FP7-ICT Future Networks
SPECIFIC TARGETTED RESEARCH PROJECT
Project Deliverable

PHYDYAS Doc. Number	PHYDYAS_ 025
Project Number	ICT – 211887
Project Acronym+Title	PHYDYAS – PHYsical layer for DYnamic AccesS and cognitive radio
Deliverable Nature	Report
Deliverable Number	D8.3
Contractual Delivery Date	July 1, 2010
Actual Delivery Date	July 31, 2010
Title of Deliverable	Impact of the FMBC physical layer on cognitive radio
Contributing Workpackage	WP8: Radio scene spectrum analysis and cognitive radio
Project starting date; Duration	01/01/2008; 30 months
Dissemination Level	CO
Author(s)	Maurice Bellanger, Didier LeRuyet, Daniel Roviras (CNAM), Markku Renfors (TUT), Andreas Merentitis, Dionysia Triantafyllopoulou (RA-CTI), Musbah Shaat, F. Carlos Bader, M. Ángel Rojas and M. Ángel Lagunas (CTTC), Yejian Chen (ALUD – new WP8 leader)

Abstract: Deliverables [D8.1] and [D8.2] are reviewed. Some complements are provided and the work carried out in WP8 is put in perspective, in order to assess the impact of FBMC on cognitive radio. The most important contribution is on opportunistic unsynchronized networks, which are able to access the spectrum on their own decision and without synchronizing and cooperating with other networks sharing the same frequency bands. It is argued that FBMC is the enabling technique for this kind of network.

List of Acronyms

3GPP	3rd Generation Partnership Project
ACF	Autocorrelation Function
AFB	Analysis Filter Bank
AWGN	Additive White Gaussian Noise
BER	Bit Error Rate
BS	Base Station
CASE	Candidate Spectral Estimation
CBS	Cognitive Base Station
CCI	Co-Channel Interference
CDF	Cumulative Distribution Function
CFO	Carrier Frequency Offset
CP	Cyclic Prefix
CR	Cognitive Radio
CRS	Cognitive Radio System
CS	Cyclostationary Signature
DoA	Direction of Arrival
DDSA	Decentralized Dynamic Spectrum Allocation
DSA	Dynamic Spectrum Access
FMBC	Filter Bank Multicarrier
FCC	The Federal Communication Commission
FDD	Frequency Division Duplex
FFT	Fast Fourier Transform
GN	Good Neighbour
i.i.d.	Independent and Identically Distributed
ICI	Inter-Carrier Interference
IDFT	Inverse Discrete Fourier Transform
IM	Interference Mitigation
KKT	Karush-Kuhn-Tucker
LPTV	Linear Periodically Time Variant
LTE	Long Term Evolution
MIMO	Multiple Input Multiple Output
MMSE	Minimum Mean Square Error
OFDM	Orthogonal Frequency Division Multiplexing
OQAM	Offset Quadrature Amplitude Modulation

PDF	Probability Density Function
PFB	Polyphase Filter Bank
PI-Algorithm	Power Interference constrained algorithm
PPN	Polyphase Network
PSD	Power Spectrum Density
PSE	Periodogram Spectrum Estimator
PSW	Prolate Sequence Window
PU	Primary User
QoS	Quality of Service
ROC	Receiver Operating Characteristic
RTG	Receive-transmit Transition Gap
SDR	Software Defined Radio
SFB	Synthesis Filter Bank
SIR	Signal-to-Interference Ratio
SINR	Signal-to-Interference-plus-Noise Ratio
SNR	Signal-to-Noise Ratio
SS	Subscriber Station
SU	Secondary User
TDD	Time Division Duplex
TTG	Transmit-receive Transition Gap
ULA	Uniform Linear Array
WiMAX	Worldwide Interoperability for Microwave Access

Contents

1 Introduction

The objective of Cognitive Radio (CR) is to maximize the usage of the spectrum at any place and any time. The PHYDYAS project contributes to this objective in two aspects

- Maximizing the bit rate in a given bandwidth;
- Enhancing the flexibility of spectrum access through new scenarios.

The first aspect has been dealt with in the work packages 2-7 and the documents which have been issued as deliverables and articles. The second aspect is mainly the subject of work package 8 (WP8), in which the technical issues of CR have been investigated and the feasibility of a scenario with opportunistic access and limited regulation has been demonstrated.

Now, the work carried out in the project must be put in perspective and the objective of the present document is to review the main contributions of the deliverables [D8.1] [D8.2], provide updates and figure out how the developed Filter Bank Multicarrier (FBMC) spectrum layer can be promoted and exploited in future cognitive radio systems and networks.

The document is organized as follows. First, it is interesting to position the work of WP8 in the field of cognitive radio and it is the subject of section 2. A huge research effort is dedicated to cognitive radio, but most of the outcome is theory with little concern for real life constraints. It is felt that a good balance between theory and applications is provided by the standardization teams and particularly the ITU-R team, because it reflects the vision of the entire world. Then, section 3 provides a review of the main characteristics of the FBMC physical layer, in comparison with OFDM. Spectrum sensing and monitoring are the subjects of section 4 and an overview of the main results is provided. Section 5 is concerned with some specific cross layer aspects. The importance of burst shortening in the time division duplex mode for cognitive radio is recalled and some additional results are presented. Also, some complements to the work reported in deliverable [D8.1] about the contribution of the MAC layer are presented. Section 6 is dedicated to the “Good Neighbour” strategy which is a major contribution of WP8. After a brief overview of the main features of the approach and some additional details, design and implementation aspects related to beamforming and interference mitigation are developed. Now, considering the PHYDYAS project as a whole, it is claimed that FBMC is the enabling technology for the most advanced concept of cognitive radio, namely the opportunistic unsynchronized network. Then, section 7 lists some potential applications and section 8 discusses some conditions for the successful introduction of this new communication paradigm and its proliferation.

2 Positioning of the Work of WP8

On the international stage, the evolution of communications is ruled by the World Radio Conference (WRC), which has introduced cognitive radio on its agenda at the 2007 meeting. Then, questions have been put to the technical arm, ITU-R, in preparation of the WRC’2012 meeting. Within ITU-R, the subject is treated by study group 5 working party A (5A) and a report entitled “Cognitive radio systems in the land mobile service” is being prepared [ITU-R-A19]. Participants to the work (from 34 countries from all continents) include administrations, registered operating agencies, scientific and industrial organizations. The PHYDYAS project has submitted (through

URSI and Alcatel-Lucent) a contribution which was discussed at the May 2009 meeting of the group [ITU-R-5A].

Within the land mobile service allocation, working party 5A are considering 5 scenarios for the deployment of Cognitive Radio Systems (CRS)

- Use of CRS technology to guide reconfiguration of connections between terminals and multiple radio systems;
- Use of CRS technology by an operator of a radio system to improve the management of its assigned spectrum resource;
- Use of CRS technology as an enabler for cooperative spectrum access;
- Use of CRS technology as an enabler for opportunistic spectrum access;
- Use of CRS technology as an enabler for opportunistic spectrum access in bands shared with other systems.

The results of the PHYDYAS project can be exploited to advantage in all these scenarios, however, in the 4th and 5th scenarios, the FBMC physical layer appears as an enabler for the opportunistic spectrum access.

Regarding operational techniques, the first item considered is "obtaining knowledge" and two approaches are listed

- Listening to the wireless channel, i.e. a cognitive control channel, a cognitive pilot channel or a common signalling channel;
- Spectrum sensing.

The wireless channel implies connection to a central data base, coordination and cooperation between the systems and the networks. The scenario presented in [D8.1] [D8.2], which proposes decentralized dynamic spectrum allocation, relies on spectrum sensing.

The next item is "decision making and adjustment of operational parameters and protocols", for which the cases of centralized and distributed decision making are distinguished. The text about distributed decision making reads

> "*A distributed approach is based on localized decisions on distributed network entities. An example is an ad hoc cognitive radio network where distributed dynamic spectrum access would be required. Each user has to gather, exchange, and process the information about the wireless environment independently. The decisions on the actions need to be carried autonomously based on the available information.*
>
> *The delay is substantially shorter to facilitate dynamic change of situations compared with centralized approach. However, there may be an issue with stability (especially when entities act independently without coordination) as it is difficult to prove that the proposed solution will always behave in a predictable manner. ……*"

The PHYDYAS approach allows distributed decision making and it avoids the stability issue through threshold regulation. The behaviour of the proposed solution has been analyzed through Markov theory and convergence has been proven.

Coexistence is an important chapter in the ITU-R document, which lists two cases

- Coexistence with existing radio systems (vertical sharing);
- Coexistence of CR systems (horizontal sharing).

Possible technical solutions for coexistence and sharing are described. The properties that coexistence mechanisms should have are presented and they are a reference to assess the “good neighbour” scheme of [D8.1] and [D8.2].

Overall, the subject of WP8 and the work carried out by the partners fit well into the vision that ITU-R have expressed about cognitive radio systems and networks. It brings potential solutions to some of the issues which have been raised, particularly regarding techniques for opportunistic networks.

3 Characteristics of the FBMC Physical Layer

Until now, cognitive radio systems, either in theoretical research or in experiments, are mainly based on OFDM. Therefore, it is appropriate to consider OFDM as the reference when recalling and assessing the characteristics of the FBMC physical layer. It is worth pointing out that WP7 in the project was dedicated to the compatibility of FBMC and OFDM.

3.1 FBMC vs. OFDM in Cellular Wireless Systems

The characteristics of OFDMA are generally considered as an almost perfect match to the requirements of today's broadband cellular wireless communications radio interface:

- Robustness and simplicity of channel equalization, which facilitates efficient implementation of advanced multi-antenna transmission schemes;
- High flexibility in allocating resources in the time-frequency domain for different users/purposes, supporting effective adaptive coding and modulation schemes and scheduling methods, and providing means utilize effectively time and frequency diversity.

As downsides, we can mention:

- Overheads due to the Cyclic Prefix (CP) and guardbands between transmission channels;
- Tight requirements for timing and frequency synchronization between uplink users, requiring complicated overall synchronization schemes and tight coordination of the radio network elements of a cell;
- High peak-to-average power ratio which is, however, significantly relieved by the SC-FDMA (or DFT-S-OFDM) approach adopted by the 3GPP-LTE uplink.

FBMC, in large extent, inherits the benefits of OFDM, while exhibiting the potential to significantly enhance the spectral efficiency of the radio interface. PHYDYAS has demonstrated a gain in spectral efficiency in the order of 20% in a WiMAX-like scenario [Rin10]. This is achieved through the elimination of CPs and through the use of considerably narrower guardbands allowed by the high spectral containment. In FBMC, channel equalization is, no doubt more involved than in OFDM, but workable schemes also for cases with significant subchannel frequency selectivity have been proposed by PHYDYAS partners [D3.1] [D3.2]. Especially, the frequency sampling based per-subcarrier equalization approach can be straightforward and efficiently extended to multiple antenna scenarios [D4.1] [D4.2], allowing OFDM-like receiver antenna diversity and spatial multiplexing techniques to be applied.

In general, the somewhat higher implementation complexity can be regarded as the main downside of FBMC, together with the higher conceptual complexity and unfamiliarity to the engineering community. However, it can be argued that the implementation complexity of FBMC is still acceptable, when considering the overall complexity of receiver implementations where the channel decoding part is usually dominating.

Another downside of FBMC is due to the usage of Nyquist pulse-shaping principle at subcarrier level, with overlapping symbol pulses extending over a few symbol intervals. This introduces 'tails' to the transmission bursts and leads to increased overheads due to the required time-domain gaps between transmission bursts originating from different stations. Significant truncation of the burst

tails may be tolerated, as studied in [D2.2]. In any case, the time-domain gaps between transmission bursts from different stations need to be increased in comparison to OFDM, if the subcarrier spacing remains the same. To reduce the overheads due to this effect, the utilized frame structures should be redesigned, avoiding tightly time-multiplexed operation. For example, some of the WiMAX uplink transmission modes are not practical to be directly adopted for an FBMC version of WiMAX.

One decisive difference is that there is more flexibility in the parameterization of FBMC systems. Compared to OFDM, considerably larger subcarrier spacing, i.e., shorter symbol duration, can be considered while using multitap subcarrier equalizers with reasonable complexity. This helps to reduce the Carrier Frequency Offset (CFO) problems in fast-fading channels and alleviates the mentioned problem of increased guard intervals between transmission bursts. On the other hand, increasing the subcarrier spacing increases the overheads due to the guardbands between groups of subcarriers used asynchronously. It also reduces the granularity in the frequency direction in spectrum sensing and utilization of spectral white spaces. A suitable compromise between these aspects should be sought when designing an FBMC system.

Regarding the transmitter power amplifier issues, it has been demonstrated in [D5.1] that the PAPR characteristics of OFDM and FBMC are quite similar. Corresponding to the reduced PAPR scheme of DFT-S-OFDM, a similar scheme, FB-S-FBMC has been developed in PHYDYAS [D5.1]. Further, it has been demonstrated that traditional single-carrier waveforms, with significantly reduced PAPR in comparison to DFT-S-OFDM, can be supported in an FBMC based radio interface by using the analysis filter bank and subcarrier equalizers as central elements in frequency-domain equalization [Iha09]. This would allow very simple and low-power devices for low data-rate communications to be supported in the same air interface with FBMC.

3.2 FBMC vs. OFDM in Dynamic Spectrum Access Cases

Let’s us turn now our attention from cellular systems with high level of coordination of different users of the radio interface to opportunistic DSA scenarios and cognitive radio. Such systems are expected to support different independent secondary users (SU) ‘cells’ operating in the same geographical region and contending for the transmission opportunities in the same spectral white spaces. In this case we cannot assume close coordination of different transmitters which would be required to reach quasi-synchronous operation which, in turn, is one of the corner-stones of OFDMA. In quasi-synchronous operation, different users’ transmissions are time-synchronized in such a way that the multipath channel delay spreads, combined with timing offsets between different transmissions, all fit within the CP of OFDM symbols.

Now if we consider scenarios where quasi-synchronous operation is not feasible, OFDMA looses many of its benefits: orthogonality of different users’ subcarriers is lost and it can only be restored if substantial guardbands are inserted between different users’ groups of subcarriers. In contrast, in FBMC one unused subcarrier is sufficient as a guardband to isolate different groups of subcarriers operating with arbitrary timing offsets. Further, a wideband receiver (e.g., in base-station) is able to process multiple asynchronous groups of subcarriers (i.e., different uplink users) efficiently based on a single analysis filter bank and multi-tap subcarrier equalizers. The orthogonality of OFDMA is quite sensitive also to the CFOs, with typical specifications for maximum CFO in the order of few percent of subcarrier spacing. In FBMC the orthogonality is based on guardbands, and CFO in the order of 10…20% of subcarrier spacing can be easily tolerated, depending also on the filter bank

design. Such CFOs can also be compensated by multi-tap equalizer based subchannel processing in a wideband receiver, as demonstrated in [D2.2].

3.3 Filter Bank Design Aspects

In the FBMC system design, the number of subchannels, or subcarrier spacing, is the primary parameter. As a rule of thumb, as long as the channel delay spread is less than quarter of the OQAM symbol interval, three-tap subcarrier equalizers provide sufficient performance if they are not expected to compensate synchronization offsets. For compensating channel delay spreads of the order of OQAM symbol interval, as well as worst-case fractional timing offsets and CFOs, we anticipate that 5 … 9-tap equalizers are required, depending on the order of the modulation. Basic synchronization and offset compensation techniques have been developed in PHYDYAS based on scattered pilots [D2.1] [D2.2]. However, there is still room for significant improvements with respect to the compensation performance and resolving phase ambiguities to allow sparser pilot structures.

The second main parameter in FB design is the overlapping factor *K*. In PHYDYAS, a highly frequency selective filter bank design based on [Bel01] and [Mar78] was adopted, and throughout the project it was found out to be an excellent choice. Mostly the overlapping factor of K=4 has been utilized, resulting in very good stopband attenuation. Smaller overlapping factor, 3 or even 2, with lower implementation complexity, could be sufficient in well-controlled cellular network scenarios, similar to WiMAX or 3GPP-LTE.

However, we feel that the benefits of FBMC are capitalized in dynamic spectrum access scenarios where high spectral containment of subcarriers is a significant asset. Using overlapping factor K=3 would significantly reduce the dynamic range in spectrum sensing and degrade the quality of isolation provided by one-subcarrier guardband with realistic power level differences of the different subcarrier groups.

On the other hand, higher stopband attenuation, provided by K=5 or higher, has little use in the presence of various non-idealities introducing spectral leakage in the transmitter end (notably power amplifier nonlinearity), and receiver end (analogue circuit and ADC nonlinearity). As a matter of fact, it is a great challenge for the analogue circuit and ADC design not to degrade the performance provided by the K=4 filter bank design.

Various generic criteria for fine optimization of the filter bank were considered in [D5.1]. These ideas can be used for example for optimizing the filter bank design for a specified maximum CFO range between different asynchronous users. This would be needed in cases where the expected CFOs might cause significant performance degradation with the basic FB design.

3.4 Channel Filtering Considerations

Another significant potentiality of FBMC is the use of the synthesis filter bank in the transmitter end and analysis filter bank in the receiver end as tools for extremely flexible waveform processing in the spirit of software defined radio [Saa08]. On the receiver side, high spectral selectivity of the analysis bank helps to separate effectively the wanted group(s) of subchannels from the other ones. In this context, the filter bank also effectively suppresses any spectrally localized interferences which might appear in the frequency band entering the AFB. These may contain narrowband interferences or adjacent channel signals utilizing FBMC, OFDM or any other communications

waveform. In fact, FBMC allows fragmented use of the spectrum where the used frequency band contains sections of completely unrelated, non-synchronized transmissions [Fet09]. In contrast, the plain FFT processing of OFDM is ineffective against any interferences which are not synchronized to the CP structure of OFDM.

If we consider the example of 3GPP-LTE, in the baseline design the channel selectivity for alternative bandwidths is implemented through configurable analogue filtering, and the baseband digital signal processing after the ADC starts with CP removal and FFT [Tos09]. However, commercial chip designs based on digital channel filtering have also been announced [Fuj10]. This is one example of the progress of SDR ideas towards practical implementations, also for latest cellular wireless technologies. On the other hand, in case of DSA, flexible digital channel filtering, with capability to suppress strong spectrally contained interferences on the DSP side, is a crucial enabler. Now considering receiver designs which utilize the digital channel selection filtering approach, the analysis filter bank of FBMC is able to implement significant portion of the needed channel filtering. In such solutions, signal processing complexity is moved from the multi-rate digital channel filtering section to the analysis filter bank processing. This basically pays back the higher complexity of the filter bank approach in signal detection.

4 Spectrum Sensing with FBMC

Spectrum sensing is an essential enabling functionality in cognitive radios to detect unoccupied spectrum holes and then dynamically adjust the radio operating parameters accordingly. In the following, first studies on spectrum sensing techniques reported in [D8.1] and [D8.2] are summarized in section 4.1. In PHYDYAS, special emphasis has been put on the spectrum monitoring functionality, which is targeted at rapid detection of reappearing primary users (PUs) during secondary transmission. A spectrum monitoring scheme based on continuous sensing subbands, proposed in [D8.2], is summarized in section 4.2 including various updates and enhancements to the basic scheme. In Section 4.3, the Candidate Spectral Estimation (CASE) spectrum sensing approach, reported in [D8.2], and various extensions to the earlier studies are presented. The method presents very good performance for FBMC primaries. Also, section 4.3 includes a brief review of multiband spectrum sensing. Section 4.4 summarizes the PHYDYAS spectrum monitoring concept.

4.1 Summary of Spectrum Sensing Studies

The main criteria for spectrum sensing are

- Minimum detectable signal levels and required sensing time to achieve the desired probabilities of detection and false alarm;
- Robustness to noise uncertainty and background interference;
- Implementation complexity and feasibility.

The different spectrum sensing schemes can be categorized into matched filter detection, energy detection, cyclostationary feature detection techniques, etc., each with its individual pros and cons. In [D8.1] these different techniques have been evaluated and tested with a special emphasis on energy detection, cyclostationarity detection and multi-band sensing.

Spectrum sensing on a single frequency band has a relatively rich literature however multi-band sensing which monitors multiple frequency bands simultaneously is an important issue from a practical point of view. The basic concept of multi-band sensing is to firstly estimate the Power Spectrum Density (PSD) and then perform energy detection in the frequency domain based on the observed power spectrum.

The PSD can be estimated using Polyphase Filter Bank (PFB) since it is well known that PFB is an efficient tool for spectral analysis. In our context, PFB can be used without additional cost since each secondary user is equipped with PFB at the receiver front end. Initial works using PFB and energy detector for multi-band sensing can be found in [She09] [Kim09]. PFB with suitable subband spacing can also be used flexibly in the detection of different types of primary signals and different SNR values by adjusting the integration range.

The decision is a binary hypothesis testing problem. Both cases follow chi-squared probability distribution, but can be well approximated by Gaussian functions. The primary SNR and the number of independent observations determine how well the distributions are separated. In [D8.1] the sensing time has been expressed for a given SNR, uncertainty of the noise variance, missed detection probability and false alarm probability. The main disadvantage of energy detector is that its performance is limited by SNR levels and noise uncertainty.

In [D8.2] we have investigated the PFB based spectrum analyzer to show its applicability for multi-band sensing in cognitive radio context. Our study includes theoretical and experimental analysis for three kinds of spectrum analyzers: conventional Periodogram Spectrum Estimator (PSE), PHYDYAS based PFB and Prolate Sequence Window (PSW) based PFB. The numerical results reveal that PSE based spectrum analyzer is sensitive to the spectral leakage. Conversely, PFB exhibits more efficient and reliable detection performance by taking advantage of its low spectral leakage property, which further enhances the multi-band sensing application of PFB in cognitive radio networks. From the view of computational complexity, the performance gain obtained by PFB doesn't come with the penalty of increased complexity due to the inherent parallel structure of PFB.

Finally, in [D8.1] detection of FBMC signal based upon Cyclostationary Signature (CS) has been proposed and investigated. The cyclic spectral correlation of both OFDM and FBMC signals has been analyzed. Using a Linear Periodically Time Variant (LPTV) model, we have derived the explicit formulas of nonconjugate and conjugate cyclic autocorrelation and spectral correlation functions for OFDM and FBMC signals, which provide the theoretical basis for further signal detection. Secondly, a strategy for the detection of MCM signals by embedding cyclostationary signature at the predefined cyclic frequency is investigated. Using the LPTV structure of the FBMC signal, the explicit formulas of nonconjugate and conjugate cyclic autocorrelation function and spectral correlation function with CS for FBMC signal are derived and CS can be accordingly easily inserted into the FBMC signal at some predetermined frequency position. A low-complexity conjugate detector has been proposed for detecting FBMC signal by embedding the CS at zero cyclic frequency in the AWGN and Rayleigh fading situations, respectively. Experimental results show that CS is a robust tool for signal detection in cognitive radio network. Using flexible CS position design for different MCM signals (different CR networks), identification among different modulated signals can also be implemented in the same way.

4.2 Spectrum Monitoring Using Sensing Subbands

In contrast to most of the spectrum sensing literature, in PHYDYAS significant emphasis has been put on spectrum monitoring, i.e., rapid detection of possibly reappearing primary users (PU), instead of focusing only on initial acquisition of spectrum holes. The spectrum monitoring function is crucial, and can be considered to be even more challenging than the basic initial acquisition setting. The reasoning here is that in the monitoring phase, the monitoring functionality introduces some overhead in the utilization of spectral resources, and this overhead should be minimized. In the basic initial acquisition scenario, all parts of the spectrum can be used for sensing PUs, and it is easier to collect sufficient statistics for the spectrum decisions.

Furthermore, in a sensible DSA scheme, like the one developed in PHYDYAS, the existence of independent uncoordinated SU systems operating in the same geographical region have to be assumed. It should be emphasized that the detection of and coexistence with other SU systems is a part of the DSA scheme, and not considered here in the spectrum monitoring context. In such a scenario, it can be argued that the pure initial acquisition setting is seldom relevant. Even if the user's own SU system is silent, it is necessary to be able to detect weak PU signals in the presence of SU transmissions at a somewhat stronger level, which would correspond to an acceptable spectral reuse case between the secondary systems.

Spectrum monitoring basically requires some way of sensing the spectrum for the presence of potential PU signals while the secondary transmissions are ongoing. It would be extremely

challenging to consider spectrum monitoring simultaneously in a transmitting station of a secondary system, but various schemes for simultaneous reception and spectrum monitoring can be conceived. Especially using FBMC waveforms for secondary transmission, commonality of data reception and spectrum sensing functions is achieved. In [D8.1], alternative spectrum monitoring techniques were discussed, including also residual interference based techniques and scattered 0-pilot based techniques. However, these approaches are practical only in case of single-user secondary transmissions, and would become extremely challenging in the uncoordinated SU system scenario. Therefore, these ideas have not been elaborated further under PHYDYAS.

Instead, we explored approaches based on the well-known idea of using silent blocks in time-frequency domain in the secondary transmissions to facilitate spectrum monitoring. It was soon realized, that in the considered DSA scheme, it is impractical to assume that different SU systems are time-synchronized, even at the transmission burst level. Fairly complicated coordination functionality would be needed to guarantee that all SU system, which can be heard at a certain geographical region, would be silent at the same time. Therefore, the studies ended up in proposing schemes with continuous sensing subbands between the groups of subcarriers used for secondary transmissions. The locations of the sensing subbands could be included as global parameters in the definition of the CR interface, and only coarse frequency synchronization of different secondary users needs to be assumed to enable the spectrum monitoring functionality. As discussed in Section 3.2, CFOs in the order of 10% of subcarrier spacing can be tolerated, and sufficient coarse synchronization can be achieved without need for specific coordination between different secondary systems.

The scheme proposed in [D8.2] uses selected subbands of analysis filter bank for spectrum sensing. These sensing subbands are inserted between groups of subcarriers. To isolate sensing subbands from the data-carrying subcarriers, three subcarriers without data modulation are inserted between subcarrier groups, two of which appear as guardbands around the spectrum sensing band (see Figure 4.1). In an example parameterization, one group consists of 18 data subcarriers and 3 zero-subcarriers. With 11 kHz subcarrier spacing (WiMAX-like case), the spacing of sensing subbands is about 230 kHz, which is adequate for primary user bandwidths of about 1 MHz or more. Naturally, for GSM and other more narrowband waveforms, other kind of parameterization should be considered.

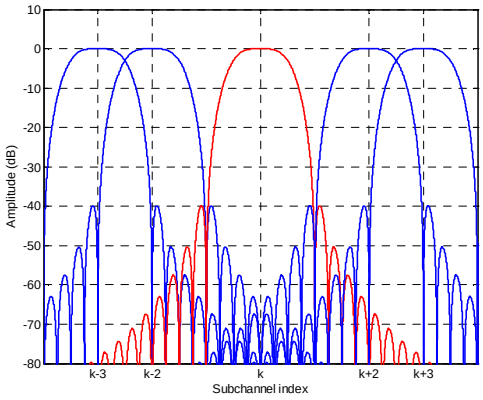

Figure 4.1: Sensing subband in FBMC spectrum

It is clear that using FBMC waveforms with highly spectrally contained filter bank design, the overheads due to sensing subbands can be minimized. As a topic for future studies, it seems possible to reduce the spectral gaps from three to two subcarriers using further filtering of the subband signals, without essentially effecting the sensing performance.

It has to be noted that the proposed sensing subband scheme is quite challenging regarding the effects of the RF imperfections mentioned in Section 3.2. Specifically, the PA nonlinearity of secondary transmitters introduces spectral regrowth, which causes interference in the sensing subbands. When this interference is at about the thermal noise level or lower, its effect can, in principle, be compensated by increasing the integration time. However, the spectral regrowth induced interference level is difficult to estimate, and in energy detection based spectrum sensing, we are faced with a severe noise uncertainty problem.

The sensing subband scheme was analyzed in [D8.2] using realistic model for the PA nonlinearity and practical operating conditions in PU sensing, with the following conclusions:

- The overheads to data transmission rate are similar in the sensing subband scheme and in a silent time-gap scheme (which would require good time synchronization of SUs).
- With realistic PA backoff (say 10 dB), the maximum SU power level could be about 25 … 30 dB above the noise level without degrading the PU sensing performance.

The resulting SU dynamic range requirement is rather tight and would require effective power control of the SUs. In practice, distributed cooperative sensing is preferred over PU sensing based on isolated sensing stations. This helps to overcome the channel fading effects, notably the large-scale fading, i.e., the fact that an isolated sensing station may experience excessive transmission loss due to shadowing in the propagation environment. Distributed sensing also helps to relive the stated SU dynamic range requirements, which can now be expressed as follows: Sufficient number (say 4 … 8, providing sufficient diversity against the fading effects) sensing stations should be in an environment where the stated SU dynamic requirement is satisfied. Preliminary discussion of different SU elements' capabilities to participate in the distributed sensing is also included in [D8.2]. However, to properly characterize the performance of such an overall scheme, system-level simulation study with adequate propagation models and user statistics should be carried out. This remains as a topic for future work.

A. Fast sequential detection of reappearing PUs

A fundamental difficulty in detecting a reappearing primary user is the fact that, during the transition phase, the integration window in spectrum sensing usually contains two parts, one where the PU is not present and another part where it is present. Then the usual assumptions of the signal statistics are not valid anymore, and the sensing performance is degraded. This effect was analyzed in [D8.2] in case of energy detection. Furthermore, a sequential detection based idea to improve the sensing performance during the transition phase was introduced in [D8.2]. The idea is based on multiple parallel sequential detection process with different starting times. Among these, the one whose starting time is closest to the actual time of reappearance is expected to converge fastest, indicating the reappearance of a PU. It is important to notice that running multiple parallel detection processes in this manner has low additional computational complexity, since the calculation of partial statistics for each block of samples is common to all of the parallel processes. After completing [D8.2], the performance of this method has been verified using FBMC signal models and the proposed sensing subband structure. The results and conclusions are consistent with the preliminary results of [D8.2], indicating significantly faster detection on the average.

In any case, in order to relax the SU dynamic range requirements, there is great interest to consider ways to mitigate the effects of the PA spectral regrowth. Some preliminary tests indicate that proper

power amplifier linearization methods would reduce the spectral leakage effects quite significantly, whereas windowing based PAPR mitigation methods [Rah09] are not effective at frequencies so close to the active subcarriers. Another direction is to consider advanced statistical signal processing methods on the receiver side for detecting the part of noise in the sensing subband which is correlated with the nearby active subcarriers (e.g., based on ideas of [Val06]). On one hand, these methods would help to estimate the power level due to spectral regrowth in the sensing subband, alleviating the noise uncertainty problem. On the other hand, it might be possible to cancel this interference, at least partially.

B. Effects of sensing filter frequency response and frequency-selective fading channel

The analysis of energy detection based spectrum sensing usually assumes that the used data samples are uncorrelated. However, in the FBMC case, correlated samples are available from each subband at two times the symbol rate. In frequency domain, the subcarrier sample sequence is characterized by the filter bank prototype frequency response, which is far from the rectangular one corresponding to the uncorrelated sequence model. In [D8.2] these effects were analyzed and proper model was developed. This model explains well the differences between basic uncorrelated model and simulations, and indicates a reduction by the factor of 0.82 in the needed sample complexity in subband-wise sensing.

The same model was also used for analyzing the effects of channel frequency selectivity. The resuting model is repeated here with some corrections and clarifications. The test statistic distributions in the absence of PU (H_o) and in the presence of PU (H_1) can be modelled as Gaussian distributions:

$$\begin{aligned} T(\mathbf{Y})|_{H_0} &\sim \mathrm{N}\left(\sigma^2, \frac{1}{N}\sigma^4\right) \\ T(\mathbf{Y})|_{H_1} &\sim \mathrm{N}\left(P+\sigma^2, \frac{1}{N}(\beta P^2 + 2P\sigma^2 + \sigma^4)\right) \end{aligned} \tag{4.1}$$

with

$$\beta = \sum_{l=1}^{L} \frac{|F_{ch}|^4}{L} \tag{4.2}$$

and

$$\sum_{l=1}^{L} \frac{|F_{ch}|^2}{L} = 1 \tag{4.3}$$

.

Here F_{ch} is the L-point FFT of the channel impulse response, σ^2 is the noise variance and P is the PU signal variance. The condition of (4.3) means that the model includes frequency selectivity but the power gain of the channel is normalized to unity.

The effect of the coefficient β can be analyzed by considered its effect for the required sample complexity $\hat{N}$ for fixed missed detection probability in terms of the required sample complexity in the AWGN case, N :

$$\frac{\hat{N}}{N} = \frac{\beta \cdot SNR^2 + 2 \cdot SNR + 1}{SNR^2 + 2 \cdot SNR + 1} \tag{4.4}$$

Experimentally, it has been verified that with the Vehicular A channel model, $\beta < 1.9$ in 99 % of the channel instances. This is in good agreement with time-domain simulations with the same channel model (with N=1000), which indicate that the experimental value of β in (4.1) satisfies the same condition, i.e., $\beta < 1.9$ in 99 % of the cases. Then we can conclude that in the interesting range (SNR<1), the effect of frequency selectivity is rather small. For example with SNR=0 or -6 dB, the sample complexity has to be increased by no more than 25 % or 8 %, respectively, if $\beta < 2$.

It is clear that the condition (4.3) is not realistic in practical spectrum sensing scenarios. However, based in the above analysis, a modest but realistic safty margin can be determined for the required sample complexity due to frequency selectivity. Then the existing knowledge for modelling flat-fading channel cases in energy detection based spectrum sensing can be utilized for handling the effects of the channel time variability.

C. CP autocorrelation approach for spectrum monitoring

OFDM is extensively used in current and emerging wireless communications standards, and thus PUs appearing in future cognitive radios will commonly use OFDM waveforms. Therefore, it is interesting to consider exploiting the specific features of OFDM in spectrum sensing. CP autocorrelation approach is an effective, low-complexity spectrum sensing method for OFDM primaries, which overcomes the noise uncertainty problem of energy detection [Cha08]. However, the time-domain approaches which are available in the literature, have some limitations in DSA and cognitive radio scenarios, because some parts of a weak PU spectrum might be masked by other SU signals. In the spectrum monitoring context, it is also very interesting to see if the sensing subband approach could be combined with the CP autocorrelation method. In [D8.2] a frequency domain implementation of the CP autocorrelation method is reported and tested successfully in a form which utilizes the sensing subcarrier signals only. This approach helps to overcome the noise uncertainty problem, discussed above, in case of OFDM PUs.

4.3 Other Techniques for Spectrum Sensing

Two additional and complementary techniques developed in the context of FBMC and reported in [D8.2] are recalled below.

4.3.1 Spectrum Sensing Using Candidate Spectral Estimation (CASE)

The Candidate Spectral Estimation (CASE) spectrum sensing approach was reported in section 6 of [D8.2]. This method is tuned to the baseband shape of the primary user; in fact the procedure is tuned to the autocorrelation matrix of the baseband transport signal of the primary user to be detected. Candidate is the name of the procedure since basically it replaces the pure sinusoid functions by a generalised function to scan the spectral power density in, let us say, traditional spectral estimation methods. Specifically, formulating power spectral estimation as a problem of correlation matching, and assuming that the data autocorrelation is given by matrix **R**, traditional power spectral estimates can be grounded on how much power can be subtracted from **R** at a pure frequency f ($\omega = 2\pi f$) with a given criterion on the resulting difference matrix (see sections 6.1.1 and 6.1.2 of [D8.2]).

The FBMC signal, considered as the primary user signature in a cognitive radio scenario, is successfully detected in the presence of narrow-band interferers, which may correspond to secondary users, in SNR regimes ranging from -15 up to -9 dB that correspond to realistic scenarios. Requiring only the spectral shape of the primary user, the CASE detector stays always with superior quality compared with traditional energy detectors. The candidate detector provides accurate power level estimates and centre frequency location, even in the presence of severe narrow-band interferences. The method presents very good performance for FBMC primaries, and seems robust even in presence of narrow-band interference.

The spectral autocorrelation matrix properties of different communications signals are usually unique. The proposed CASE detector takes this advantage to differentiate between a particular primary user and other users or interferences. The basic steps of the CASE detector are

1. Sensing the candidate user including the noise level and the interference effects
2. Estimate the autocorrelation matrix of the received signal
3. Define the autocorrelation matrix of the primary user $\mathbf{R_c}$ (see filter bank spectral analysis in section 6.1.1 of [D8.2]) at unit power level and band frequency
4. Find the minimum eigenvalue λ_{min} and the associate eigenvector **a** (λ_{min} and **a** values detailed in [D8.2])
5. Compute the estimate spectral density of the candidate

A. Robustness analysis of the CASE estimator

The claimed performance of the candidate power level estimation has been undertaken first under high SNR scenario. For the evaluation a FBMC signal (as primary user) has been used with 256 subcarriers, a bandwidth of 20 MHz and a frequency carrier of 90 MHz. The synthesis filter parameters used for the analysis are those specified in [D5.1]. It has been noticed that the candidate signal is still detectable in a robust manner despite of its contamination with different SNRs (-5 dB, 2 dB and 9 dB respectively) values. The CASE estimator robustness has been compared with the periodogram and Capon estimators [Roj08] [Roj09]. Requiring only the spectral shape of the primary user, the CASE detector allows a superior accuracy than traditional energy detectors, providing precise power level estimate and central frequency location.

The performance of CASE detector has been also analysed when a narrow-band interference radiating at a very near frequency carrier (analysed example at 80 MHz) of the candidate (primary) signal (at 90 MHz of frequency carrier). It has been shown in [D8.2] that the CASE still detects with accuracy the transmit power of primary user at its frequency location despite the interference.

Probability of detection versus probability of false alarm, namely Receiver Operating Characteristic (ROC), has been analysed to test the candidate estimate. It is observed that even having an SNR of -9 dB the system still presents good performances in terms of probability of detection. The ROC performance has been also analysed in presence of narrow-band interference, the Signal-to-Interference Ratio (SIR) has been set to -10 dB and in accordance with the low sensitivity of the CASE estimator to narrow-band interference the system still achieves high-quality performance in terms of probability of detection.

The performance of the CASE detector based on generalized spectral subtraction is reported for FBMC signals. The FBMC signal, considered as the primary user signature in a cognitive radio scenario, is detected in presence of narrow-band interferers that may correspond to secondary users and in SNR regimes ranging from -15 up to -9 dB what correspond to realistic scenarios. Requiring only the spectral shape of the primary user, the CASE detector presents in all our simulation tests superior accuracy than traditional energy detectors (Periodogram and Capon methods), providing precise power level estimate and central frequency location, even in the presence of severe narrow-band interferences.

B. Candidate method for detecting spectrum holes

A spectrum hole is defined as the set of successive frequencies not occupied in a multicarrier transmission as FBMC. The bandwidth of the hole that is available for secondary transmission use to be greater than the corresponding to a single carrier. Nevertheless, searching single carrier holes is not longer a problem for CASE.

For wide bandwidth, i.e. 20 MHz, systems the power spectrum used by primary where a spectrum hole of bandwidth B exist. The basic spectral shape that fills the occupied spectrum is the magnitude of the corresponding baseband or prototype filter of the multicarrier scheme. In consequence for a single carrier analysis of the occupied spectrum, the Autocorrelation Function (ACF) that is used in the $\mathbf{R}_C$ (define the candidate autocorrelation matrix) matrix of the CASE formulation will be the inverse Fourier transform of the baseband or prototype filter magnitude response.

In fact, the usual number of carriers associated per a single user is within the range 30-60, in consequence, the spectrum sensing will look for holes with size equal to the number of carriers assigned to a single user. Figure 4.2, shows the spectral density estimate, using the Welch's procedure, of a FBMC 512 carriers system with a spectral hole equal to 30 carriers.

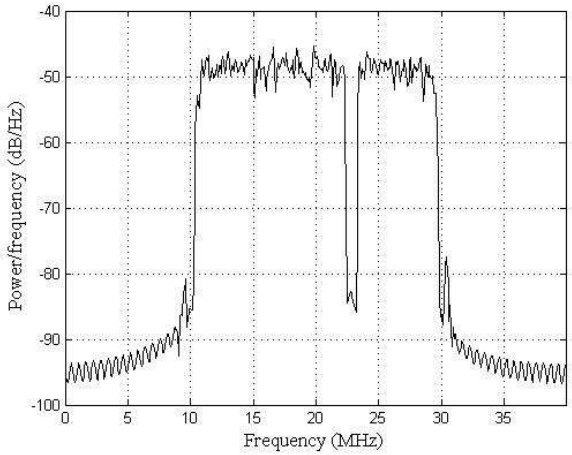

Figure 4.2: Spectral density, estimated with the Welch's procedure, of a Filter Bank Multi-Carrier transport signal of 512 subcarriers showing a spectral hole of 1.17 MHz, corresponding to 30 subcarriers.

In summary, a more realistic approach than single carrier sensing is to concentrate the interest of the spectrum sensing station on detecting and monitoring spectrum holes of a minimum bandwidth B_0, where realistic secondary transmissions may take place, with affordable complexity and delay in the detection process. For this reasons, the candidate matrix $\mathbf{R}_C$ is set to M successive carriers such that

a hole is defined when at least *M* successive carriers are empty. Note, as mentioned before, that the order of the candidate matrix, for good detection, will be close to the quotient between the global number of carriers *N* and the number of carriers occupied by a single user *M*.

Once the basic spectral shape is selected, the ACF that provides the entries of the ACF matrix is derived from its IFFT. Also it can be derived from the autocorrelation of the impulse response of the aggregate. Inserting this matrix ($\mathbf{R}_C$) in the CASE framework it is expected that the resulting power estimate will depict those frequencies where a set of *M* consecutive carriers remain used/un-used.
The scenario where the performance of CASE was tested is formed by a FBMC signal of 512 carriers occupying a global bandwidth of 20 MHz or equivalently 39.0625 KHz. per carrier. From this transport signal a hole is produced when 30 carriers are not used, i.e. the corresponding symbols are set to zero. The hole produced in the power spectral density is 1.015 MHz wide. Concerning the CASE detector, and to illustrate the performance depending on the candidate selected, two different candidates have been used: First candidate is equal to the size of the actual hole we are looking for; in the second, it has been assumed erroneously that the candidate is formed by 60 carriers which is twice the actual size of the searched spectrum hole.

From Figure 4.3 it is clear that CASE defines the borders of the hole more properly than traditional methods. In fact, the performance of the traditional methods is roughly achieved when the candidate is selected erroneously to twice the actual bandwidth of the spectrum hole. The high resolution and robustness of the CASE was reported in [Per09] proving its superiority with respect traditional methods as well as with respect cyclo-stationary approaches.

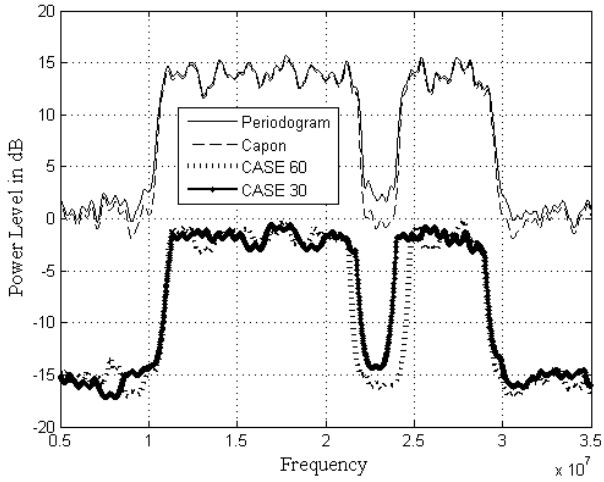

Figure 4.3: Response of the methods of Welch and Capon above, together with CASE detector for two different candidates corresponding to 30 and 60 subcarriers. The sample size was 2000 and CASE order was set to 100.

In addition, to the mentioned features in the previous paragraph, the major advantage of CASE with respect the rest of the available procedures is the robustness against secondary transmission or interferences. This performance is due to the fact that CASE is tuned to a spectral pattern, in our case the spectrum hole characterized by its bandwidth. This promotes that CASE does not responds to opportunistic transmissions already scheduled on the hole. In fact, the hole is precisely detected whenever no primary transmission occurs regardless other potential transmissions. To show briefly this performance, in the following scenario, the hole is partially occupied by a secondary narrow-band transmission (single subcarrier) corresponding to an opportunistic user. The goal of the spectral monitoring is to show the actual presence of the hole regardless opportunistic users already

scheduled for transmission. It is assumed that narrow-band opportunistic transmissions do not use completely the spectrum hole.

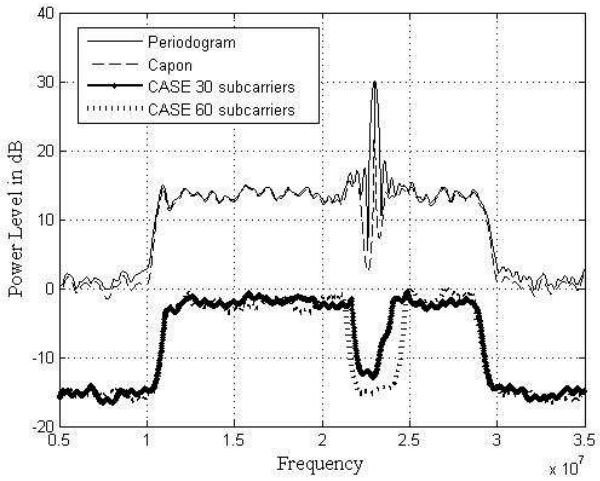

Figure 4.4: Response for the same scenario of previous figure when an opportunistic transmission appears in the Filter bank multicarrier spectrum hole.

For the sake of comparison, the performance obtained with traditional Welch's Periodogram and minimum variance method of Capon will be also depicted on the plot. Figure 4.4 shows the resulting plots with the same procedures used in Figure 4.3.

It is remarkable that the CASE method detects properly the hole in both cases regardless the presence of the opportunistic interferer. Note that the dynamic range depicted is equal and greater than 10 dB, which guarantees proper detection of the presence of the hole and its size with false alarm rates below the prescribed of 10^{-3}.

As a general summary of the undertaken analysis using CASE method:

- The named Candidate detector, based on generalized spectral subtraction, and applied to FBMC signals with PHYDYAS prototype filter bank [D5.1] has been developed and analysed. The FBMC signal, considered as the primary user signature in a cognitive radio scenario, is successfully detected in the presence of narrow-band interferers, which may correspond to secondary users, in SNR regimes ranging from -15 up to -9 dB that correspond to realistic scenarios. Requiring only the spectral shape of the primary user, the CASE detector stays always with superior quality compared with traditional energy detectors. The candidate detector provides accurate power level estimates and centre frequency location, even in the presence of severe narrow-band interferences. The method presents very good performance for FBMC primaries, and seems robust even in presence of narrow-band interference.

- Focusing on the spectrum sensing station of a cognitive radio scenario, it has been shown that the CASE can be tuned to detect spectrum holes in Filter Bank Multicarrier transmission systems. Basically tuning the candidate autocorrelation to a prescribed set of *M* successive subcarriers, the method is able to properly detect the presence/absence of these groups within the scanned bandwidth. The resulting method shows very good resolution, robustness and, most important, perfect rejection of secondary transmissions from secondary users or co-channel interferers.

- The developed implementation complements in a certain way the set of listed and developed tools in Section 4.1 of deliverable [D8.2], where the autocorrelation based sensing property is used to detect OFDM primary user. The analysis assumes a FBMC system as PU and uses, besides the autocorrelation properties to detect the signature of desired PUs, a process to detect its power level.

From a practical perspective, some more issues have to be considered, particularly latency and computational complexity, and they are a subject for further work.

4.3.2 Multiband spectral sensing

The basic concept of multi-band sensing is to firstly estimate the power spectrum density (PSD) and, then, perform energy detection in the frequency domain based on the observed power spectrum. The PSD can be estimated using Polyphase Filter Bank (PFB) since it is well known that PFB is an efficient tool for spectral analysis. In our context, PFB can be used without additional cost since each secondary user is equipped with PFB at the receiver front end. Initial works using PFB and energy detector for multi-band sensing can be found in [She09] [Kim09]. PFB with suitable subband spacing can also be used flexibly in the detection of different types of primary signals and different SNR values by adjusting the integration range.

The decision is a binary hypothesis testing problem. Both cases follow chi-squared probability distribution, but can be well approximated by Gaussian functions. The primary SNR and the number of independent observations determine how well the distributions are separated. In [D8.1] the sensing time has been expressed for a given SNR, uncertainty of the noise variance, missed detection probability and false alarm probability. The main disadvantage of energy detector is that its performance is limited by SNR levels and noise uncertainty.

In [D8.2] we have investigated the PFB based spectrum analyzer to show its applicability for multi-band sensing in cognitive radio context. Our study includes theoretical and experimental analysis for three kinds of spectrum analyzers: conventional Periodogram Spectrum Estimator (PSE), PHYDYAS based PFB and Prolate Sequence Window (PSW) based PFB. The numerical results reveal that PSE based spectrum analyzer is sensitive to the spectral leakage. Conversely, PFB exhibits more efficient and reliable detection performance by taking advantage of its low spectral leakage property, which further enhances the multi-band sensing application of PFB in cognitive radio networks. From the view of computational complexity, the performance gain obtained by PFB doesn't come with the penalty of increased complexity due to the inherent parallel structure of PFB. Finally, in [D8.1] detection of FBMC signal based upon Cyclostationary Signature (CS) has been proposed and investigated. The cyclic spectral correlation of both OFDM and FBMC signals has been analyzed. Using a Linear Periodically Time Variant (LPTV) model, we have derived the explicit formulas of nonconjugate and conjugate cyclic autocorrelation and spectral correlation functions for OFDM and FBMC signals, which provide the theoretical basis for further signal detection. Secondly, a strategy for the detection of MCM signals by embedding cyclostationary signature at the predefined cyclic frequency is investigated. Using the LPTV structure of the FBMC signal, the explicit formulas of nonconjugate and conjugate cyclic autocorrelation function and spectral correlation function with CS for FBMC signal are derived and CS can be accordingly easily inserted into the FBMC signal at some predetermined frequency position. A low-complexity conjugate detector has been proposed for detecting FBMC signal by embedding the CS at zero cyclic frequency in the AWGN and Rayleigh fading situations, respectively. Experimental results

show that CS is a robust tool for signal detection in cognitive radio network. Using flexible CS position design for different MCM signals (different CR networks), identification among different modulated signals can also be implemented in the same way.

4.4 Spectrum Monitoring Concept for PHYDYAS DSA

In this subsection we summarize a possible spectrum monitoring concept which is consistent with the Dynamic Spectrum Access (DSA) scheme developed in the PHYDYAS project. The proposed spectrum monitoring scheme includes the following elements:

- Sensing subband model with energy detection, or frequency-domain CP autocorrelation based method for OFDM PUs. Possibilities to adapt other effective spectrum sensing techniques (like CASE) to this scheme remains as a topic for future studies.
- Co-operative spectrum sensing, possibly together with antenna diversity in some of the SU elements.
- Using sequential detection at all levels (basic sensing, antenna combining, and sensor fusion). Sequential detection is tuned for rapid detection of reappearing PUs through multiple parallel sensing processes.
- Using the base station as the fusion centre to achieve high sensitivity in co-operative detection.
- In addition, the boosting protocol [Wei03b] is used to reach rapid action in case of reappearing strong PUs. In this context, the sensing subcarriers within the frequency band of the detected PU can be used for sending signalling information between the elements of the SU system. In parallel, the active subcarriers of the SUs are used for finalizing the on-going transmissions and providing further signalling information for re-organizing the SU system (assuming, of course, that the PU is at a power level which allows the SU to operate).

The key elements of this concept have been developed and tested, or they have been introduced in [D8.2] based on literature. However, validation of this overall concept, as well as some details and more complete analytical and simulation based performance studies remain topics for future work.

5 FBMC PHY/MAC Layers

Cognitive radio networks can use either of the two conventional duplexing techniques, namely Frequency Division Duplex (FDD) and Time Division Duplex (TDD). The topic has been dealt with in deliverables [D6.1] [D6.2]. However, in the most challenging context, opportunistic unsynchronized networks, where spectrum sensing and allocation are critical, the fact that FDD requires two allocations while TDD requires only one is a clear advantage for TDD. Thus, the issue of burst transmission with FBMC is worth reviewing and the first part of this section is dedicated to this issue. In the second part of this section, resource management is considered, recalling the results given in [D8.1] for downlink and introducing uplink. The third part of this section deals with the role that the MAC layers can play in power control, when cooperation is considered.

5.1 Time Division Duplex in Cognitive Radio

In the TDD mode, data are transmitted in bursts which alternate for downlink and uplink in the same channel. Then, the impulse response of the prototype filter imposes transition phases at the beginning and at the end of each burst, which increase the length of the burst of the emitted signal, as shown in Figure 5.1, for overlapping factor $K = 4$ and number of sub-channels $M = 256$.

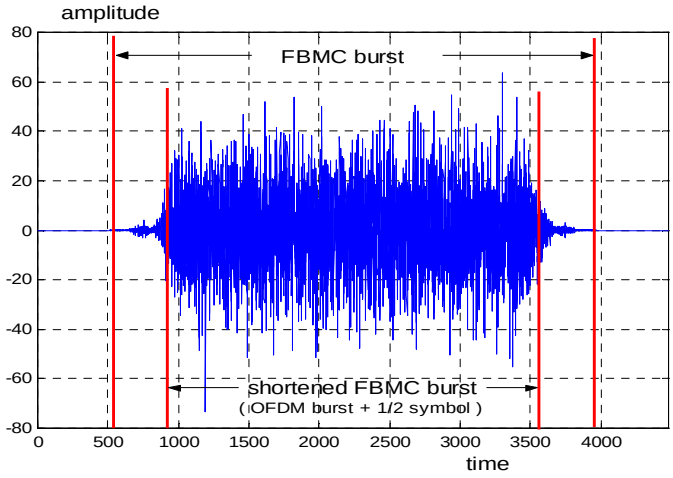

Figure.5.1: Transmitted FBMC burst

Specifically, if N_s symbols have to be transmitted, if the duration of a symbol is T, then the length of the burst is $(N_s + K - 1) \cdot T$. In addition, with OQAM modulation, considering that real and imaginary parts alternate and are shifted by half a symbol duration, the quantity $T/2$ must be added, which leads to the total burst length B_L expressed by

$$B_L = (N_s + K - \frac{1}{2}) \cdot T . \qquad (5.1)$$

With OFDM, the length of the burst would be $N_s T$ and, therefore, at first glance, the penalty of using FBMC is $(K - \frac{1}{2}) \cdot T$. However, looking at Figure 5.1, it is obvious that significant parts of the transitions may be cut with minor effect. Then, the impulse response of the system consisting of

a truncated filter impulse response at the transmitter and the full filter impulse response at the receiver must be analyzed. In the sub-channels, only the terms which are simultaneous to the reference and those coming after, the post-cursors, must be taken into account. This analysis reveals that only the reference symbol and the symbol next to the reference are significantly impacted by the burst cut. The magnitudes of the interfering signals in the neighbouring sub-channels, simultaneous to the reference pulse, when the first 384 coefficients (1.5 symbols) of the filter impulse response are cut, are shown in Figure 5.2. The decrease with the distance to the reference sub-channel is worth pointing out and the maximum interference level is –37 dB. Note that the figure represents the spectral temporary leakage.

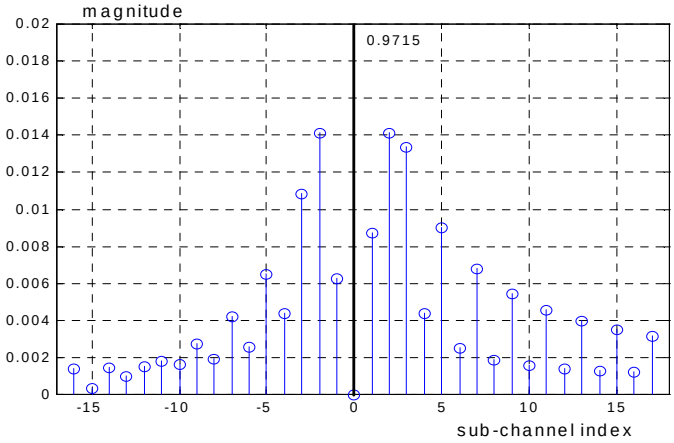

Figure 5.2: Interference in neighbouring sub-channels for shortened transmitter filter

Now, different cuts are considered and the results are given in Table 5.1.

Table 5.1: Impact of burst cuts on the first and last symbols

Number of coefficient cut		256	320	384	448
SNR (dB)	S1/1	47	47	27	13
	S1/2	65	59	38	33
	S2/1	65	65	63	37

For example, when the first 384 samples of the burst are cut, the Signal-to-Interference Ratio (SIR) is 27 dB for the first half of the first OQAM symbol, S1/1, it is 38 dB for the second half, S1/2, and it is 63 dB for the first half of the second symbol S2/1. The consequence is that, if the OQAM constellation has the size 256 for example, i.e. the first and the second half of a symbol carry 4 bits each, the first half of the first symbol has to be limited to 3 or 2 bits, while the second half and the subsequent symbols may carry the full load. The same reasoning applies to the last symbol in the burst, when the last 384 samples of the burst are deleted.

From Table 5.1, it appears that no reduction in bit loading is required for cuts of 320 and 256 samples (1 symbol), while a cut of 448 samples leads to the loss of half an OQAM symbol. Therefore, among the proposed cuts, the most efficient cut is 384 samples, which yields an increase in burst length of $T/2$, half a symbol duration, with respect to OFDM and it is illustrated in Figure 5.1.

In the TDD access mode of OFDM systems, the frames are divided into sub-frames for downlink and uplink and guard intervals are introduced for the transitions, the so-called Transmit-receive Transition Gap (TTG) and Receive-transmit Transition Gap (RTG). The sizes of these gaps are generally smaller than the duration of a symbol.

In an FBMC system, assuming filtering with overlapping factor $K = 4$ and the truncation of the bursts by 1.5 symbol length (384 samples) at the beginning and the end, the total length of each burst is increased by $T/2$, which implies that the TDD frame is expanded by T, the duration of a symbol. In the comparison of the efficiencies of the OFDM and FBMC systems, this quantity has to be subtracted from the gains due to the absence of cyclic prefix.

In radio systems, the bursts often include a preamble at the beginning, which is used for time and frequency alignment and for measuring the channel characteristics, in order to optimize the performance. An example of such a burst structure is shown in Figure 5.3, where the preamble consists of two identical symbols, followed by N_s data symbols. Since the preamble signal samples are exploited for measurements, no overlapping with other signals is generally permitted. In the FBMC context, this means that a transition must be introduced between the preamble and the data, to allow for the preamble signal to vanish and the data signal to raise, as sketched in Figure 5.3.

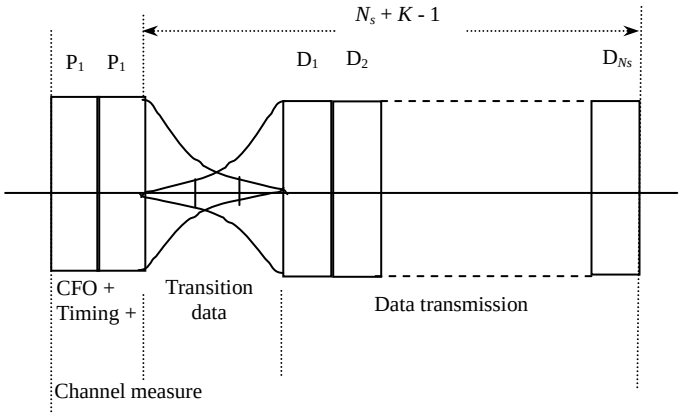

Figure 5.3: Structure of the packet and preamble-data transition

The principle of filter impulse response shortening can be applied to the preamble case, in a straightforward manner. First, the preamble signals are exploited independently of the data transmission constraints, by separate operations and devices. Then, the beginning of the data section in the burst can be cut as described above and with the same effect, namely the bit loading of the first data symbol has to be reduced. Therefore, the impact of FBMC in the presence of a preamble is again an increase of burst length of $T/2$.

In conclusion, in an opportunistic network exploiting TDD, the penalty incurred by FBMC with respect to OFDM due to the burst edges is half a multicarrier symbol and, if a preamble is included, it is one symbol.

5.2 Resource Management in downlink and uplink-OFDM/FBMC comparison

This work, is a continuation of the work on downlink presented in D8.1, under section 6. It describes an efficient resource allocation algorithm in uplink/downlink OFDM/FBMC based CR systems. The objective is to maximize the total CR data rate while limiting the interference introduced to the primary system. The proposed resource allocation is divided into two phases. The assignment of subcarriers to users is performed first and then the power is allocated to the different subcarriers. For downlink case, the subcarriers are allocated to the user with the highest SNR. However, for uplink case, the scheme for subcarrier to user assignment proposed in [Kim05] for non-cognitive systems are adopted in order to be suitable for cognitive ones. Subcarriers are allocated based on the channel quality, amount of interference imposed to the primary bands, instantaneous rate achieved by every user and the increment in the total data rate. For the power allocation phase, an efficient power allocation algorithm is proposed to distribute the powers among the subcarriers under the power and interference constraints. Moreover, the efficiency of using FBMC in CR systems is investigated and compared to OFDM based CR systems.
The contents of section 6 of D8.1 about downlink is recalled for convenience, with some additional results. The subsections are organized as follows. Section 5.2.1 introduces the system model while Section 5.2.2 formulates the problem. The resource allocation schemes are discussed for uplink and downlink in Section 5.2.3. Finally, the section is concluded.

5.2.1 System Model

The scenario in which the primary and cognitive systems co-exist in the same geographical location is assumed as described in Figure 5.4.

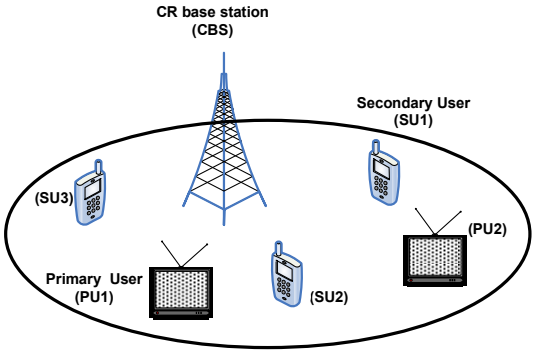

Figure 5.4: Cognitive Radio Network

In the downlink case, the Cognitive Base Station (CBS) transmits to its SUs and causes interference to the PUs. Moreover, the PU's base station interferes with the SU's.

For the uplink case, SUs are opportunistically accessing the unused primary system's spectrum bands to transmit to their CBS without causing harmful interference to PUs. The CR system's frequency spectrum is divided into N subcarriers each having a Δf bandwidth. The side by side frequency distribution of the PUs and SUs will be assumed (see Figure 5.5).

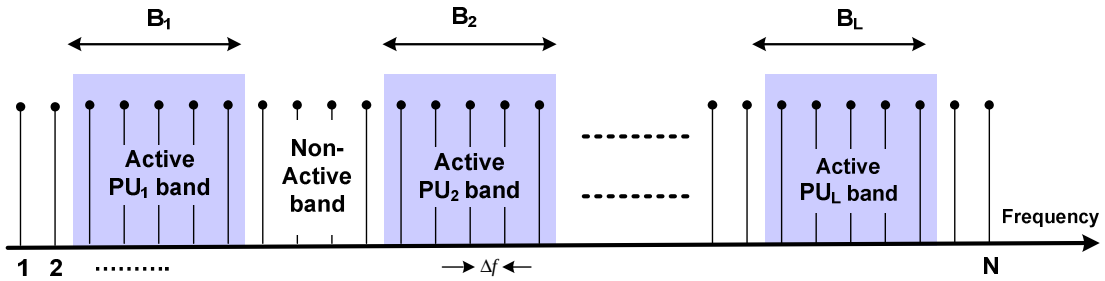

Figure 5.5: Frequency distribution of the active and non-active primary bands

The frequency bands B_1, $B_2, \cdots, B_L$ has been occupied by the PUs (active PU bands) while the other bands represent the non-active PU bands. . There is no synchronization between the primary and CR systems, and hence the transmission of the CR system will cause interference to the PUs due to side-lobes of its filter frequency response. The interference caused by the CR system to the l^{th} PU band should not exceed the predefined interference temperature limit I_{th}^{l}. The same maximum interference constraint can be found in [Ban08][Zha09-4][Has09][Sha10] and [Zha10-1].

The interference introduced by the transmission of the i^{th} subcarrier of the CR system to l^{th} PU band, $I_i^l\left(d_i^l, P_i\right)$, is the integration of the Power Spectrum Density (PSD) of the i^{th} subcarrier across the l^{th} PU band, B_l. If an ideal Nyquist pulse is assumed, the mutual interference can be expressed as [Wei04]

$$I_i^l\left(d_i^l, P_i\right) = P_i \Omega_i^l; \quad \Omega_i^l = \int_{d_i^l - B_l/2}^{d_i^l + B_l/2} \left|g_i^l\right|^2 \Phi_i\left(f\right) df \tag{5.2}$$

where Φ_i is the PSD of the i^{th} subcarrier which depends on the used multicarrier technique and d_i^l is the spectral distance between the i^{th} subcarrier and the l^{th} PU band. g_i^l denotes the channel gain between the i^{th} subcarrier and the l^{th} PU band while P_i is the total transmit power emitted by the i^{th} subcarrier. $T_s = 1/\Delta f$ is the symbol duration and Ω_i^l denotes the interference factor of the i^{th} subcarrier to the l^{th} PU band. By the same way, the interference power introduced by the l^{th} PU signal into the band of the i^{th} subcarrier is [Wei04]

$$J_i^l = \int_{d_i^l - \Delta f/2}^{d_i^l + \Delta f/2} \left|y_i^l\right|^2 \psi_l\left(e^{j\omega}\right) d\omega \tag{5.3}$$

where $\psi_l\left(e^{j\omega}\right)$ is the power spectrum density of the l^{th} PU signal and y_i^l is the channel gain between the i^{th} subcarrier and l^{th} PU signal. The OFDM and FBMC PSD's are described in the following subsections.

5.2.1.1 OFDM System and its PSD Model

The OFDM symbol is formed by taking the Inverse Discrete Fourier Transform (IDFT) to a set of complex input symbols $\{X_k\}$ and adding a cyclic prefix. The block diagram of the OFDM system is depicted in Figure 5.6.

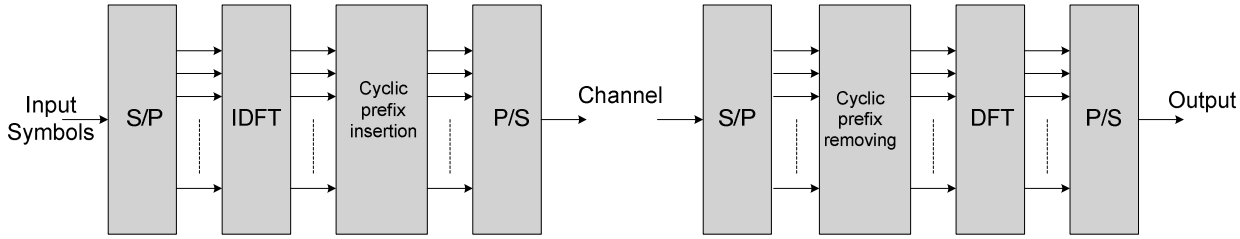

Figure 5.6: OFDM system block diagram

This is can be written mathematically as

$$x(n) = \sum_{k}\sum_{w\in Z} X_{k,w} g_T(n - wT) e^{j2\pi(n-wT-C)k/N} \tag{5.4}$$

where $\{k\}$ is the set of data subcarrier indices and is a subset of the set $\{0,1,\cdots,N-1\}$, N is the IDFT size, C is the length of the cyclic prefix in number of samples, $T = C + N$ is the length of the OFDM symbol in number of samples, and w denotes the w^{th} OFDM symbol index.

Following the derivation of the PSD for general baseband signal given in [Pro02], it can be shown that the OFDM PSD is:

$$\Phi_{OFDM}(f) = \frac{\sigma_x^2}{T}\sum_{k}\left|G_T\left(f - \frac{k}{N}\right)\right|^2 \tag{5.5}$$

where $G_T(f)$ is the Fourier transform of $g_T(n)$, and σ_{x^2} is the variance of the zero mean (symmetrical constellation) and uncorrelated input symbols. The assumption of the uncorrelated input symbols can be justified because of coding and interleaving in practical symbols [Bal07]. $g_T(n)$ can be chosen as

$$g_T(n) = \begin{cases} 1 & n = 0,1,\cdots,T-1 \\ 0 & \text{otherwise} \end{cases} \tag{5.6}$$

and hence its Fourier transform is

$$\left|G_T(f)\right|^2 = T + 2\sum_{r=1}^{T-1}(T-r)\cos(2\pi fm). \tag{5.7}$$

5.2.1.2 FBMC System and its PSD Model

Each subcarrier in FBMC system is modulated with a staggered QAM (offset QAM) [Bal07]. The basic idea is to transmit real-valued symbols instead of transmitting complex valued ones. Due to this time staggering of the in-phase and quadrature components of the symbols, orthogonality is achieved between adjacent subcarriers. The modulator and the demodulator are implemented using the synthesis and analysis filter banks. The filters in the synthesis and analysis filter bank are obtained by frequency shifts of a single prototype filter. Figure 5.7 depicts the structure of the synthesis and analysis filter bank at the transmitter and receiver in FBMC based multicarrier systems.

The FBMC signal can be written mathematically as [Skr06],

$$x(n) = \sum_{k}\sum_{w\in Z} a_{k,w} h(n - w\tau_o) e^{j2\pi\frac{k}{N}n} e^{j\phi_{k,w}} \tag{5.8}$$

where $\{k\}$ is the set of subcarrier indices, h is the pulse shape, $\phi_{k,w}$ is an additional phase term and τ_o is FBMC symbol duration. $a_{k,w}$ are the real symbols obtained from the complex QAM symbols having a zero mean and variance σ_x^2 . Hence the symbols have a zero mean and finite variance $\sigma_r^2 = \frac{\sigma_x^2}{2}$. The PSD of the FBMC can be expressed by [Skr06]:

$$\Phi_{FBMC} = \frac{\sigma_r^2}{\tau_\circ} \sum_{k} \left| H\left(f - \frac{k}{N} \right) \right|^2 \tag{5.9}$$

where $H(f)$ is the frequency response of the prototype filter with coefficients $h[n]$ with $n = 0, \cdots, W-1$, where $W = KN$ and K is the length of each polyphase components (overlapping factor). Assuming that the prototype coefficients have even symmetry around the $\left(\frac{KN}{2}\right)^{th}$ coefficient, and the first coefficient is zero [Bal07], we get

$$\left|H(f)\right| = h[W/2] + 2\sum_{i=1}^{\frac{W}{2}-i} h\left[(W/2) - i\right] \cos(2\pi fi). \tag{5.10}$$

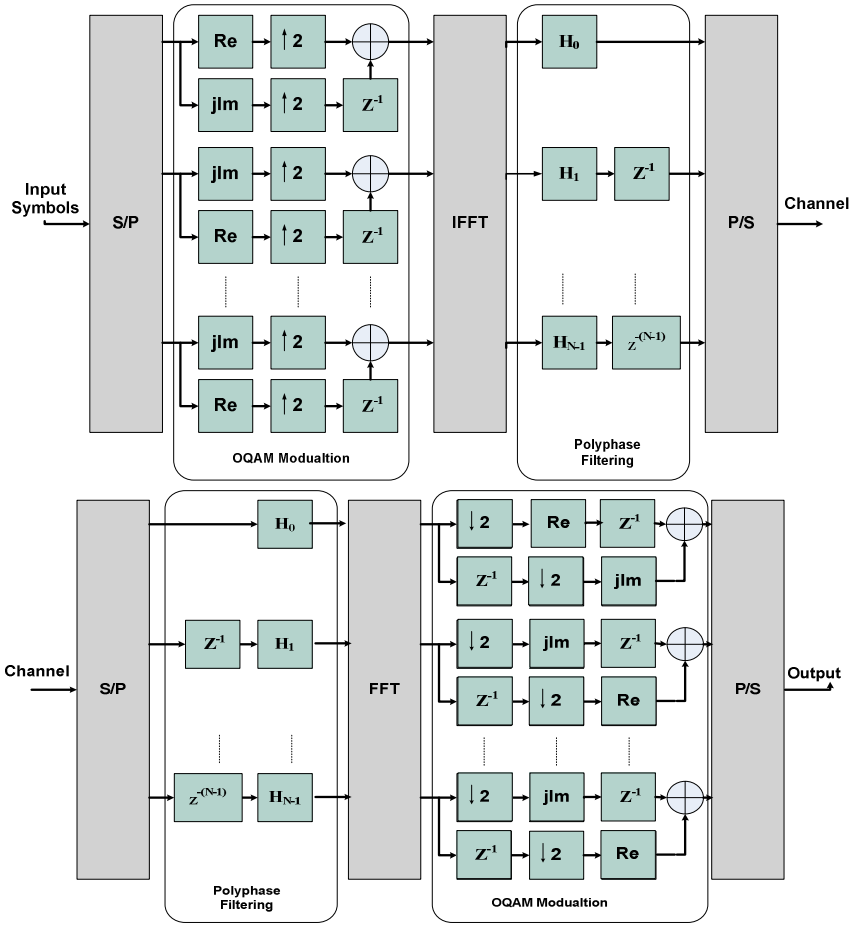

Figure 5.7: FBMC system's transmitter and receiver

To make a parallel between OFDM and FBMC, we place ourselves in the situation where both systems transmit the same quantity of information. This is the case if they have the same number of subcarriers N together with duration of τ_o samples for FBMC real data and $T = 2\tau_o$ for the complex QAM ones [Bal07] [Skr06].

From the relations above we can notice that the PSDs of OFDM and FBMC are the summation of the spectra of the individual subcarriers. Using the PHYDYAS prototype filter [PHY], Figure 5.8 plots single subcarrier power spectral densities of the OFDM and FBMC systems.

It can be noted that the FBMC system has very small side lobes with comparison to that of the OFDM system.

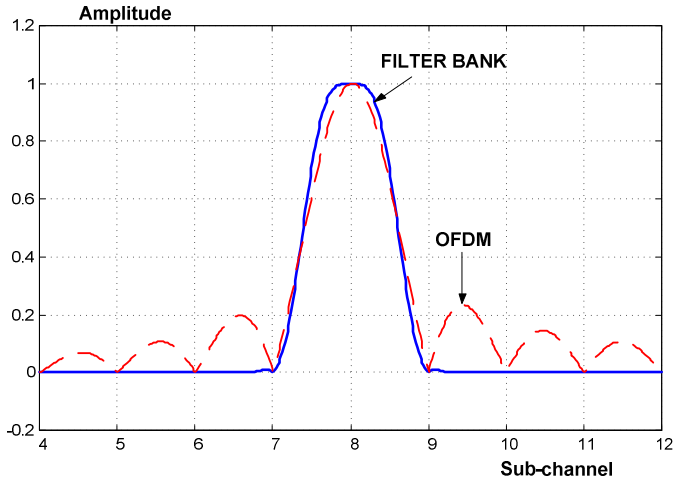

Figure 5.8: Single subcarrier PSD's of the OFDM and FBMC systems

5.2.2 Problem Formulation

The transmission rate for the i^{th} subcarrier, R_i can be evaluated as

$$R_i\left(P_{i,m}, h_{i,m}\right) = \Delta f \log_2\left(1+\frac{P_{i,m}\left|h_{i,m}\right|^2}{\sigma_i^2}\right) \tag{5.11}$$

where $P_{i,m}$ is the transmission power and $h_{i,m}$ is the i^{th} subcarrier fading gain from the m^{th} SU to the CBS. $\sigma_i^2 = \sigma_{AWGN}^2 + \sum_{l=1}^{L} J_i^l$ where σ_{AWGN}^2 is the variance of the additive white Gaussian noise (AWGN) and J_i^l is the interference introduced by the l^{th} PU band into the i^{th} subcarrier which is evaluated using (5.3) and can be modelled as AWGN as described in [Ban08]. Throughout this paper, all the instantaneous fading gains are assumed to be perfectly known at the CBS. The channel gains between the SUs and the CBS can be obtained practically by the classical channel estimation techniques while the channel gains between the SUs and the PUs can be obtained by estimating the received signal power from each primary terminal when it transmits, under the assumptions of pre-knowledge on the primary transmit power levels and the channel reciprocity [Zha09-2][Zha08-3]. Based on the channel gains, the CBS assigns the subcarriers and powers to each SU through a reliable low-rate signalling channel.

Let $v_{i,m}$ to be a subcarrier allocation indicator, i.e. $v_{i,m} = 1$ if and only if the subcarrier is allocated to m^{th} user. It is assumed that each subcarrier can be used for transmission to at most one user at any given time. Our objective is to maximize the total capacity of the CR system subject to the instantaneous interference introduced to the PUs and total transmit power constraint in downlink and per user power constraints in uplink. Therefore, the optimization problem in downlink case can be formulated as follows

$$P1: \max_{P_i} \sum_{m=1}^{M}\sum_{i=1}^{N} v_{i,m} R_i\left(P_i, h_{i,m}\right) \tag{5.12}$$

subject to

$$\upsilon_{i,m} \in \{0,1\}, \forall i,m \tag{5.13}$$

$$\sum_{m=1}^{M} \upsilon_{i,m} \leq 1, \forall i \tag{5.14}$$

$$\sum_{m=1}^{M}\sum_{i=1}^{N} \upsilon_{i,m} P_{i,m} \leq P_T \tag{5.15}$$

$$P_i \geq 0, \forall i \in \{1,2,\cdots,N\} \tag{5.16}$$

$$\sum_{m=1}^{M}\sum_{i=1}^{N} \upsilon_{i,m} P_i \Omega_i \leq I_{th}^{l}, \forall l \in \{1,2,\cdots,L\} \tag{5.17}$$

where N denotes the total number of subcarriers , M is the number of users, I_{th}^{l} denotes the interference threshold prescribed by the l^{th} PU and P_T is the total SU's power budget. Inequality (5.14) ensures that any given subcarrier can be allocated to at most one user.

For the uplink case, the total power constraint given in (5.15) should be rewritten to consider the per user power constraint as follows

$$\sum_{i=1}^{N} \upsilon_{i,m} P_{i,m} \leq \overline{P_m}; \forall m \tag{5.18}$$

where $\overline{P_m}$ is the m^{th} SU total power budget. The optimization problem $P1$ is a mixed optimization problem in which achieving the optimal solution needs high computational complexity. Additionally, the minimum rate constraints increase the complexity of the problem. In order to solve the problem, we propose an algorithm to perform the resource allocation in two phases. In the first phase, a heuristic sub-optimal algorithm is used to allocate the subcarriers to the different users. Afterwards, the optimal power allocation is evaluated in the second phase. The optimal power allocation algorithm requires high computational complexity and hence a low complexity power algorithm is proposed to perform the power allocation phase.

5.2.3 Resource Allocation in Multicarrier Based CR Networks

The schemes to solve the optimization problem presented in the previous section will be discussed in detail in this section. We will start reviewing the schemes described in the deliverable [D8.1] considering the downlink resources allocation. Afterwards, the uplink resource allocation will be discussed.

5.2.3.1 Resource Allocation in Downlink (Review of the Work Presented in [D8.1])

The optimization problem $P1$ in (5.12) is a combinatorial optimization problem and its complexity grows exponentially with the input size. In order to reduce the computational complexity, the problem is solved in two steps by many of the suboptimal algorithms

[Jan03][Kiv03][She03][Won99]. In the first step, the subcarriers are assigned to the users and then the power is allocated for these subcarriers in the second step. Once the subcarriers are allocated to the users, the multiuser system can be viewed virtually as a single user multicarrier system.

5.2.3.1.1 Subcarriers to Users Allocation in Downlink

As proofed in [Jan03], the maximum data rate in downlink can be obtained if the subcarriers are assigned to the user who has the best channel gain for that subcarrier as described in Algorithm 1.

Algorithm 1 Subcarriers to User Allocation in Downlink

Initialization:
Set $\upsilon_{i,m} = 0 \; \forall i, m$

Subcarrier Allocation:
for $i = 1$ to N **do**

$$m^* = \arg\max_m \{h_{i,m}\}; \; \upsilon_{i,m^*} = 1$$

end for

By applying the Algorithm 1, the values of the channel indicators $\upsilon_{i,m}$ are determined and hence for notation simplicity, single user notation can be used. The different channel gains can be determined form the subcarrier allocation step as follow

$$h_i = \sum_{m=1}^{M} \sum_{i=1}^{N} \upsilon_{i,m} h_{i,m} \tag{5.19}$$

and hence problem $P1$ can be reformulated as follow

$$P2: \quad \max_{P_i} \sum_{i=1}^{N} \log_2 \left(1 + \frac{P_i |h_i|^2}{\sigma^2} \right) \tag{5.20}$$

subject to

$$\sum_{i=1}^{N} P_i \Omega_i \le I_{th}^l \qquad \forall l \in \{1, 2, \cdots, L\} \tag{5.21}$$

$$\sum_{i=1}^{N} P_i \le P_T \tag{5.22}$$

$$P_i \ge 0 \qquad \forall i \in \{1, 2, \cdots, N\}. \tag{5.23}$$

5.2.3.1.2 Subcarriers Power Loading (Optimal Solution)

The problem $P2$ in (5.20) is a convex optimization problem. Solving for the optimal solution (see [D8.1] for the derivation), we can get

$$P_i^* = \left[\frac{1}{\sum_{l=1}^{L} \alpha_l \Omega_i + \beta} - \frac{\sigma^2}{|h_i|^2} \right]^+ \tag{5.24}$$

where $[x]^+ = \max(0, x)$. α_l and β are the non-negative Lagrange multipliers. Solving for $L+1$ Lagrangian multipliers is computational complex. These multipliers can be found numerically using ellipsoid or interior point method with a complexity $\mathrm{O}\left(N^3\right)$ [Boy04]. In what follows we will propose a low complexity algorithm that achieve near optimal performance.

5.2.3.1.3 Proposed Sub-optimal Downlink Power Allocation Algorithm

The optimal solution for the optimization problem has a high computational complexity which makes it unsuitable for the practical applications. A low complexity algorithm is proposed in [Zha08-2]. The subcarriers nulling and deactivating throughout this algorithm degrades the system capacity and causing the algorithm to have a limited performance in low interference constraints. To overcome the drawbacks of this algorithm, a low complexity power allocation algorithm will be presented.

As described in [Wei04], most of the interference introduced to the PU bands is induced by the cognitive transmission in the subcarriers where the PU is active as well as the subcarriers that are directly adjacent to the PU bands. More restrictive way with dealing with the interference constraint will be described later for the uplink case. Considering this fact, it can be assumed that each subcarrier is belonging to the closet PU band and only introducing interference to it, then the optimization problem $P2$ can be reformulated as follow

$$P3: \quad \max_{P_i^{'}} \sum_{i=1}^{N} \log_2 \left(1 + \frac{P_i^{'} |h_i|^2}{\sigma^2} \right) \tag{5.25}$$

subject to

$$\sum_{i \in N_l} P_i^{'} \Omega_i \le I_{th}^l \qquad \forall l \in \{1, 2, \cdots, L\} \tag{5.26}$$

$$\sum_{i=1}^{N} P_i^{'} \le P_T \tag{5.27}$$

$$P_i^{'} \ge 0 \qquad \forall i \in \{1, 2, \cdots, N\} \tag{5.28}$$

where N_l denotes the set of the subcarriers belong to the l^{th} PU band. Solving for the optimal we can get (see [D8.1] for the derivation)

$$P_i^{'} = \left[\frac{1}{\alpha_l^{'} \Omega_i + \beta'} - \frac{\sigma^2}{|h_i|^2} \right]^+ \tag{5.29}$$

where $\alpha_l^{'}$ and β' are the non-negative dual variables corresponding to the interference and power constraints respectively. The solution of the problem is still has high computational complexity which encourage us to find a faster and efficient power allocation algorithm.

If the interference constrains are ignored in $P3$, the solution of the problem will follow the well known waterfilling interpretation [Lek97],

$$P_i^{'(P_T)} = \left[\lambda - \frac{\sigma^2}{|h_i|^2} \right]^+ \tag{5.30}$$

where λ is the waterfilling level. On the other side, if the total power constraint is ignored, the Lagrangian of the problem can be written as

$$\mathrm{G}^{(Int)} = -\sum_{i \in N_l} \log_2 \left(1 + \frac{P_i^{'(Int)} |h_i|^2}{\sigma^2} \right) + \alpha_l^{'(Int)} \left(\sum_{i \in N_l} P_i^{'(Int)} \Omega_i - I_{th}^l \right) \tag{5.31}$$

where $\alpha_l^{'}$ is the Lagrange multiplier. Equating $\frac{\partial \mathrm{G}^{(\mathrm{Int})}}{\partial P_i^{'(Int)}}$ to zero, we get

$$P_i^{'(Int)} = \left[\frac{1}{\alpha_l^{'(Int)} \Omega_i} - \frac{\sigma^2}{|h_i|^2} \right]^+ \tag{5.32}$$

where the value of $\alpha_l^{'}$ can be calculated by substituting (5.32) into $\sum_{i \in N_l} P_i^{'(Int)} \Omega_i = I_{th}^l$ to get

$$\alpha_l^{'(Int)} = \frac{|N_l|}{I_{th}^l + \sum_{i \in N_l} \frac{\Omega_i \sigma^2}{|h_i|^2}} \tag{5.33}$$

It is obvious that if the summation of the allocated power under only the interference constraints is lower than or equal the available total power budget, i.e. $\sum_{i=1}^{N} P_i^{'(Int)} \le P_T, \forall i \in \{1, 2, \cdots, N\}$, then (5.25)-(5.28) will be the optimal solution for the optimization problem $P3$. In most of the cases, the total power budget is quite lower than this summation and hence the Power Interference (PI) constrained algorithm, referred to as *PI-Algorithm*, is proposed to allocate the power under the both the total power and interference constraints.

In order to solve the optimization problem $P3$, we can start by assuming that the maximum power that can be allocated for a given subcarrier P_i^{Max} is determined according to the interference constraints only by using (5.25)-(5.28) for every set of subcarriers $N_l, \forall l \in \{1, 2, \cdots, L\}$. By such an assumption, we can guarantee that the interference introduced to PU bands will be under the pre-specified thresholds. Once the maximum power P_i^{Max}, the total power constraint is tested. If the

total power constraint is satisfied, then the solution has been found and equal to the maximum power that can be allocated to each subcarrier, i.e. $P_i^{'} = P_i^{Max}$. Otherwise, the available power budget should be distributed among the subcarriers giving that the power allocated to each subcarrier is lower than or equal to the maximum power that can be allocated to each subcarrier P_i^{Max} and hence the following problem should be solved

$$P4: \quad \max_{P_i^{W.F}} \sum_{i=1}^{N} \log_2\left(1+\frac{P_i^{W.F}\left|h_i\right|^2}{\sigma^2}\right) \tag{5.34}$$

subject to

$$\sum_{i=1}^{N} P_i^{W.F} \le P_T \tag{5.35}$$

$$0 \le P_i^{W.F} \le P_i^{Max} \tag{5.36}$$

The problem $P4$ is called *"cap-limited"* waterfilling [Pap08] [Zha10-2]. The problem can solved efficiently using the concept of the conventional waterfilling. Given the initial waterfilling solution, the channels that violate the maximum power P_i^{Max} are determined and upper bounded with P_i^{Max}. The total power budget is reduced by subtracting the power assigned so far. At the next step, the algorithm proceeds to successive waterfilling over the subcarriers that not violated the maximum power P_i^{Max} in the last step. These procedures are repeated until the allocated power $P_i^{W.F}$ doesn't violate the maximum power P_i^{Max} in any of the subcarriers in the new iteration. The *"cap-limited"* waterfilling algorithm implementation is described in Algorithm 2.

Algorithm 2 Cap-Limited Waterfilling

1. ***Initialize*** $\mathrm{F} = \mathrm{M} = \mathrm{N} = \{1,2,\cdots,N\}$, $\bar{P}_i = P_i^{Max}$, and $S = P_T$.
2. Sort $\left\{T_i = \frac{\sigma^2}{\left|h_i\right|^2}, i \in \mathrm{N}\right\}$ in decreasing order with J being the sorted index. Find the waterfilling λ as follows:
   (a) $T_{sum} = \sum_{i\in\mathrm{N}} T_i$, $\lambda = \left(T_{sum} + S\right)/\left|\mathrm{N}\right|$, $n = 1$.
   (b) **while** $T_{J(n)} > \lambda$ **do**
   $T_{sum} = T_{sum} - T_{J(n)}$, $\mathrm{N} = \mathrm{N} \setminus \left\{J\left(n\right)\right\}$, $\lambda = \left(T_{sum} + S\right)/\left|\mathrm{N}\right|$, $n = n+1$
   end while
   (c) Set $P_i^{W.F} = \left[\lambda - T_i\right]^+, \forall i \in \mathrm{F}$
3. **repeat**
   if $P_i^{W.F} \ge \bar{P}_i$
   Let $P_i^{W.F} = \bar{P}_i$, $S = S - P_i^{W.F}$, $\mathrm{M} = \mathrm{M} \setminus \{i\}$, $\mathrm{N} = \mathrm{M}$, and go to step 2;
   end if
   until $P_i^{W.F} \le \bar{P}_i, \forall i \in \mathrm{F}$

The solution $P_i^{W.F}$ of the problem $P4$ is satisfying the total power constraint of the problem $P3$ with equality which is not the case for the different interference constraints I_{th}^l. Since it's assumed that $P_i^{W.F} \le P_i^{Max}$, some of the powers allocated to subcarriers will not reach the maximum allowable values which will make the interference introduced to the PU bands below the thresholds I_{th}^l. In order to use all the allowable interference values, the values of the maximum power that can be allocated to each subcarrier P_i^{Max} should be updated depending on the left available interference. The left available interference can be determined as follow

$$I_{Left}^l = I_{th}^l - \sum_{i \in N_l} P_i^{W.F} \Omega_i \tag{5.37}$$

Assuming that $A_l \subset N_l$ is the set of the subcarriers that reach its maximum, i.e. $P_i^{W.F} = P_i^{Max}, \forall i \in A_l$, then, $P_i^{Max}, \forall i \in A_l$ can be updated by applying the equations (5.38)-(5.39) on the subcarriers in the set A_l with the following interference constraints

$$I_{th}^{'l} = I_{Left}^l + \sum_{i \in A_l} P_i^{W.F} \Omega_i \tag{5.38}$$

After determining the updated values of P_i^{Max}, the *"cap-limited"* waterfilling is performed again to find the final solution $P_i^{'} = P_i^{W.F}$. Now, the solution $P_i^{'}$ is satisfying approximately the interference constraints with equality as well as guaranteeing that the total power used is equal to P_T. A graphical description of the *PI-Algorithm* is given in Figure 5.9 while the implementation procedures are described in Algorithm 3.

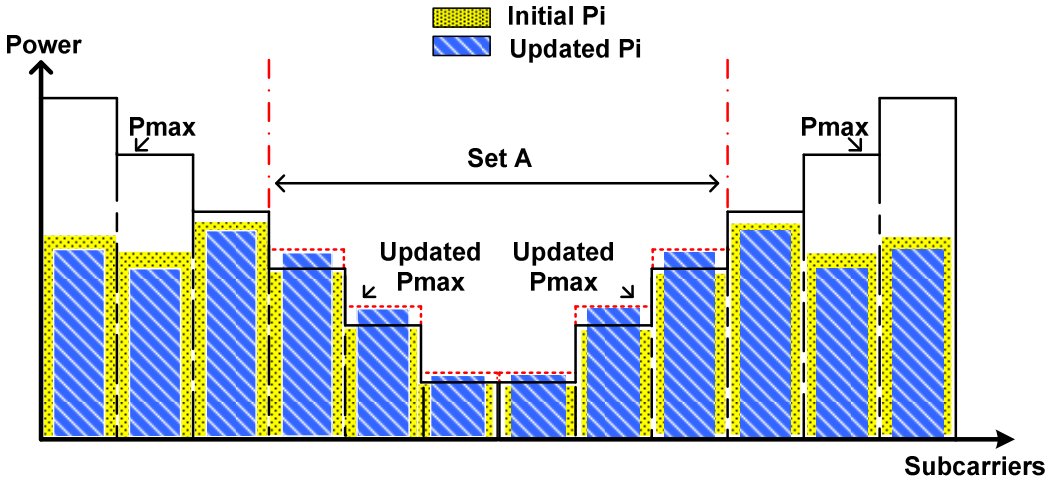

Figure 5.9: An Example of the SUs allocated power using PI-Algorithm

Algorithm 3 PI-Algorithm

1. **Initialize** $\mathrm{N} = \{1, 2, \cdots, N\}$, $\mathrm{N}_l = N_l$, $I_{Left}^l = 0$, $S = P_T$ and $\mathrm{A}_l = \varnothing$.

2. $\forall l \in \{1,2,\cdots,L\}$, sort $\left\{ H_i = \frac{\sigma^2}{|h_i|^2}\Omega_i, i \in \mathrm{N}_l \right\}$ in decreasing order with k being the sorted index. Find the P_i^{Max} as follows:

(a) $H_{sum} = \sum_{i\in \mathrm{N}_l} H_i$, $\alpha_l^{'(Int)} = |\mathrm{N}_l| / \left(I_{th}^l + H_{sum} \right)$, $n = 1$.

(b) **while** $\alpha_l^{'(Int)} > H_{k(n)}^{-1}$ **do**

$$H_{sum} = H_{sum} - H_{k(n)},\ \mathrm{N}_l = \mathrm{N}_l \setminus \{k(n)\},\ \alpha_l^{'(Int)} = |\mathrm{N}_l| / \left(I_{th}^l + H_{sum} \right),\ n = n+1$$

end while

(c) Set $P_i^{Max} = \left[\frac{1}{\alpha_l^{'(Int)}\Omega_i} - \frac{\sigma^2}{|h_i|^2} \right]^+$

3. **if** $\sum_{i\in \mathrm{N}} P_i^{Max} \le P_T$

Let $P_i^{'} = P_i^{Max}$ and stop the algorithm.

end if

4. Execute the *"cap-limited"* waterfilling (Algorithm 2) and find the set $\mathrm{A}_l \subset N_l$ where $P_i^{W.F} = P_i^{Max}$.

5. Evaluate $I_{Left}^l = I_{th}^l - \sum_{i\in N_l} P_i^{W.F}\Omega_i$ and set $\mathrm{N}_l = \mathrm{A}_l$, $I_{th}^l = I_{Left}^l + \sum_{i\in \mathrm{A}_l} P_i^{W.F}\Omega_i$ and apply again only step 2 to update P_i^{Max}.

6. Execute the *"cap-limited"* waterfilling (Algorithm 2) and set $P_i^{'} = P_i^{W.F}$.

The computational complexity of Step 2 in the proposed PI-Algorithm (Algorithm 3) is $\sum_{l=1}^{L} \mathrm{O}\left(|N_l| \log |N_l| \right) \le \mathrm{O}\left(N \log N \right)$. Steps 4 and 6 of the algorithm execute the *"cap-limited"* waterfilling which has a complexity of $\mathrm{O}(N) \le \mathrm{O}(N \log N)$ [Che10]. Step 5 has a complexity of $\sum_{l=1}^{L} \mathrm{O}\left(|A_l| \log |A_l| \right) + \mathrm{O}(L) \le \mathrm{O}\left(N \log N \right) + \mathrm{O}(L)$. Hence, the overall complexity of the algorithm is lower than $\mathrm{O}\left(N \log N \right) + \mathrm{O}(L)$. Comparing to the computational complexity of the optimal solution, $\mathrm{O}\left(N^3 \right)$, the proposed algorithm has much lower computational complexity specially when the number of the subcarriers N increased.

5.2.3.1.4 Simulation Results for the Downlink Case

The simulation is performed under the scenario given in Figure 5.5. A multicarrier system of $M = 3$ cognitive users and $N = 32$ subcarriers is assumed. The value of T_s, Δf and P_T are assumed to be 4μ second, 0.3125 MHz and 1 watt respectively. Additive White Gaussian Noise (AWGN) of variance 10^{-6} is assumed. Without loss of generality, the interference induced by PUs to the SU's band is assumed to be negligible. The channel gains *h* and *g* are outcomes of independent, identically distributed (i.i.d.) Rayleigh distributed random variables (rv's) with mean equal to "1" and assumed to be perfectly known at the CBS. OFDM and FBMC based cognitive

radio systems are evaluated. The OFDM system is assumed to have a 6.67% of its symbol time as CP. For FBMC system, the prototype coefficients are assumed to be equal to PHYDYAS coefficients with overlapping factor $K = 4$ [PHY]. The optimal solution is implemented using the interior point method. We refer to the method proposed in [Zha08-2] by Zhang algorithm. All the results have been averaged over 1000 iterations.

Two interference constraints belonging to two active PU bands, i.e. $L = 2$, are assumed as given in Figure 5.10.

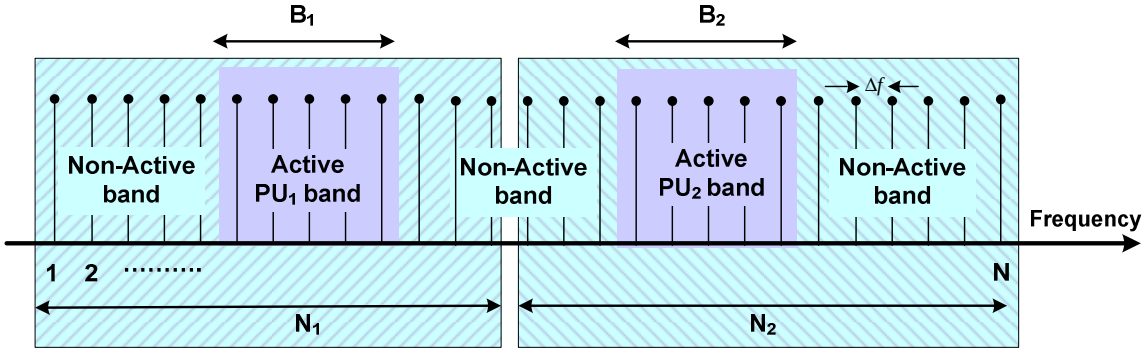

Figure 5.10: Frequency distribution with two active PU bands

Each active PU band is assumed to have six subcarriers where $|N_1| = |N_2| = 16$. The achieved capacity using optimal, PI and Zhang algorithms for different interference constraints where $I_{th}^1 = I_{th}^2$ is plotted in Figure 5.11.

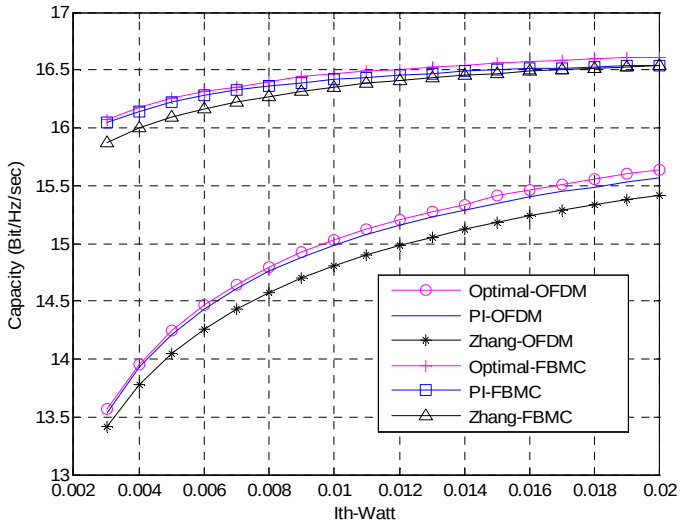

Figure 5.11: Achieved capacity vs. allowed interference threshold for OFDM and FBMC based CR systems - Two active PU bands

It can be noted that the proposed PI-algorithm approaches the optimal solution and outperforms Zhang algorithm. The effect of assuming that every subcarrier is belonging to the closest PU band and introducing interference to it only on the net interference introduced to the active PU bands is studied in Figure 5.12 and Figure 5.13 for PU_1 and PU_2 respectively.

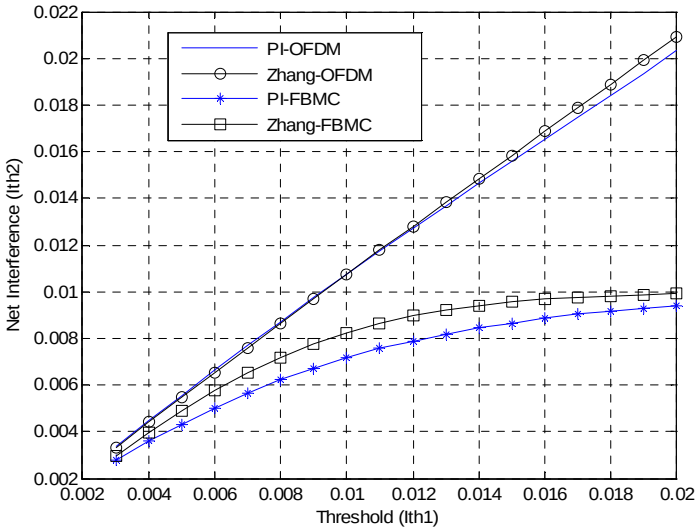

Figure 5.12: Total interference introduced to the PU_1 vs. interference threshold

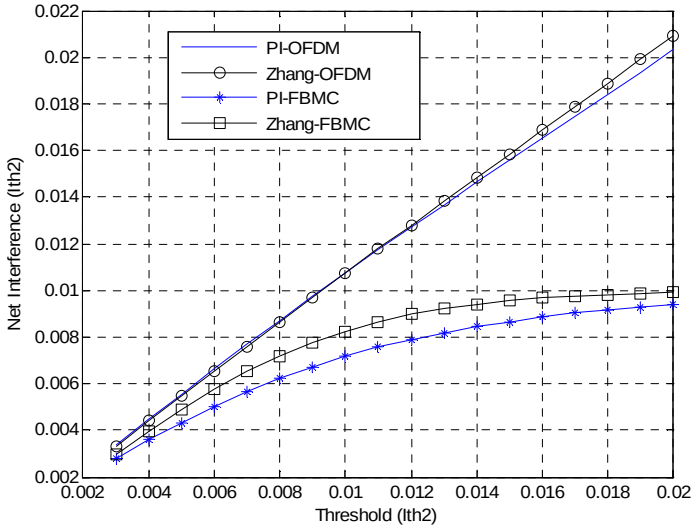

Figure 5.13: Total interference introduced to the PU_2 vs. interference threshold

It can be observed that the net interference induced using the PI-algorithm is approximately equal to the pre-specified thresholds which make the assumption reasonable. The achieved capacity of the different algorithms is plotted in Figure 5.14 with lower values of the interference constraints.

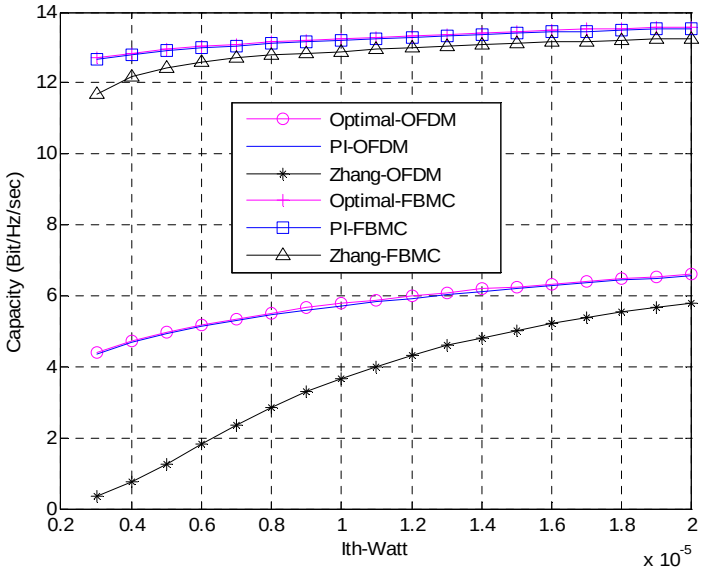

Figure 5.14: Achieved CR vs. allowed interference threshold (low) for OFDM and FBMC based CR systems - Two active bands

One can notice that Zhang algorithm has a limited performance with low interference constrains because the algorithm turns off the subcarriers that have a noise level more that the initial waterfilling level and never uses these subcarriers again even if the new waterfilling level exceeds its noise level. Moreover, the algorithm deactivates some subcarriers, i.e. transmit zero power, in order to ensure that the interference introduced to PU bands is below the pre-specified thresholds. The lower are the interference constraints, the more are the deactivated subcarriers which justify the limited performance of this algorithm in low interference constraints.

To show the efficiency of transmitting over the active PU bands as well as the non-active bands, Figure 5.15 and Figure 5.16 plot the achieved capacity using the PI algorithm with and without allowing the SUs to transmit over the PU active bands.

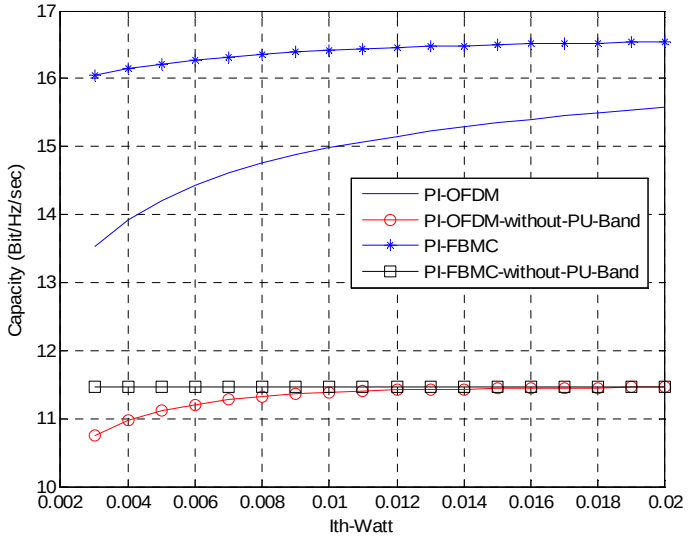

Figure 5.15: Achieved capacity vs. allowed interference threshold with and without transmitting over active bands- Two active PU bands

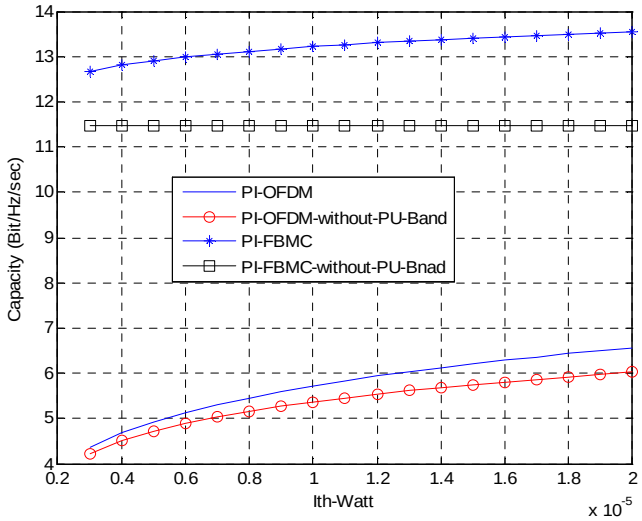

Figure 5.16: Achieved capacity vs. allowed interference threshold (low) with and without transmitting over active bands - Two active PU bands

The capacity of the CR system transmitting on both the active and non-active bands is more than that one transmitting only on the non-active band. Since the cognitive transmission in the active PU band introduces more interference to the PUs than the other subcarriers, low power levels can be used in these bands with low interferences constraints which justify why when the interference constraints decrease ,the difference between the two systems decreases.

For all the so far presented results, the capacity of FBMC based CR system is higher than that of OFDM based one because the sidelobes in FBMC's PSD is smaller than that in OFDM which introduce less interference to the PUs. Moreover, the inserted CP in OFDM based CR systems reduces the total capacity of the system. It can be noticed also that the interference condition introduce a small restriction on the capacity of FBMC based CR systems which is not the case in OFDM based CR systems. The significant increase in the capacity of FBMC based CR systems over the OFDM based ones recommends the FBMC as a candidate for the CR network applications. More simulation results can be found in [D8.1].

5.2.3.2 Resource Allocation in Uplink

As described in the previous section that the problem of resource allocation will be solved in two steps. In the first step, the subcarriers are allocated to the users and then powers are allocated to these subcarriers.

5.2.3.2.1 Subcarriers to Users Allocation in Uplink (Single PU Case)

The scheme of subcarrier allocation by which the subcarrier is allocated to the user with maximum SNR is not efficient in uplink case due to the per-user power constraints. In this section, a heuristic subcarrier and power allocation algorithm is presented. To better describe the proposed algorithm, only one PU band, i.e. single interference constraint, will be considered in this section. The solution will be generalized next to consider multiple interference constraints. We will refer to the single interference constraint by I_{th}^{l*} and hence, the interference constraint in the optimization problem $P1$ can be rewritten as follows

$$\sum_{m=1}^{M}\sum_{i=1}^{N}\nu_{i,m}P_{i,m}\Omega_{i,m}^{l*} \le I_{th}^{l*} \tag{5.39}$$

where $\Omega_{i,m}^{l*}$ denotes the interference factor of the i^{th} subcarrier to the PU band ($l*$) when the i^{th} subcarrier is allocated to m^{th} SU.

To achieve an efficient subcarrier allocation, the proposed algorithm should assign the subcarriers to the different SUs considering not only their channel quality and per-user power constraints but also the interference that will be induced to the PU band.

The scheme assumes that the interference introduced to the primary system, i.e. I_{th}^{l*}, is divided uniformly among the different subcarriers. Accordingly, the maximum amount of interference that can be introduced by any subcarrier is

$$I_{Uniform}^{l*} = \frac{I_{th}^{l*}}{N}. \tag{5.40}$$

By using (5.2), the maximum power, $P_{i,m}^{Uni}$, that can be allocated to the i^{th} subcarrier when it is allocated to the m^{th} SU is

$$P_{i,m}^{Uni} = \frac{I_{Uniform}^{l*}}{\Omega_{i,m}^{l*}}. \tag{5.41}$$

Let us define the following sets

- C: the set of unassigned subcarriers.
- A_m : the set that includes the subcarriers already allocated to the m^{th} user with powers equal to the maximum power $P_{i,m}^{Uni}$.
- B_m : the set that includes the subcarriers already allocated to the m^{th} user with powers equal to the average power. The average power means that the remaining power for the m^{th} user ($\overline{P_m} - \sum_{i\in \mathrm{A}_m} P_{i,m}^{Uni}$) is divided equally among the subcarriers in the set B_m.

According to the previous definition, the instantaneous rate of the m^{th} user is

$$R\left(m, \mathrm{A}_m, \mathrm{B}_m\right) = \sum_{i\in \mathrm{A}_m} R_i\left(P_{i,m}^{Uni}, h_{i,m}\right) + \sum_{i\in \mathrm{B}_m} R_i\left(\frac{\overline{P_m} - \sum_{x\in \mathrm{A}_m} P_{x,m}^{Uni}}{\left|\mathrm{B}_m\right|}, h_{i,m}\right) \tag{5.42}$$

where $R_i\left(P_{i,m}, h_{i,m}\right)$ is evaluated using (5.11) and $\left|\mathrm{B}_m\right|$ means the cardinality of the set B_m. Note that the allocated powers according either the maximum or average power are only used to simplify the calculation of the increment in the data rate. The optimal power allocation will be derived later based on the subcarrier allocation information.

The algorithm begins by allocation of the subcarriers that are located next to the PU band, i.e. subcarriers that have more interference to the PU, and moving towards the distant ones. The subcarriers are allocated sequentially to the users until all the subcarriers are assigned. Remark that the subcarriers that will introduce high interference to the PU bands should have a low transmitting power even that they have a good channel quality which will reduce the total data rate. Therefore, the limitation that will be introduced to any subcarrier assignment due the interference constraints should be considered and the subcarriers should be classified according to their interference to the PU band. The algorithm initially assigns the subcarrier to the set B_m and evaluates the new average power, P_{Test}. If the average power exceeds the maximum power, i.e. $P_{Test} \geq P_{i,m}^{Uni}$, then the subcarrier should be moved to the set A_m. Afterwards, the increments of the individual data rates due to the allocation of a particular subcarrier to different SUs are evaluated and the subcarrier is allocated to the SU with maximum data rate increment. The scheme is repeated until the allocation of all subcarriers. Note that the final set of allocated subcarriers to m^{th} SU is $\mathrm{N}_m = \mathrm{A}_m \cup \mathrm{B}_m$. The assigning procedures of a particular subcarrier $i^* \in \mathrm{C}$ are as follows

Algorithm 4 Subcarriers to User Allocation in Uplink

1. $\forall m$,

   Evaluate $P_{Test} = \dfrac{\overline{P_m} - \sum_{r \in \mathrm{A}_m} P_{r,m}^{Uni}}{|\mathrm{B}_m| + 1}$

   if $P_{Test} \geq P_{i^*,m}^{Uni}$

   let $\mathrm{A}_m^* = \mathrm{A}_m \cup \{i^*\}$ and $\mathrm{B}_m^* = \mathrm{B}_m$

   else let $\mathrm{B}_m^* = \mathrm{B}_m \cup \{i^*\}$ and $\mathrm{A}_m^* = \mathrm{A}_m$.

2. Compute the amount of increment Δ_m in the data rate when the subcarrier $\{i^*\}$ is assigned to m^{th} SU, i.e,

$$\Delta_m = R_m^{new} - R_m^{old} = R\left(m, \mathrm{A}_m^*, \mathrm{B}_m^*\right) - R\left(m, \mathrm{A}_m, \mathrm{B}_m\right)$$

where $R\left(m, \mathrm{A}_m^*, \mathrm{B}_m^*\right)$ and $R\left(m, \mathrm{A}_m, \mathrm{B}_m\right)$ are evaluated using (5.42).

3. Find m^* satisfying $m^* = \arg\max_m(\Delta_m)$, set $v_{i^*,m^*} = 1$, and update the sets $\mathrm{A}_{m^*} = \mathrm{A}_{m^*}^*$ and $\mathrm{B}_{m^*} = \mathrm{B}_{m^*}^*$.

4. Remove the subcarrier i^* form the set C and repeat the above procedures until the set C is empty.

5.2.3.2.2 Proposed Sub-optimal Uplink Power Allocation Algorithm (Single PU Case)

By the subcarrier to users assignment phase, the subcarriers are allocated to the different users with the consideration of the minimum rates constraints. Therefore, the values of the subcarrier indicators, i.e. $v_{i,m}$, are already known from the previous phase. The multiuser system can be viewed

virtually as a single user multicarrier system and the power allocation problem can be formulated as follows

$$\begin{aligned} P5: \quad & \max_{P_{i,m}} \sum_{i=1}^{N} R_i\left(P_{i,m}, h_{i,m}\right) \\ s.t. \quad & \sum_{i=1}^{N} P_{i,m}\Omega_{i,m}^{l^*} \le I_{th}^{l^*} \\ & \sum_{i\in \mathrm{N}_m} P_{i,m} \le \overline{P_m} \quad \forall m \\ & P_{i,m} \ge 0 \qquad \forall i \end{aligned} \tag{5.43}$$

where m in $P_{i,m}$, $h_{i,m}$ and $\Omega_{i,m}^{l^*}$ refers to the user who's already got the subcarrier i, i.e. $v_{i,m}=1$. N_m denotes the set of subcarriers allocated to the m^{th} SU. Remark that having too much power comparing to the interference constraint will lead to an interference-only optimization problem while having high interference constraint in relative with the total power will lead to a non-cognitive, i.e. classical, resource allocation problem.

The problem $P5$ is a convex optimization problem. Solving for the optimal solution (See the Appendix for the derivation), we can get

$$P_{i,m}^{*} = \left[\frac{1}{\alpha^{l^*}\Omega_{i,m}^{l^*} + \sum_{m=1}^{M}\beta_m} - \frac{\sigma_i^2}{\left|h_{i,m}\right|^2}\right]^{+} \tag{5.44}$$

where α^{l^*}, μ_i, and β_m are the non-negative Lagrange multipliers and $[x]^{+} = \max(0,x)$. Solving for $(M+1)$ Lagrangian multipliers is computational complex. The optimal solution can be found numerically using ellipsoid or interior point method with a complexity $\mathrm{O}\left(N^3\right)$ [Boy04]. The high computational complexity makes the optimal solution unsuitable for practical application and hence a low complexity algorithm is proposed.

On one side, ignoring the interference constraint in problem $P5$ will let the optimal solution to be the distribution of the per-user power budget $\overline{P_m}$ among the set of subcarriers N_m according to the well known waterfilling interpretation [Lek97]. On the other side, if the per-user power constraints are ignored, the analysis given in [Ban08] can be followed where the Lagrangian of the problem can be written as

$$\mathrm{G}^{(Int)}\left(l^*\right) = -\sum_{i=1}^{N} R_i\left(P_{i,m}^{(Int)}, h_{i,m}\right) + \alpha_{l^*}^{(Int)}\left(\sum_{i=1}^{N} P_{i,m}^{(Int)}\Omega_{i,m}^{l^*} - I_{th}^{l^*}\right) \tag{5.45}$$

where $\alpha_{l^*}^{(Int)}$ is the Lagrange multiplier. (Int) stands for optimization under the interference constraint only. Equating $\dfrac{\partial \mathrm{G}^{(\mathrm{Int})}\left(l^*\right)}{\partial P_{i,m}^{(Int)}}$ to zero, we get

$$P_{i,m}^{(Int)}\left(l^*\right)=\left[\frac{1}{\alpha_{l^*}^{(Int)}\Omega_{i,m}^{l^*}}-\frac{\sigma_i^2}{\left|h_{i,m}\right|^2}\right]^+. \tag{5.46}$$

Hence, substituting (5.46) into $\sum_{i=1}^{N}P_{i,m}^{(Int)}\Omega_{i,m}^{l^*}=I_{th}^{l^*}$ we get

$$\alpha_{l^*}^{(Int)}=\frac{\left|N\right|}{I_{th}^{l^*}+\sum_{i=1}^{N}\frac{\Omega_{i,m}^{l^*}\sigma_i^2}{\left|h_{i,m}\right|^2}}. \tag{5.47}$$

One can note that if the solution found by (5.46)-(5.47) satisfies the different per-user power constraints, i.e. $\sum_{i\in \mathrm{N}_m}P_{i,m}^{(Int)}\left(l^*\right)\le\overline{P_m},\forall m$, then (5.46)-(5.47) will be the optimal solution for the optimization problem $P5$ where the case of interference-only optimization problem occurred. In most of the cases, this relation doesn't hold which motivates developing an efficient algorithm considering both the interference and per-user power constraints.

The downlink power allocation problem is solved considering one total power constraint. The algorithm presented in the downlink part will be extended to consider the uplink scenario with several per-user power constraints. We can start by assuming that the maximum power $P_{i,m}^{Max}$ that can be allocated to each subcarrier is determined according to the interference constraint only using (5.46)-(5.47), i.e. $P_{i,m}^{Max}=P_{i,m}^{(Int)}\left(l^*\right)$. Afterwards, the per-user power constraints are tested to check whether $\sum_{i\in \mathrm{N}_m}P_{i,m}^{(Int)}\left(l^*\right)\le\overline{P_m},\forall m$ holds or not. If the relation is satisfied, then the solution is found where $P_{i,m}^{*}=P_{i,m}^{Max}$. Otherwise, the available power $\overline{P_m}$ for each SU should be distributed among the subcarriers in N_m giving that the power allocated to each subcarrier is lower than or equal to $P_{i,m}^{Max}$. For every SU, the following problem should be solved

$$\begin{aligned} P6:\ & \max_{P_{i,m}^{W.F}}\sum_{i\in \mathrm{N}_m}R_i\left(P_{i,m}^{W.F},h_{i,m}\right)\\ s.t.\ & \sum_{i\in \mathrm{N}_m}P_{i,m}^{W.F}\le\overline{P_m};\\ & 0\le P_{i,m}^{W.F}\le P_{i,m}^{Max} \end{aligned}. \tag{5.48}$$

The problem $P6$ is called *"cap-limited"* waterfilling (see Algorithm 3) [Pap08][Zha10-2]. Since it is assumed that $P_{i,m}^{W.F}\le P_{i,m}^{Max}$, some of the powers allocated to subcarriers will not reach the maximum allowable values which will make the interference introduced to the primary system below the threshold $I_{th}^{l^*}$. In order to take the advantage of the allowable interference, some power can be taken from one subcarrier and given to another hoping to increase the total system capacity. Therefore, the values of the maximum power that can be allocated to each subcarrier $P_{i,m}^{Max}$ should

be updated depending on the remaining interference. The residual interference can be determined as follows

$$I^{l*}_{Residual} = I^{l*}_{th} - \sum_{i=1}^{N} P^{W.F}_{i,m} \Omega^{l*}_{i,m} . \quad (5.49)$$

Assuming that $S_m \subset N_m$ is the set of the subcarriers that reach its maximum, i.e. $P^{W.F}_{i,m} = P^{Max}_{i,m}, \forall i \in S_m$, then, $P^{Max}_{i,m}, \forall i \in S_m$ can be updated by applying the equations (5.46)-(5.47) on the subcarriers in the set $S = \{S_1 \cup S_2 \cdots \cup S_m\}$ with the following interference constraint

$$I^{l*}_{updated} = I^{l*}_{Residual} + \sum_{i \in S} P^{W.F}_{i,m} \Omega^{l*}_{i,m} . \quad (5.50)$$

After determining the updated values of $P^{Max}_{i,m}$, the *"cap-limited"* waterfilling is performed again for every SU to find the final solution $P^{*}_{i,m} = P^{W.F}_{i,m}$. A graphical description of the proposed power allocation algorithm is given in Figure 5.17.

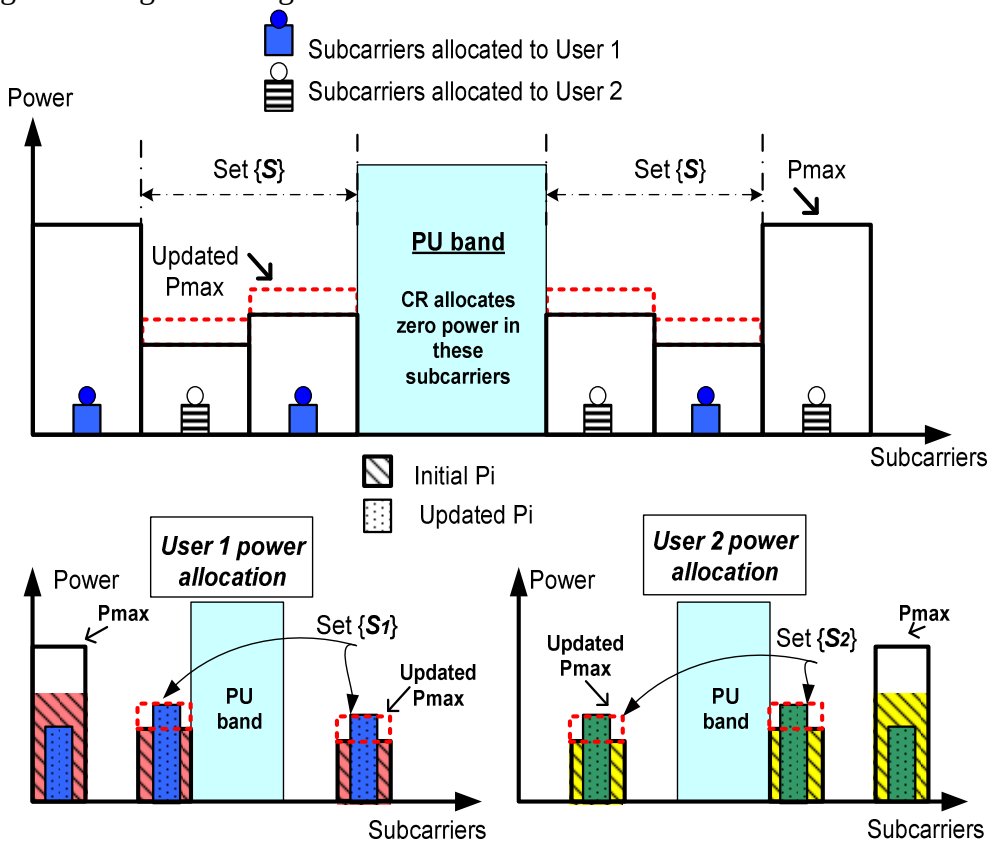

Figure 5.17: An example of the SUs allocated power using proposed power allocation algorithm

5.2.3.2.3 Generalization of the Proposed Algorithm (Multiple PUs Case)

In this section, the algorithm presented in the previous section to solve the optimization problem $P1$ considering only one interference constraint will be generalized to consider L interference constraints, i.e. multiple PU bands.

For the subcarrier allocation phase, considering the same assumption in which every subcarrier is able to introduce the same amount of interference to the different PU bands, the value of the maximum power that can be allocated to each subcarrier, i.e. $P_{i,m}^{Uni}$, is determined by choosing the minimum among the different maximum powers evaluated according to the different interference constraints. Therefore, equation (5.41) can be generalized as follows

$$P_{i,m}^{Uni} = \min\{\frac{I_{Uniform}^{1}}{\Omega_{i,m}^{1}}, \frac{I_{Uniform}^{2}}{\Omega_{i,m}^{2}}, \cdots, \frac{I_{Uniform}^{L}}{\Omega_{i,m}^{L}}\}. \tag{5.51}$$

Once the maximum power $P_{i,m}^{Uni}$ is determined, the same subcarrier assigning procedures presented previously can be used for the multiple PU bands case.

In the power allocation phase, if multiple interference constraints are considered in the optimization problem $P2$, the solution given in (5.47) can be generalized as follows

$$P_{i,m}^{*} = \left[\frac{1}{\sum_{l=1}^{L} \alpha^{l} \Omega_{i,m}^{l} + \sum_{m=1}^{M} \beta_{m}} - \frac{\sigma_{i}^{2}}{\left| h_{i,m} \right|^{2}} \right]^{+} \tag{5.52}$$

where α_l, μ_i, and β_m are the non-negative Lagrange multipliers. Therefore, the problem become more computationally complex where $(M+L)$ Lagrangian multipliers should be determined. To find a suboptimal solution for the multiple PUs case, the values of the allocated power $P_{i,m}^{(Int)}(l)$ under every interference constraint I_{th}^{l} are determined using (5.46)-(5.47). Then, the maximum power $P_{i,m}^{Max}$ that can be allocated to each subcarrier is determined according to the following formula

$$P_{i,m}^{Max} = \min\{P_{i,m}^{(Int)}(1), P_{i,m}^{(Int)}(2), \cdots, P_{i,m}^{(Int)}(L)\}. \tag{5.53}$$

Afterwards, the per-user power constraints are tested and the *"cap-limited"* waterfilling is applied for every user m. Using (5.49) and (5.50), the updated values of the interference thresholds can be found and then (5.46)-(5.47) are applied to find the values of $P_{i,m}^{(Int)}(l)$ $\forall i \in \mathrm{S}$. Accordingly, the new values of $P_{i,m}^{Max}$ can be determined using (5.53). The *"cap-limited"* waterfilling is performed again for every SU considering the updated maximum values to find the final solution. The implementation procedures of the power allocation algorithm with multiple interference constraints are described in Algorithm 5.

Algorithm 5 Power Allocation Algorithm in Uplink Case

1. **Initialize** $\mathrm{N} = \{1, 2, \cdots, N\}$, $I_{Left}^{l} = 0$ and $\mathrm{S} = \varnothing$.

2. $\forall l \in \{1,\cdots,L\}$, Sort $\left\{ H_i = \frac{\sigma_i^2}{\left|h_{i,m}\right|^2}\Omega_{i,m}^l, i \in \mathrm{N} \right\}$ in decreasing order with k being the sorted index.

Find the P_i^{Max} as follows:

(a) $H_{sum} = \sum_{i\in \mathrm{N}_l} H_i$, $\alpha_l^{(Int)} = \left|\mathrm{N}\right| / \left(I_{th}^l + H_{sum}\right)$, $n = 1$.

(b) $\alpha_l^{(Int)} > H_{k(n)}^{-1}$ $H_{sum} = H_{sum} - H_{k(n)}$, $\mathrm{N} = \mathrm{N} \setminus \{k(n)\}$, $\alpha_l^{(Int)} = \left|\mathrm{N}\right| / \left(I_{th}^l + H_{sum}\right)$, $n = n+1$

(c) Set $P_{i,m}^{(Int)}(l) = \left[\frac{1}{\alpha_l^{(Int)}\Omega_{i,m}^l} - \frac{\sigma_i^2}{\left|h_{i,m}\right|^2} \right]^+$

3. Evaluate $P_{i,m}^{Max} = \min\{P_{i,m}^{(Int)}(1), P_{i,m}^{(Int)}(2), \cdots, P_{i,m}^{(Int)}(L)\}$

4. **if** $\sum_{i\in \mathrm{N}_m} P_{i,m}^{Max} \le \overline{P_m}; \forall m$

Let $P_{i,m}^* = P_{i,m}^{Max}$ and stop the algorithm.

end if

5. $\forall m$, Perform the *"cap-limited"* waterfilling on the set of subcarriers N_m under the per-user constraint $\overline{P_m}$ and the maximum power that can be allocated to each subcarrier $P_{i,m}^{Max}$ and find the set $\mathrm{S}_m \subset \mathrm{N}_m$ where $P_{i,m}i^{W.F} = P_{i,m}^{Max}$.

6. Let $\mathrm{S} = \{S_1 \cup S_2 \cdots \cup S_m\}$, evaluate $I_{Residual}^l = I_{th}^l - \sum_{i=1}^N P_{i,m}^{W.F}\Omega_{i,m}^l$, set $\mathrm{N} = \mathrm{S}$, $I_{updated}^l = I_{Residual}^l + \sum_{i\in \mathrm{S}} P_{i,m}^{W.F}\Omega_{i,m}^l$ and apply again only steps $(2-3)$ to update $P_{i,m}^{Max}$.

7. $\forall m$, Perform the *"cap-limited"* waterfilling on the set of subcarriers N_m under the per-user constraint $\overline{P_m}$ and the maximum power that can be allocated to each subcarrier $P_{i,m}^{Max}$ and set $P_{i,m}^* = P_{i,m}^{W.F}$.

The exhaustive enumeration scheme needs to iterate M^N times to exhaust all the cases and its complexity of $\mathrm{O}\left(N^3 M^N\right)$ is very hard to afford. Moreover, the algorithm proposed by Wang et al. in [Wan09] has a complexity larger than $\mathrm{O}\left(N^2 M\right)$ and lower than $\mathrm{O}\left(N^3 M\right)$.

Recall that our proposed algorithm to solve problem $P1$ is divided into two phases: the subcarriers to user's allocation phase and the power allocation phase. Each subcarrier in the first phase requires no more than M function evaluations to be assigned to one user depending on the size of the set U. Hence, the computational complexity of the proposed subcarrier to user allocation algorithm is lower than or equal $\mathrm{O}(NM)$. In the power allocation algorithm, Step 2 in Algorithm 4 has a computational complexity of $\mathrm{O}(N \log N)$ while Steps 5 and 7 of the algorithm execute the *"cap-limited"* waterfilling for every SU with a complexity of $\sum_{m=1}^{M} \mathrm{O}\left(\mathrm{N}_m\right) \le \mathrm{O}(N) \le \mathrm{O}(N \log N)$ [Zha10-2]. Step 6 has a complexity of $\mathrm{O}\left(\left|\mathrm{S}\right| \log \left|\mathrm{S}\right|\right) \le \mathrm{O}(N \log N)$. Hence, the complexity of the power

allocation algorithm is lower than $\mathrm{O}\left(N \log N\right)$. Thus, the overall asymptotic complexity of the proposed uplink resource allocation algorithm is lower than $\mathrm{O}\left(N \log N\right)+\mathrm{O}\left(NM\right)$. Table 5.2 summarizes the complexity of the different algorithms.

Table 5.2: Complexity comparison

Algorithm	Complexity
Optimal	$\mathrm{O}\left(N^3 M^N\right)$
Wang	$\in \left[\mathrm{O}\left(N^2 M\right), \mathrm{O}\left(N^3 M\right)\right]$
Proposed	$\leq \mathrm{O}\left(N \log N\right)+\mathrm{O}\left(NM\right)$
Classical+Pr	$\leq \mathrm{O}\left(N \log N\right)+\mathrm{O}\left(NM\right)$

5.2.3.2.4 Simulation Results for the Uplink Case

The simulations are performed under the scenario given in Figure 5.4. The values of T_s, Δf, and σ_i^2 are assumed to be 4μ seconds, 0.3125 MHz and 10^{-6} respectively. For simplicity, the channel gains *h* and *g* are outcomes of independent Rayleigh distributed random variables with mean equal to1. Two interference constraints belonging to two active PU bands, i.e. $L = 2$, are assumed with $B_1 = B_2$ and $I_{th}^1 = I_{th}^2$ (see Figure 5.5). Perfect synchronization is assumed between the SUs. All the results have been averaged over 1000 iterations. OFDM and FBMC based cognitive radio systems are evaluated. The OFDM system is assumed to have a 6.67% of its symbol time as CP. For FBMC system, the prototype coefficients are assumed to be equal to PHYDYAS coefficients with overlapping factor $K = 4$ [PHY]. For the purpose of performance comparison, the following algorithms are considered:

1. **Optimal**: the subcarriers are allocated by exhaustive enumeration while the power is allocated using (5.52). The optimal capacity is found without considering the minimum rate requirements.
2. **Wang**: the method proposed in [Wan09] is used. The interference constraint is converted into per-subcarrier power constraints using (5.51).
3. **Classical+Pr**: the subcarriers are allocated according to the scheme used in non-cognitive OFDM systems [Kim05], while the power is allocated using our proposed algorithm.

Figure 5.18 plots the average capacity of a CR system with $M = 2$ SUs versus the interference threshold when the number of subcarriers is $N = 8$, the per-user power budget $\overline{P_m} = 1m$ Watt and $B_1 = B_2 = 1.25$ MHz. The proposed algorithm achieves a good performance in comparison with optimal and outperforms the other algorithms. Moreover, the capacity of FBMC based CR system is higher than that of OFDM based one because the sidelobes in FBMC's PSD are smaller than that in OFDM which introduces less interference to the PUs. Moreover, the inserted CP in OFDM based CR systems reduces the total capacity of the system. For the rest of the results, the optimal solution will not be simulated due to its high computational complexity when the numbers of subcarriers and users are increased.

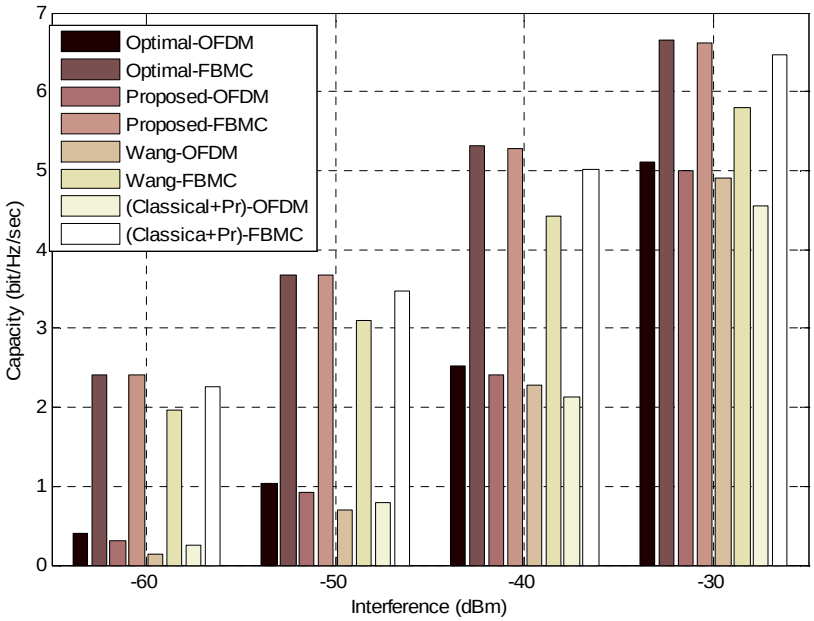

Figure 5.18: Achieved capacity vs. interference threshold

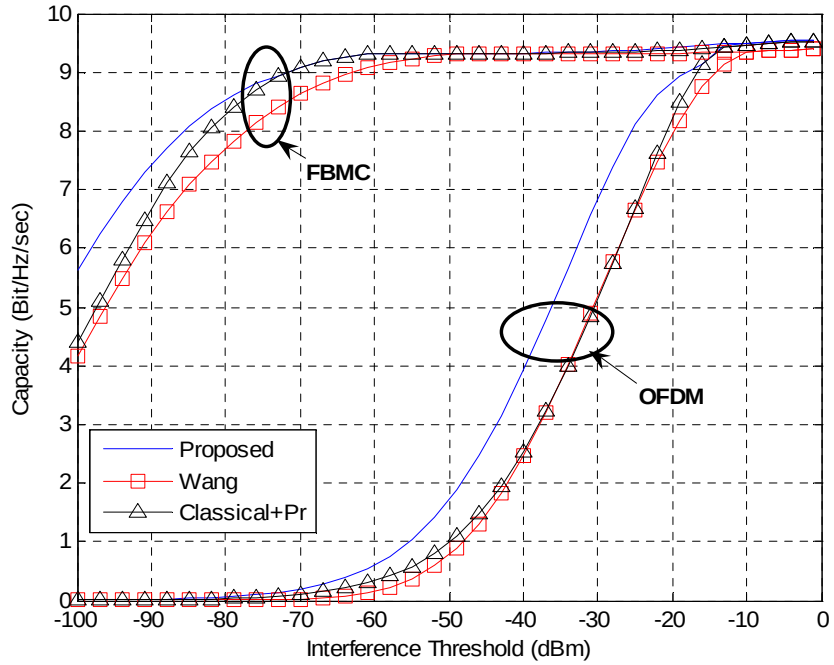

Figure 5.19: Achieved capacity vs. allowed interference threshold

Figure 5.19 plots the average capacity versus the interference threshold when the number of subcarriers N=64 and M=10 SUs versus the interference threshold when the number of subcarriers is, the per-user power budget $\overline{P}_m = 1m$ Watt and $B_1 = B_2 = 10$ MHz. It can be observed that as the interference threshold increases, the capacity increases since each SU is allowed to have more flexibility in allocating more power on its subcarriers. The performance of the proposed algorithm outperforms other algorithms. Moreover, the gap between the different algorithms decreases with the interference threshold as the CR system becomes closer to the classical (non-cognitive) system. The capacity of FBMC based CR system is higher than that of OFDM.

In the case of OFDM system, the interference has a high effect on the system performance where the efficiency of the proposed algorithm appears. Moreover, the inefficiency of the Classical algorithm is shown when the interference constraint affects the optimization problem. In FBMC systems, the difference between the Classical+Pr and the proposed is very small. The reason behind that is in the low interference induced by the FBMC system to the primary system which makes the CR system very close to the non-cognitive one. In FBMC CR system with an extremely small interference threshold (or with high power budget), the proposed algorithm will be useful and achieves more capacity than the classical one as in the region below −70dBm in Figure 5.8 for example. Since the Classical+Pr and the proposed algorithm apply the same power allocation algorithm, it's clear that the capacity increase of the proposed algorithm over the Classical+Pr one results from the subcarrier allocation step. In addition to the subcarrier allocation, the conversion of the total interference constraint into several per-subcarrier maximum power constraints, choosing he minimum waterfilling level, and the assumptions made to decrease the computational complexity affect the performance of Wang's algorithm.

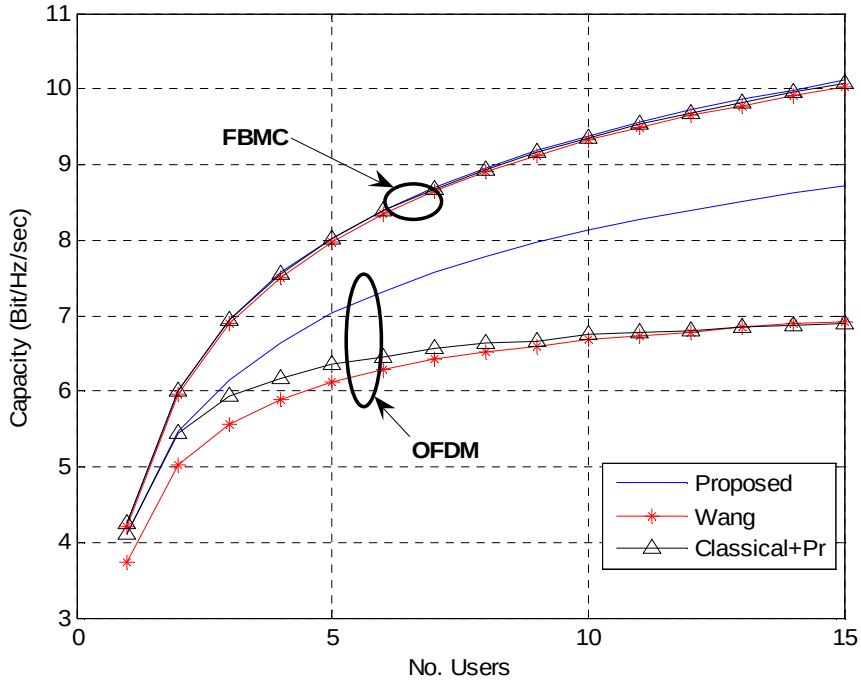

Figure 5.20: Achieved capacity vs. No. of SUs

Figure 5.20 shows the average capacity versus the number of SUs when the number of subcarriers is N = 64, the interference thresholds is −25 dBm, the per-user power is P_m = 1mWatt and B = 10 MHz. The capacity increases with the number of users due to the multiuser diversity. In OFDM based CR system, the lower the number of SUs, the smaller the difference between the proposed and Classical+Pr algorithm. This is because the number of subcarriers that will be allocated to each user will increase which reduces the amount of power that will be allocated to each subcarrier and consequently the amount of interference imposed to the primary system which makes the CR system acts relatively as a non-cognitive system. FBMC based CR system has more capacity than the OFDM based one and the different algorithms have approximately the same capacity because the interference introduced to the primary system by the FBMC based CR system is less than the prescribed threshold and hence, works virtually like the non-cognitive schemes.

From the presented results, one can notes that when the interference constraint affects the optimization the problem (like the OFDM case), the proposed algorithm enhances the total data rate and outperforms the other algorithms. Additionally, due to its small interference to the PU, the throughput of FBMC systems is more than the OFDM ones and the classical ways of subcarrier allocation can be used (depending on the values of power and interference constraints) which recommends the FBMC as a candidate for the CR applications.

5.2.4 Summary

In this report, we proposed an efficient resource allocation algorithm for uplink/downlink multicarrier based CR networks. The allocation process is separated into two steps. In the first step, the subcarriers are allocated to the users while in the second step; the per-user power budget is distributed among the subcarriers so that the total system capacity is maximized without causing excessive interference to the primary system.
For downlink scenario, the maximum data rate can be achieved by allocating the subcarrier to the user with maximum SNR. It's shown that the proposed power allocation algorithm achieves a near optimal performance and outperforms the sub-optimal algorithms proposed so far. Its found that the net total interference introduced to the PU's band is relatively not affected by assuming that each subcarrier is belong to the closest PU band and only introducing interference to it. It's demonstrated also that the capacity of the CR system that uses the non-active as well as the active bands is more than the capacity of the system that only uses the non-active bands.

For uplink scenario, the allocation of subcarriers to the user with maximum SNR is not efficient in uplink due to the per user power constraint. Therefore, the subcarriers are allocated to the users according to their channel quality, interference to the primary user and the incremental data rate.

Moreover, simulation results prove that the FBMC based CR systems have more capacity than OFDM based ones. The obtained results contribute in recommending the use of FBMC physical layer in the future cognitive radio systems.

5.3 Synergistic Power Control in Cognitive Radio Networks with MAC Layer Cooperation

This part is an extension of section 7 in deliverable [D8.1] and it assumes the same context, which is recalled for convenience.

For cognitive radio systems operating in licensed spectrum bands with co-existence of both primary and secondary users, spectrum sensing and spectrum mobility are of key importance. On the other hand, Cognitive Radio systems operating in license exempt spectrum bands (e.g. case of different operators in unlicensed spectrum bands), require efficient spectrum decision and spectrum sharing, as well as power control mechanisms for interference mitigation. For example, if all users transmit at the maximum valid power level then every user is causing significant interference to all other users, which can result in reduced total utility from the network perspective and poor QoS from the user perspective.

In this scope, algorithms that employ power control in order to maximize the overall utility are required. At the same time, these algorithms need to be distributed in order to be applied efficiently

in ad-hoc networks operating in unlicensed spectrum bands (e.g. only users from the same operator are synchronized). Such algorithms should be able to utilize message exchange schemes between the users in order to maximize the overall utility (therefore the related systems are classified as cooperative CR systems); however, uncertainties in message exchange should also be considered. Furthermore, they should be able to converge in an optimal solution within a finite number of iterations in order to be applicable in real systems. Finally, the algorithms need to be flexible in order to take advantage of improvements in the physical layer (e.g. FBMC). The overall assumptions and definitions for the proposed algorithm are the following.

We propose an algorithm based on the spectrum sharing scheme of [Hua05] for distributed interference compensation in Cognitive Radios that operate in license exempt spectrum. The proposed algorithm refines the utility function used in [Hua05] to take into account uncertainties that may be the result of user mobility and large delays in the update of the interference prices. More specifically, a fuzzy logic reasoner is utilized in order to take into account the effect of a large number of users and the related interference, as well as to cope for uncertainties in the message exchange process. The performance of the proposed algorithm is evaluated through simulations. In this direction, the overall utility value of the algorithm is compared to the utility of a simple "always select the maximum valid power" policy. The proposed algorithm is also applied in both Filter Bank Multicarrier (FBMC) and Orthogonal Frequency Division Multiplexing (OFDM) systems in order to show its flexibility and capability of transparently exploiting an improved Physical layer, without any further modifications. Moreover, comparison with the distributed algorithm of [Hua05] is used to validate the improvement in terms of the overall utility level under uncertainties that cause 25% underestimation of the interference. In order to quantify the improvement using conventional network metrics and to show the relation between a higher overall utility value and parameters that directly affect the user experience, comparison with the algorithm of [Hua05] in terms of Signal-to-Interference-plus-Noise Ratio (SINR) is also performed. Experimental results indicate that SINR is consistently improved with the use of the proposed algorithm. Finally, the optimal period for triggering the power control mechanism in order to minimize energy consumption has been defined using Markov models.

5.3.1 Algorithm Outline

Various pricing mechanisms have been proposed for allocating resources in various types of networks, targeting both wired and wireless network topologies. However, the problem in distributed networks that operate in license exempt spectrum bands is different from most of the previous works, since the interference that each user is causing to the rest of the users implies that the users' utility functions are coupled. This means that in the general case the overall network utility is not necessarily concave in regard to the transmission power of each user. We assume a scenario similar to [Hua05], in which the communication is not fixed-rate but the transmission rate can be adaptive ("elastic" data applications) and the goal is to maximize the total utility of the network without guaranteeing interference margins for each user. The proposed algorithm refines the algorithm of [Hua05] for distributed interference compensation, with the addition of a fuzzy logic reasoner that caters for the effect of a large number of users in the impact of interference as well as to cope for uncertainties in the message exchange (e.g. from high mobility or a large time interval for the update of interference prices).

The main idea of the algorithm is that the users exchange information about their interference levels, using for this purpose explicit message exchange mechanisms at the MAC layer. A transmitter sets its power level by considering not only its own Signal-to-Interference-plus-Noise Ratio (SINR)

information but also the negative impact in utility for other users caused from the increased interference that will come as side effect of the increase in power of that particular transmitter. This functions as a counter-motive that prevents users from always setting their transmission power to the maximum valid level.

Assuming that there are a total of *L* users in a spectrum band with *k* available channels, the SINR of the *i*th user in channel *k* is given by the equation

$$\gamma\left(p_i^{\,k}\right)=\frac{p_i^{\,k}\cdot h_{ii}}{n_0+\sum_{j\neq i} p_j^{\,k}\cdot h_{ji}}$$

where p_i^k is the transmission power for *i* user on channel *k*, h_{ii} is the link gain between *i*th receiver and *i*th transmitter, $n_0=10^{-2}$ is the noise level, p_j^k is the transmission power for all other users on channel *k* and h_{ji} is the link gain between *i*th receiver and *j*th transmitter. It should be noted that $h_{ij} \neq h_{ji}$, since the first expresses the gain between *i*th transmitter and *j*th receiver and the latter expresses the gain between *j*th transmitter and *i*th receiver.

In the general case, the carrier frequency of a signal is varied; therefore the magnitude of the change in amplitude will vary. The coherence bandwidth measures the separation in frequency after which two signals will experience uncorrelated fading. Specifically, in the case of frequency-selective fading, the coherence bandwidth of the channel is smaller than the bandwidth of the signal. Thus, different frequency components of the signal experience decorrelated fading. On the other hand, in the case of flat fading, the coherence bandwidth of the channel is larger than the bandwidth of the signal. Therefore, all frequency components of the signal will experience the same magnitude of fading. In the following analysis we assume a flat-faded channel without shadowing effects. For a flat-faded channel there is no delay spread and no frequency selectivity, as mentioned previously. This means that a single coefficient is used for channel attenuation. Since the described channel is static, i.e., the coefficient is fixed, the only attenuation present is the path loss. Therefore, in this particular case *h* is strictly the channel attenuation or channel gain. We assume that the environment causes average to high loss (path loss exponent is three, typical for indoor urban environments), thus the channel gain $h_{ji} = d_{ji}^{\,3}$, where *d* is the distance between the *j*th transmitter and *i*th receiver.

In order to model the impact in utility for user *i* caused by the transmission of all other users, we adopt from [Hua05] the notion of interference price. Interference price is defined as

$$\pi_i^{\,k}=\frac{\partial u_i\left(\gamma\left(p_i^{\,k}\right)\right)}{\partial\left(\sum_{j\neq i} p_j^{\,k}\cdot h_{ji}\right)}$$

where $u_i\left(\gamma_i\left(p_i^k\right)\right)=\theta_i\log\left(\gamma_i\left(p_i^k\right)\right)$ is the logarithmic utility function and θ_i is a user dependent parameter. As shown, the interference price expresses the marginal utility degradation due to a marginal increase in sustained interference. Interference prices are exchanged between the users in a completely asynchronous fashion, while every user is able to update its own price and power level at different times. Each user selects an appropriate transmission power level in order to maximize the difference between the increase in its own utility minus the utility degradation for others, caused

by the increased interference as expressed by the interference price. Specifically, the mathematical formula that [Hua05] attempts to maximize is given below

$$u_i\left(\gamma\left(p_i^{\,k}\right)\right) - p_i^{\,k}\sum_{j\neq i}\pi_j^{\,k}\cdot h_{ji}\,. \tag{5.54}$$

The first part of this equation is closely **related to the Shannon capacity** for user *i* (the constant term is excluded in order to have a form that can be proved to converge in all cases). Increasing that part is directly related to an increase in the maximum bit rate. However, since the transmission of every user is seen as noise by the other users, the second term expresses what the other users will lose if user *i* increases its transmission power level.

The algorithm is comprised by the following steps:

1. **Initialization:** For every user $i \in L$ transmitting in channel k select a valid transmission power level p_i^k and a positive value for the interference price π_i^k;
2. **Power Update:** For every user i at a time interval $t_{ai} \in T_i$, where T_i is a set of positive time instances in which the user i will update its transmission power level and $t_{a1} \neq t_{a2} \neq \ldots \neq t_{ai}$, update its transmission power level p_i^k trying to maximize equation (5.54);
3. **Interference Price Update:** For every user i at a time interval $t_{bi} \in T'_i$, where T'_i is a set of positive time instances in which the user i will update its interference price and $t_{b1} \neq t_{b2} \neq \ldots \neq t_{bi}$, calculate and announce the updated interference price π_i^k and notify the rest of the users for the updated value.

Steps 2 and 3 are repeated asynchronously for all users until the algorithm reaches its final steady state. In order to perform the power update in step 2, users select p_i^k from the set *TP* of the allowable transmission power levels, so that the surplus of is maximized. Provided that the allowable power levels are equidistant values that can be derived from the previous value by adding a constant increment, then it can be proved that the algorithm converges, as long as the increment is sufficiently small. Moreover, if the problem is partitioned so that there is a single available spectrum area or if the algorithm is executed only for subgroups selecting the same spectrum area *M*, then it can be proved that the algorithm converges to a **global maximum** under arbitrary asynchronous updates [Hua05].

In order to execute the algorithm, every user in the network needs to know its own SINR and channel gain, as well as the channel gains and the interference prices announced by other users. The SINR and the channel gain between a user pair can be calculated at the receiver and forwarded to the transmitter. The channel gains between users can be calculated if receivers periodically broadcast a beacon [Hua05] (h_{ii} message between Receiver *i* and Transmitter *i* in Figure 5.21). This information can also be provided on demand through a specially defined message sent from the receiver. Thus, in case the transmitter requires channel gain information before the reception of the next scheduled beacon, it can request this information from the receiver who will respond with the relative measurements. Finally, interference price values can be also conveyed in the same manner (message p_{ij} from Receiver *i* to Transmitter *j* in Figure 5.21). Every user announces a single interference price, therefore the delay that is introduced by the algorithm scales linearly with the number of users. This also implies that, given the fact that the updates are distributed in an asynchronous manner; the complexity of the algorithm is polynomial to the number of users and available power levels (that depend on the size of the increment in the Power Update step).

In the original version of the algorithm of [Hua05], an underestimation of the interference prices is likely to occur in some cases. This can be caused by problems in message exchange, for example due to users' mobility, or increased update time intervals for the interference prices, considering that updates are asynchronous for all users. The effect of this underestimation is the convergence of the algorithm to a non optimal solution. Moreover, as the number of user pairs increases, the highest allowable transmission power level is more likely to be chosen, since the previous problems escalate. This is not desirable, since it will often result in increased interference to a potentially large number of neighboring users, especially in the case that the interference is underestimated for the reasons mentioned above.

Therefore, in this work, a coefficient "α" is introduced in order to improve the scalability of the algorithm in case a large number of users are sharing the same spectrum band and to cope with uncertainties, such as large update intervals and problems in the message exchange mechanism. In both cases, there is a danger that the impact of the interference to other users due to the increase in transmission power will be underestimated as explained above. Thus, factor α needs to avert this scenario by increasing the weight of the second term of (5.54), which expresses the utility loss other users will experience from a transmission power increase. In such cases, it will compensate for the underestimation of interference, by increasing the value of the second term and, therefore it can result in a system that approximates the case of "perfect" message exchange (without long delays, reduced message range, etc. that reduce the second term in (5.54)).

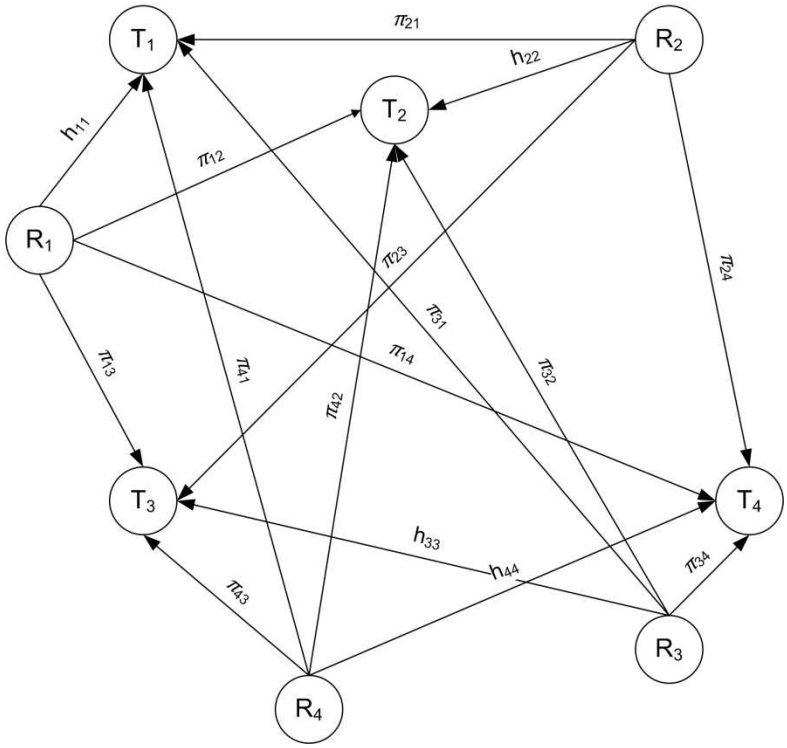

Figure 5.21: An example network topology with four transmitter-receiver pairs

If coefficient α is included as a weight multiplied with the subtracted interference term, then the following equation is derived, that is the objective to be maximized

$$u_i\left(\gamma\left(p_i^{\,k}\right)\right) - a \cdot p_i^{\,k} \sum_{j \neq i} \pi_j^{\,k} \cdot h_{ji} \,. \tag{5.55}$$

In a "real" protocol implementation, parameters such as the storage requirements and scalability of the message exchange mechanism should be addressed. Moreover, the overhead and delays introduced by message exchange should be taken into consideration together with parameters such as timeliness and path optimality (for increased reliability in message transmission). However, the performance of the original version of the algorithm in [Hua05] was shown not to degrade sharply in case the message exchange is imperfect (e.g., if the nodes can only exchange messages with their closest neighbors up to a specific range, or if some messages are lost). This characteristic is the outcome of the fact that, in the case of imperfect message exchange, the algorithm gracefully degrades towards the "worst case" scenario of unregulated transmission with the maximum allowable power level, as the value of the subtracted term is gradually underestimated in (5.55). The term "graceful degradation" refers to fact that when a certain number of messages are lost, the performance of the system does not drop sharply towards the worst case. This characteristic is greatly desirable for systems that operate in faulty or unreliable environments (e.g., [Raw08]). In this work, the previous property is further improved with the introduction of coefficient α that provides the capability to handle uncertainties.

5.3.2 Fuzzy Inference

Fuzzy logic is well suited for the purpose of defining the value of factor α since it can address vague and unclear requirements efficiently and the system can be easily fine-tuned to exhibit the desirable behavior. Fuzzy logic is based on fuzzy set theory in which every object has a grade of membership in various sets. Inputs are mapped to membership functions, or sets (fuzzification process). Knowledge of a restricted domain is captured in the form of linguistic rules. Relationships between two goals are defined using fuzzy inclusion and non-inclusion between the support and hindering sets of the corresponding goals [Fou96]. As a last step, the required output is defuzzified (to numerical) from the 'THEN' part of the rules in order to produce the consequent.

An important advantage of fuzzy logic is that it can be applied transparently in combination with other well known decision methods, such as multi-objective genetic algorithms [Bul08] and game theoretic approaches [Wei03]. Moreover, proper definition of the linguistic rules can be used to reduce signaling overhead by avoiding the ping-pong, i.e. when decisions or selections are made and the input variables are not constant but temporarily present regressive behavior. Finally, Fuzzy logic can handle vague requirements more efficiently than Boolean algebra. Network-related decision making and resource allocation based on fuzzy logic approaches have been proposed in various works (e.g. [Mer08]) with promising results.

For the previous reasons, but mainly due to it is effectiveness in dealing with uncertainties and vague requirements, fuzzy logic was selected for defining the value of coefficient α that is the weight of the subtracted interference-related term in (5.55). Specifically, α is defined as:

$$\alpha = \frac{1}{\beta} \cdot IW + \gamma \tag{5.56}$$

where *IW* is the Interference Weight derived after defuzzification. *IW* takes values in the range [$\beta_{min,}$ β_{max}] in order to provide adequate resolution capabilities for the fuzzy reasoner, also according to the specific ranges of the membership functions. Parameter β has the value of β_{max}, while γ equals 1. This implies that α cannot be greater than two, meaning that the underestimation of the interference is not expected to be greater than 100%. Beyond that point, message exchange is not considered very reliable and the algorithm degrades towards the "always transmit with the maximum power" case (although a portion of the underestimation is still alleviated). On the other hand, if uncertainties are very low, the first term of the sum is converging to zero and the value of the equation is approximately equal to that of the original algorithm. For all other cases the first term is a non-zero value in the (0, 1) interval that compensates for a typical underestimation of the interference due to imperfect message exchange [Mer10].

The Fuzzy reasoner used for deriving α is of type "Mamdani", because it is intuitive, well suited for human input, flexible and widely accepted. It receives three inputs (number of users, mobility level and update time interval for the interference prices) and generates one output (the Interference Weight). The input membership functions are triangular (selected mainly for simplicity in calculations) and three membership functions per input variable are defined, therefore the number of fuzzy rules is 3^3=27.
The membership functions for the output variable "Interference Weight" are five and the output value is set in the range [0, 500], in order to achieve a greater degree of resolution and flexibility for the output of the fuzzy reasoner. The membership functions mf1-mf5 are given the labels "very low", "low", "moderate", "high" and "very high" respectively in Table 5.3.

As can be seen, the number of users is selected to be the dominant factor, which has the greatest effect in the final outcome. This is a result of the fact that if the number of users is large, even a small increase in the transmission power of a user has the potential to cause increased interference and reduce the QoS to a large number of users if its effect is underestimated due to uncertainties in message exchange. The update time interval and the mobility level have similar weights but different behavior. The first has a uniform effect over the entire valid range of update times, while the latter starts to affect the outcome only after a relatively high level, but after which it increases sharply, as only after a relatively high level of mobility is reached, users are likely to underestimate the interference they will cause to others (due to problems in message exchange, etc.).

The Defuzzification method used for generating the final crisp value is "Centroid", also known as "Center of Gravity - COG". This method determines the center of the area below the combined membership function; therefore the final output u_{COG} is given from the following equation, where u_i are the centers of the membership functions $\mu_F(u)$

$$u_{COG} = \frac{\sum_1^{27} u_i \cdot \mu_F(u_i)\ du}{\sum_1^{27} \mu_F(u_i)\ du}.$$

The defuzzification method takes into account the area as a whole, counting overlapping regions only once.

The three-dimensional (3D) representation of the Interference Weight (crisp value in the range [0,500]) as a function of the interference price update time interval and the mobility level is presented in Figure 5.22.

Table 5.3: Rules of the fuzzy reasoner

Rule Number	Users	Update Interval	Mobility Level	Consequent
1	Low	Low	Low	Very Low
2	Low	Low	Moderate	Very Low
3	Low	Low	High	Low
4	Low	Moderate	Low	Low
5	Low	Moderate	Moderate	Low
6	Low	Moderate	High	Low
7	Low	High	Low	Low
8	Low	High	Moderate	Low
9	Low	High	High	Moderate
10	Moderate	Low	Low	Low
11	Moderate	Low	Moderate	Low
12	Moderate	Low	High	Moderate
13	Moderate	Moderate	Low	Moderate
14	Moderate	Moderate	Moderate	Moderate
15	Moderate	Moderate	High	High
16	Moderate	High	Low	Moderate
17	Moderate	High	Moderate	High
18	Moderate	High	High	High
19	High	Low	Low	Moderate
20	High	Low	Moderate	High
21	High	Low	High	High
22	High	Moderate	Low	High
23	High	Moderate	Moderate	High
24	High	Moderate	High	Very High
25	High	High	Low	High
26	High	High	Moderate	Very High
27	High	High	High	Very High

The coefficient increases with the update time interval, as it is more likely that transmitters do not have the updated interference price information for other users. The increase is approximately uniform for the entire valid update time range. On the other hand, the coefficient also increases as the level of mobility increases. However, in this case the increase is not uniform but begins after a relatively high mobility level is reached, and then rises quickly. The exhibited behavior is the outcome of the fuzzy rules defined in Table 5.3.

The 3D representation of the Interference Weight derived from the specified rule base and defuzzification method as a function of the interference price update time interval (defined as up to 100 seconds but normalized in the [0,1] range) and the number of users (up to 20 user pairs) is presented in Figure 5.23.

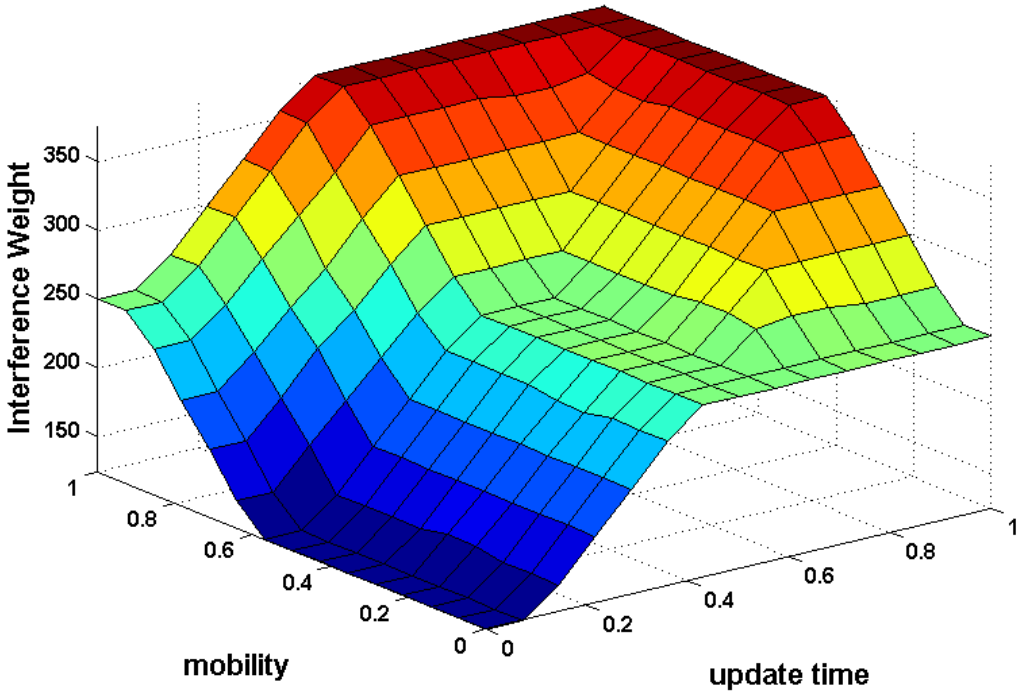

Figure 5.22: Interference weight as a function of the update interval and the mobility level

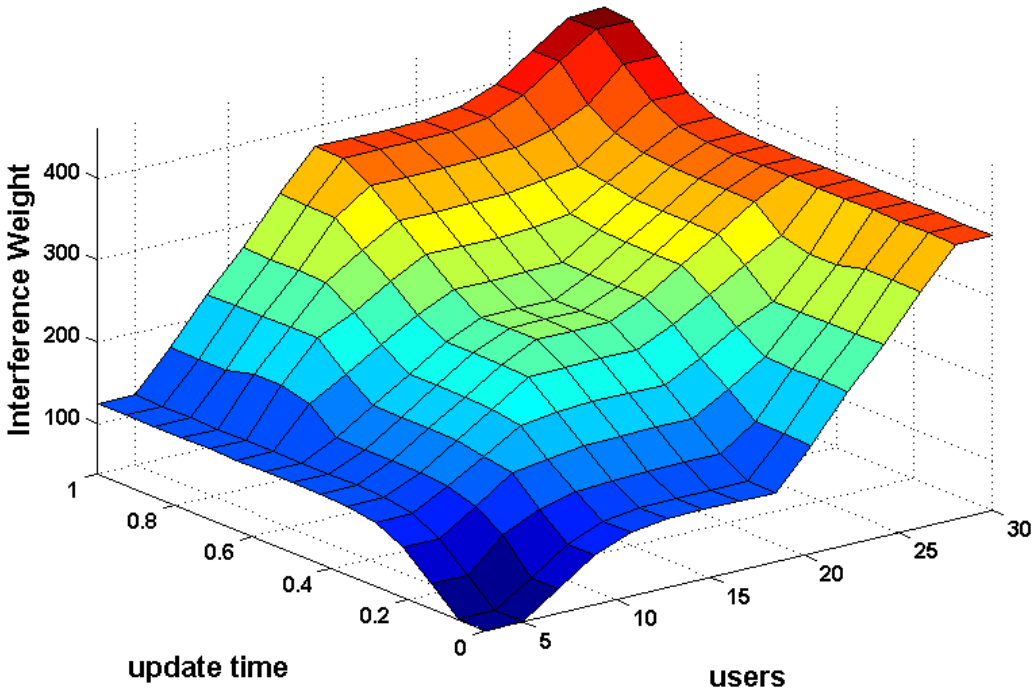

Figure 5.23: Interference weight as a function of the update interval and the number of users

For the update time interval the behavior is similar to that in the previous case. On the other hand, the coefficient also increases with the number of users. The increase is rather sharp (as determined by the rules in Table 5.3) and the value of the coefficient is rising quickly even for a relatively small

number of users. This is necessary because, as mentioned previously, when the number of user pairs is large, even a small increase in interference has the potential to affect many users and significantly decrease the overall utility of the network.

The 3D representation of the Interference Weight as a function of the number of users and the mobility level, Fig.5.24, is presenting for both parameters the behavior explained above. The overall form of the figure resembles the previous, however the mobility level is starting to affect the outcome only after a threshold is crossed, as expected according to the selected set of fuzzy rules.

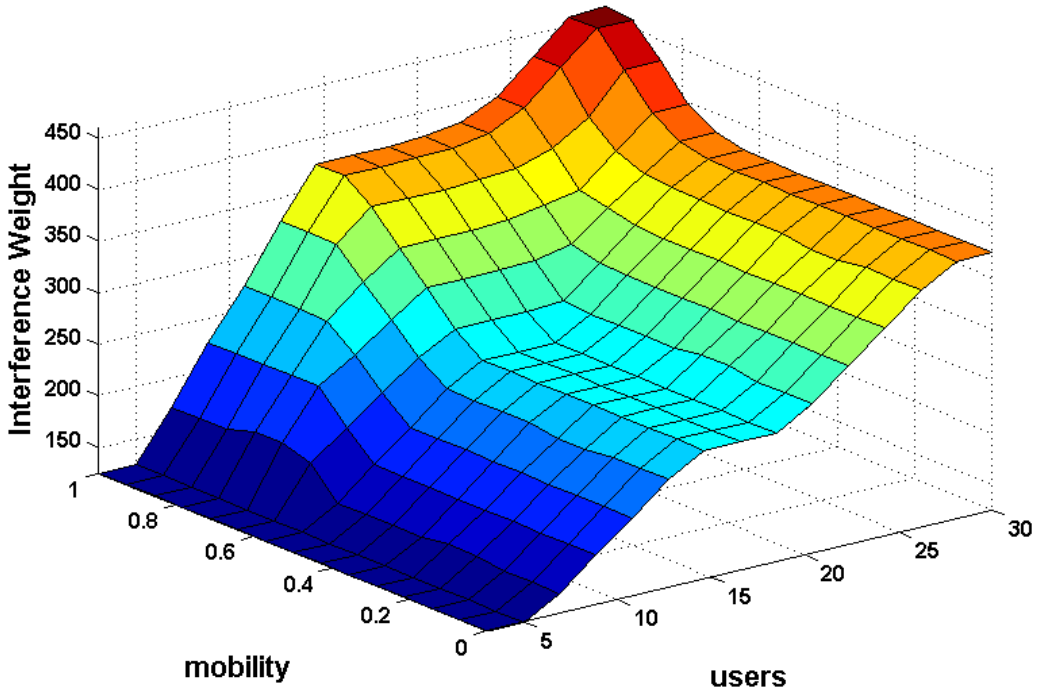

Figure 5.24: Interference weight as a function of the mobility level and the number of users

The overall methodology [Mer10] for the derivation of the optimal transmission power of every user pair is depicted in Figure 5.25. Initially, the number of user pairs is defined, together with the mobility level and the update time interval for the interference prices. As a next step, fuzzification of the values takes place in order to prepare them for elaboration in a fuzzy logic context. Following the fuzzification process, fuzzy reasoning based on a set of predefined rules (Table 5.3) is applied. These rules describe the desired behavior of the system and define the impact of the input parameters (number of users, mobility level and update time interval) in the value of the Interference Weight. After fuzzy reasoning is completed, the result is defuzzified to numerical, giving the crisp value of the Interference Weight. The topology characteristics are used to initialize the simulator and every user selects a valid initial value for the transmission power level p_i^k and the interference price π_i^k. Finally, the users proceed to update their transmission power levels and interference prices asynchronously in order to maximize (5.55). The process is completed when the system reaches a steady point in which no user is requesting to modify its transmission level.

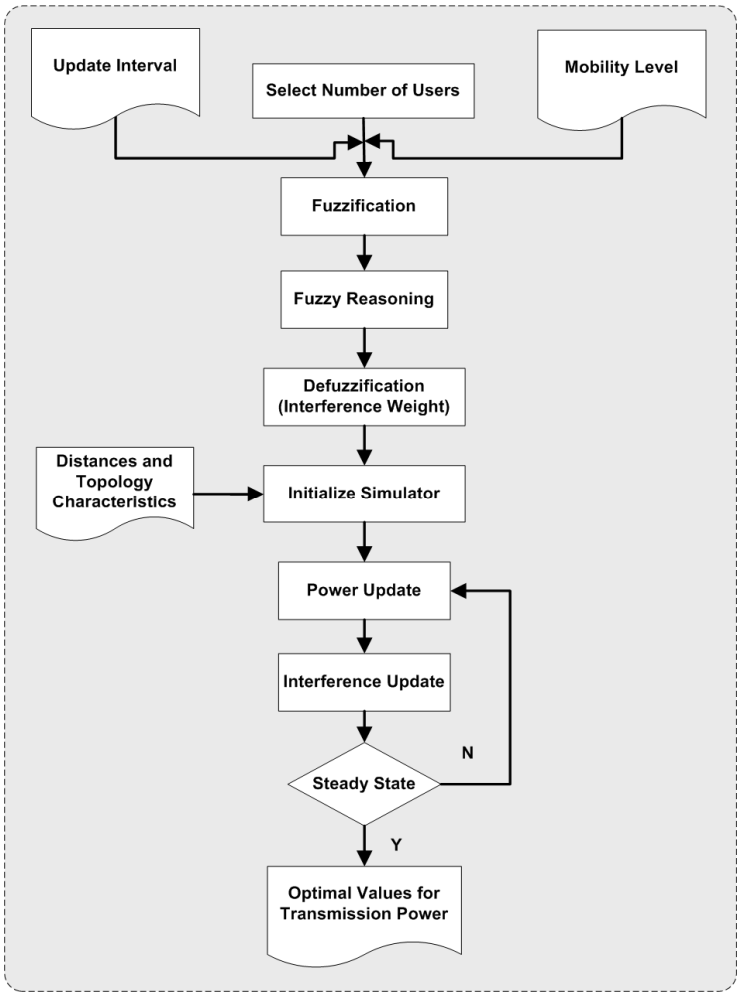

Figure 5.25: Overall methodology for deriving the transmission power levels

5.3.3 Performance Evaluation

The performance of the proposed algorithm is evaluated through extensive MATLAB simulations. In this direction, the overall utility value of the algorithm is initially compared to the utility of a simple "always select the maximum valid power" policy, as well as the utility of the original algorithm. The proposed algorithm is also applied in both FBMC and OFDM systems in order to validate its flexibility and capability of transparently exploiting an improved Physical layer, without any further modifications. Moreover, a scenario of long update time intervals in which some of the messages are delayed causing other nodes to not have the latest interference price information is considered, in order to study the performance of both algorithms in a specific case of non-ideal message exchange. Finally, in order to quantify the improvement using conventional network metrics and to show the relation between a higher overall utility value and parameters that directly affect the user experience, comparison with the algorithm of [Hua05] in terms of SINR is also performed.

As explained previously, users set their power level so as to maximize (5.55). The total "useful" utility for the network is the sum of the utilities for every user pair. The distance between users that constitute a pair is a random number in the [1, 20] meters range, while the distance between users

that are not a pair is a random value in the [5, 50] meters range. This is a more common and more practically significant scenario than using entirely random values, (e.g., it is often encountered in a conference room, as well as an airport or train station, where co-workers are initiating a point-to-point ad hoc communication). The value of β in (5.56) is set to 500, since the Interference Weight takes values in the range [0, 500], in order to provide adequate resolution capabilities. For all cases we assume the presence of uncertainties due to imperfect message exchange (one in every four messages is lost) that cause 25% underestimation of the interference. If such uncertainties are not present, then the algorithm behaves similarly to the algorithm of [Hua05]. In the presence of uncertainties, parameter α compensates for the underestimation of interference and helps the system converge near its optimal point, as described in the previous sections.

The improvement in the total utility of the network if the proposed algorithm is utilized over the scenario in which every user transmits using the maximum allowable power level, as well as over the original version of the algorithm that does not include the coefficient α is depicted in Figure 5.26. The vertical axis depicts the achieved useful utility while the horizontal axis represents the corresponding topology instance. The considerable range over which the distance values are selected, coupled with the randomness of the relative positions between nodes and the presence of uncertainties that cause underestimation of the interference in ways that are not necessarily uniform (e.g., only some messages may be delayed), causes the final value of the utility function to vary significantly between different experiments both for the original and the proposed algorithm. Thus, the final utility of each topology instance is the average utility of ten experiments for the same instance. Finally, in order to study the effect of the number of users in the system, a scenario of 10 user pairs and 20 user pairs was simulated.

The utility for the scenario in which the users transmit always using the maximum power level defines the lower bound for the behavior of the system. The proposed algorithm outperforms the original one, for the majority of times, with a more significant improvement for the lower utility values. This property is very important since it can improve the Bit Error Rate (BER) and raise QoS from poor to acceptable levels. Furthermore, the proposed algorithm always outperforms the always maximum power scenario, while the original algorithm in some cases results in similar performance. The reason for this is that the existence of the coefficient α in the proposed algorithm does not allow the system to reach the worst case of completely unregulated transmission since it always compensates for at least a portion of the underestimated interference. Another interesting point is that, as the number of users increases, the average utility of the system decreases, although extreme values are not affected significantly. This is justified by the fact that the interference exhibits a cumulative behavior that affects all other user pairs, therefore reducing the average utility. However, extreme values are mainly the outcome of the topology and the relative distance of the user pairs, thus are less sensitive to the number of users.

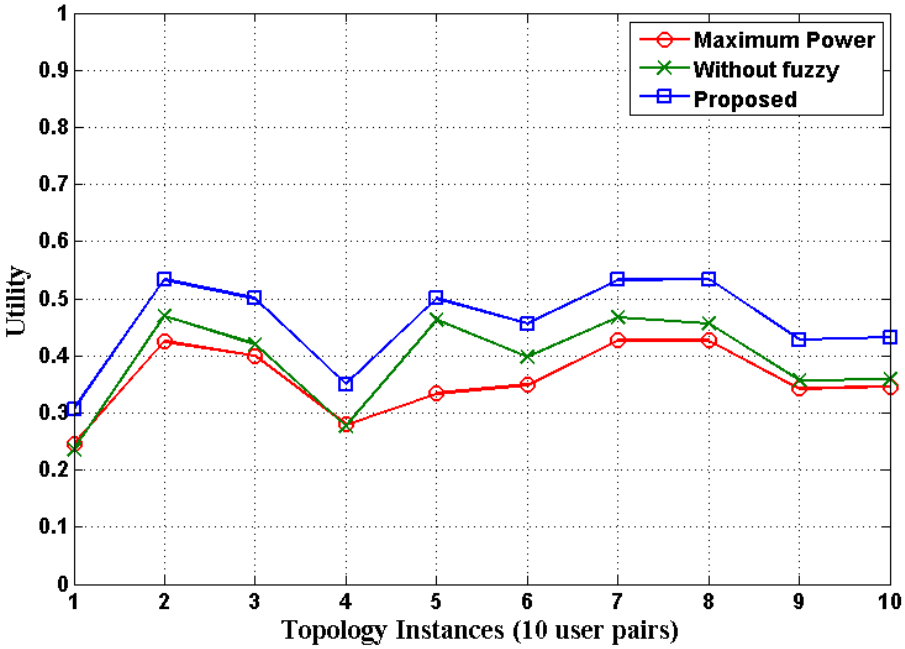

(a)

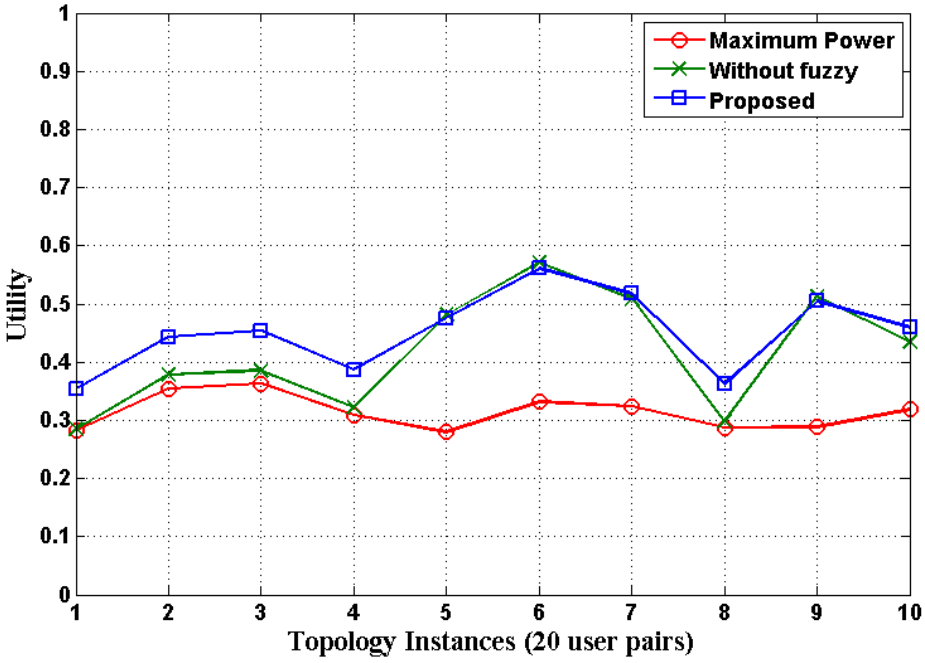

(b)

Figure 5.26: Utility values for the proposed algorithm, the always transmit with the maximum valid power scenario and the original algorithm without coefficient α for (a) 10 and (b) 20 user pairs

The next step is to compare the results of the proposed algorithm using OFDM and FBMC systems. However, a short outline of the FBMC technique is required. According to the principle of transmission based on filter banks, the transmitter incorporates A Synthesis Filter Bank (SFB) while the receiver incorporates an Analysis Filter Bank (AFB). In the structure, the Fast Fourier Transform (FFT) is present as in OFDM [Zha10-3]. It is however augmented, to complete a filter bank, by the Polyphase Network (PPN) which is comprised of a set of digital filters, whose

coefficients, globally form the impulse response of the so-called prototype low-pass filter. FBMC systems have somewhat increased hardware complexity compared to the classical OFDM approach, but compensate for this with a number of advantages. Among others, they do not require guard time and cycle prefix, while the use of Offset QAM (OQAM) implies that the full capacity of the transmission bandwidth is achieved. The improvement in the total utility of a network consisting of ten user pairs if the proposed algorithm is used with FBMC over OFDM is depicted in Figure 5.27.

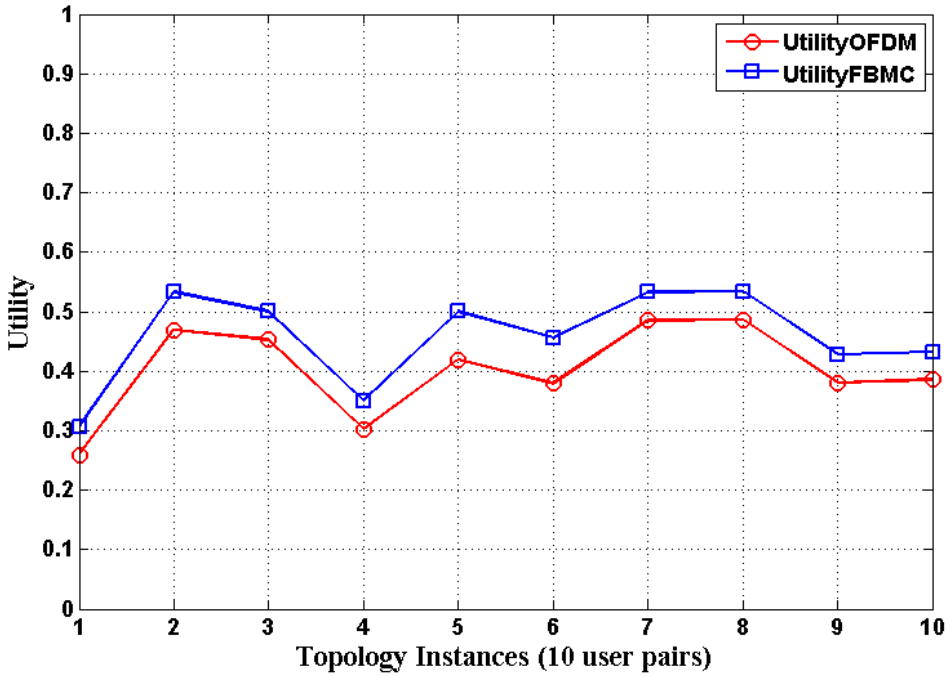

Figure 5.27: Utility function for the proposed algorithm with FBMC and OFDM

This improvement stems from the fact that FBMC uses lower transmission power for the same bandwidth compared to OFDM [Wal08] and therefore causes reduced interference. The proposed algorithm is able to transparently exploit this improvement and translate it in increased utility values. To evaluate the resilience of the algorithm in the presence of long update time intervals we perform simulations with the assumption that some of the messages are delayed and, consequently, other nodes do not have the latest interference price information that has been announced. Thus, the definition of “long update times” that we consider in this work is to be at least equal to twice the average update time (so that other nodes have updated the announced interference price in this interval). Since it is already established that transmitting with the maximum power is the lower bound of performance for both the original and the proposed algorithm, in this scenario we evaluate the behavior of the original and the proposed algorithm with both FBMC and OFDM, in order to study the effect of increased delays on each of these cases.

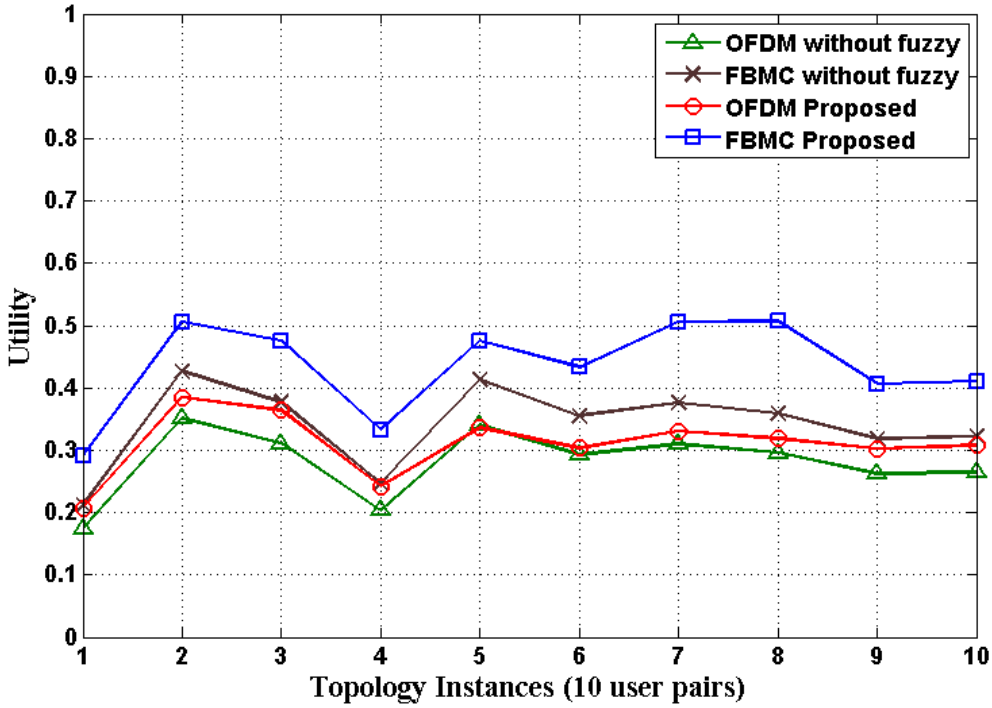

Figure 5.28: Utility values for the original and the proposed algorithm with both FBMC and OFDM, under the assumption of long message delays (10 user pairs)

A first point that is noteworthy is the fact that the improved Physical layer of FBMC in this scenario provides a significant advantage that even surpasses the advantage offered by the proposed algorithm. Therefore, using FBMC with the original algorithm is better for this case than using OFDM with the proposed algorithm. The best option is to use the proposed algorithm with FBMC, combining the advantage of improved Physical layer capabilities and improved upper layer functions. Regarding the latter point, the proposed algorithm consistently outperforms the original one when both use the same Physical layer (FBMC) under the assumption of long delays. Furthermore, if we juxtapose Figure 5.28 with Figure 5.26 we can derive some additional conclusions. Specifically, although the average utility values are reduced for all algorithms, the proposed algorithm is not affected as much as the original from the increased delays, thus the property of "graceful degradation" is indeed enhanced. Since real systems usually have to cope with non-ideal conditions, this property is highly desirable.

Finally, it is very important to quantify the performance improvement in terms of conventional network metrics, to show the relation between a higher overall utility value and parameters that directly affect the user experience. Since the main comparison is between the original algorithm and the proposed one, their behavior in terms of SINR is compared in Figure 5.29. SINR is chosen as the most appropriate metric for comparison as it reflects directly on the QoS and the final user experience and can also be compared without considering external parameters, such as modulation and coding schemes that will impact for example the final BER of the system. The two graphs are following a similar pattern but the proposed algorithm consistently outperforms the original when the interference is underestimated, as it compensates for the interference underestimation and raises SINR to acceptable levels, especially for the lower values.

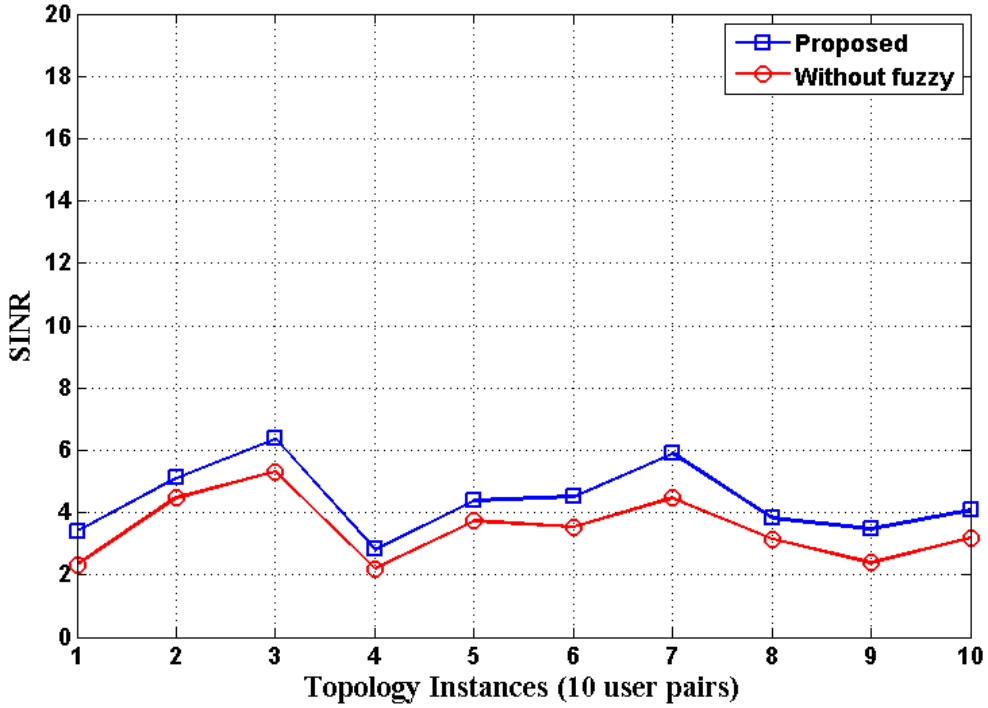

Figure 5.29: SINR for the original and the proposed algorithm under 25% underestimation of interference

Regarding the overall simulation time and scalability properties of the algorithm, for all cases, the number of iterations for convergence is comparable to the number of user pairs. More specifically, for 10-30 user pairs usually less than thirty and up to fifty iterations are required for reaching the final steady state. Furthermore, the average execution time on a Core2 Quad Q9400 CPU operating at 2.66 GHz is less than two minutes for up to 20 user pairs and approximately five minutes for up to 30 user pairs [Mer10].

5.3.4 Optimal Period Definition for Triggering Power Control

One of the most important issues in cooperative Cognitive Radio networks is to define how often the network nodes trigger the decision making modules. In the case of the previously described algorithm, the decision making module is the power control unit. Thus, we need to define the t_{ai} time instances of section 5.3.2 where users update their transmission power levels. Many factors influence this choice, including the hardware capabilities of the devices, the total number of nodes, as well as the nature of the Cognitive Radio network. If the power control mechanism is not executed very often, the users tend to transmit using higher power than required, which is not efficient from an energy point of view. On the other hand, very frequent triggering of the transmission power decision module will result in better regulation of the transmission power between different user pairs, but will also imply an increased cost in terms of energy and overhead for the additional signaling required. These two factors need to be balanced in order to achieve an optimal operation of the entire system in terms of energy consumption. In this direction, the counterbalancing factors shall be modeled analytically in order to proceed to the derivation of the optimal solution.

The status of the user is modeled as a two-state continuous-parameter Markov model, similar to the one described in [Mer09]. State 0 corresponds to an appropriate transmission power level, while state 1 corresponds to an excessive transmission power level. Let λ and μ denote the rates of leaving states 0 and 1, respectively, and let S_t denote the user's state at time t. For this model, the time interval during which the transmission power is at the appropriate (state 0) or excessive level (state 1) follows an exponential distribution with a mean time that equals the parameters $1/\lambda$ and $1/\mu$, respectively. Thus, the transition probabilities $P_{i,j}(t)$ from state i at time t_0 to state j at time t_0+t are

$$P_{0,1}(t) = \frac{\lambda}{\lambda+\mu}\left(1-e^{-(\lambda+\mu)t)}\right)$$
$$P_{0,0}(t) = 1-P_{0,1}(t)$$
$$P_{1,0}(t) = \frac{\mu}{\lambda+\mu}\left(1-e^{-(\lambda+\mu)t)}\right)$$
$$P_{1,1}(t) = 1-P_{1,0}(t).$$

The steady-state probabilities, upon an arbitrary observation instant, are $\pi_0=\mu/(\lambda+\mu)$ and $\pi_1=\lambda/(\lambda+\mu)$, respectively. If the transmission power increases beyond the appropriate level (as determined by (5.55)) during a transmission cycle, the user has to detect this event and thus select a lower transmission power level so as to reduce the interference caused to other users. In order to select the "optimal" transmission power level the user triggers the power control unit. Each execution of the power control unit is assumed to have a finite duration D and energy cost E.

We are focusing on a periodic power update strategy where the nth power control action is executed at time $t_n = nT$, $1 \le n \le N$, T is the update period, B is the duration of the session and $N = \lfloor B/T \rfloor$ is the total number of power control actions performed during a session (for simplicity we disregard the floor function). In every execution of the power control module, if excessive transmission power is detected, the user sets its transmission power using (5.55). Let p_d denote the probability of detecting excessive transmission power with a single execution of the power regulation mechanism, $p_{fd}(n)$ denote the probability of detecting excessive transmission power with the nth execution, and p_{fd} denote the probability of detecting excessive transmission power with any one of the N executions of the power control module. For the above model and power update strategy, we have

$$p_d = P_{0,1}(T) = \frac{\lambda}{\lambda+\mu}\left(1-e^{-(\lambda+\mu)T)}\right)$$
$$p_{fd}(n) = (1-p_d)^{n-1}p_d = P_{0,0}(T)^{n-1}\cdot P_{0,1}(T)$$
$$p_{fd} = \sum_{n=1}^{N} p_{fd}(n) = 1-P_{0,0}(T)^{\frac{B}{T}}.$$

We define q as the probability that the transmission power becomes excessive during the time interval [0, B] that is required for finishing a session (B is assumed to be considerably larger than the time required for the algorithm to converge). Let d denote the probability that the transmission power exceeds the appropriate level during the time interval [0, B], and this is detected by any of the N monitoring actions. Under these assumptions, the detection probability is given from the following formula

$$d = q \cdot p_{fd}.$$

If the transmission power becomes excessive during an active session, the user will detect this in the next execution of the power control module and will be forced to perform a transmission power update and, consequently, proceed to announce the updated interference price. However, the additional power P_{extra}, which is used in the time interval before the identification of the excessive transmission power, is considered as wasted and results in a factor $E_{extra} = P_{extra} T$ of wasted energy. We can analyze P_{extra} as the difference between the optimal transmission power and the utilized transmission power level. Then, the value W_E of the wasted energy can be written as follows

$$W_E = \frac{B}{T}(E + E_{extra}) \cdot (1 - p_{fd}) + \sum_{n=1}^{B/T} N \cdot (E_{extra} + E) \cdot p_{fd}(n).$$

The first part of W_E expresses the energy that is wasted for the entire session duration if no excessive energy is detected, while the second part expresses the wasted energy if the fact that the user is transmitting with higher energy than actually required is alleviated by the nth power control action. Then we define the cost function $C(T)$ that expresses the energy cost incurred when selecting a periodic power update strategy with period T

$$C(T) = (1 - q) \cdot N \cdot E + q \cdot W_E.$$

The first part of $C(T)$ represents the energy that is wasted in power update actions, when the transmission power level is appropriate (an event of probability $(1-q)$). This part of the cost function favors the selection of large monitoring periods. The second part of $C(T)$ represents the energy wasted when the transmission power level is excessive (an event of probability q). Thus, the second part of $C(T)$ favors the selection of small monitoring periods (i.e., it favors frequent monitoring actions). The optimal period can be derived by solving the following equation

$$\frac{dC(T)}{dT} = 0.$$

However, the previous equation does not have a simple closed-form solution and it can only be solved numerically, using techniques such as Newton's method. Solving it in mathematics we derive the graph presented in Figure 5.30. The figure depicts the energy cost $C(T)$ for periodic monitoring as a function of the monitoring period T, for typical rates of leaving state 0 (appropriate transmission power level) and state 1 (excessive transmission power level) and the average session duration B. Selection of the optimal period can result in considerable energy gains; specifically, Figure 5.30 shows that the improvement in terms of energy consumption can be almost up to 40%.

A three-dimensional graph showing the energy cost $C(T)$ as a function of the monitoring period and the session duration is presented in Figure 5.31. The graph shows the reduction of the optimal monitoring period, favoring more frequent power updates, if the time during which the user remains in state 1 is increased, meaning that it is more probable to allocate excessive transmission power level. Moreover, it shows that frequent updates are also becoming more favorable when the session duration is larger than, in that case, the potential for excessive transmission power and consequently increased interference is more significant. Specifically, we derive that for this scenario the energy

cost $C(T)$ is minimized if the test period T is approximately 100 times smaller than the average session duration.

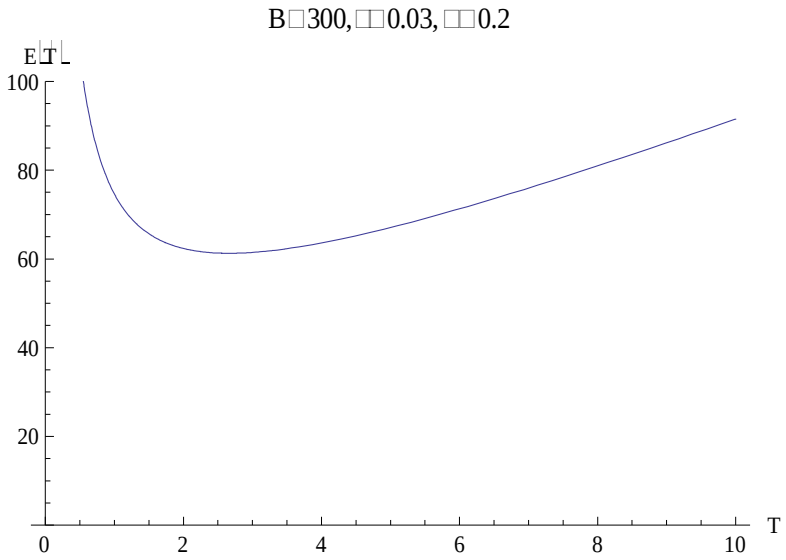

Figure 5.30: Energy cost as a function of monitoring period T

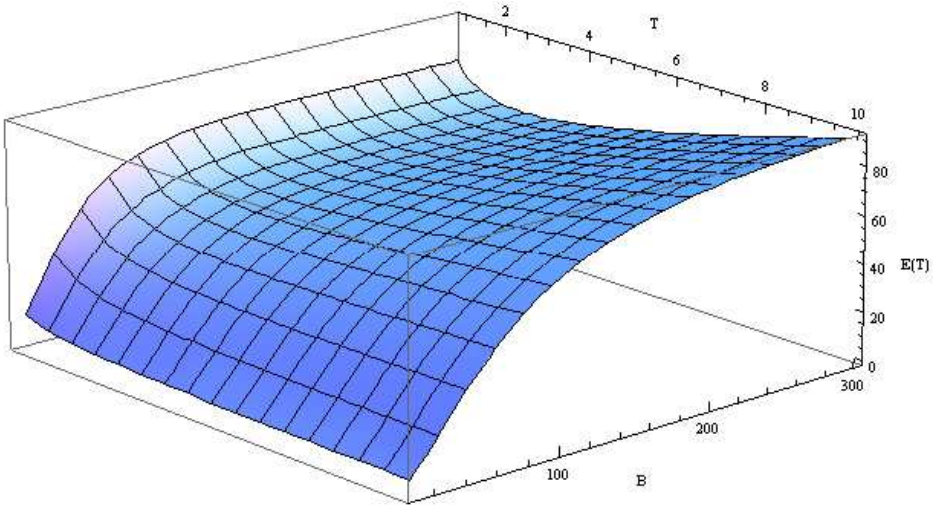

Figure 5.31: Energy cost as a function of T and B

5.3.5 Summary

A power control algorithm, based on the algorithm of [Hua05], was presented for cooperative DSA in unlicensed bands, utilizing MAC layer mechanisms for message exchange ("interference prices") between the secondary nodes, in order to achieve interference mitigation. The main improvement in this work [Mer10] compared to [Hua05] is the introduction of a coefficient α that is serving as the weight of the interference term, increasing its impact in cases of imperfect message exchange, long update time intervals for interference prices, as well as increased number of users. In such cases, the interference that is caused to other user pairs by an increase in the transmission power of a user is often underestimated, resulting in a convergence of the algorithm to a non-optimal solution. In the presence of such uncertainties, if this underestimation is compensated by a properly defined weight

parameter, the system approximates its optimal behavior as in the case of "perfect" message exchange.

The value of the weight parameter was derived from a fuzzy logic reasoner. Fuzzy logic was selected because it is particularly effective in dealing with uncertainties and vague requirements. Moreover, the outcome of the proposed algorithm has been compared to the original algorithm in terms of the overall utility level (defined as the sum of the user utilities) under uncertainties that cause 25% underestimation of interference. Furthermore, comparison was also made between the proposed algorithm in FBMC and OFDM systems. In this case, using FBMC increased the achieved utility. The improvement stems from the fact that FBMC uses lower transmission power for the same bandwidth compared to OFDM and therefore causes reduced interference. Additionally, a scenario of long update time intervals in which some of the messages are delayed causing other nodes to not have the latest interference price information was considered, and the performance of both algorithms in a this case of non-ideal message exchange was evaluated. Results indicate that the algorithm consistently outperforms previous schemes in terms of SINR under uncertainties and can transparently exploit the improved physical layer offered by FBMC. Finally, the optimal period for triggering the power control module has been defined using Markov models.

5.4 Appendix - Derivation of the Optimal Power Allocation in (5.44) and (5.52)

We want to find the optimal solution for the following optimization problem

$$\max_{P_{i,m}} \sum_{i=1}^{N} \log_2 \left(1 + \frac{P_{i,m} \left| h_{i,m} \right|^2}{\sigma_i^2} \right) \tag{5.57}$$

$$s.t. \qquad \sum_{i=1}^{N} P_{i,m} \Omega_{i,m}^{l} \le I_{th}^{l} \qquad \forall l \in \{1, \cdots, L\} \tag{5.58}$$

$$\sum_{i \in \mathrm{N}_m} P_{i,m} \le \overline{P_m} \qquad \forall m \tag{5.59}$$

$$P_{i,m} \ge 0 \qquad \forall i \,. \tag{5.60}$$

The problem above is a convex optimization problem. Introducing the lagrange multipliers α^l, μ_i, and β_m for the inequality constraints in (5.58), (5.59) and (5.60) respectively, The Lagrangian can be written as

$$G = -\sum_{i=1}^{N} R_i \left(P_{i,m}, h_{i,m} \right) + \sum_{l=1}^{L} \alpha^l \left(\sum_{i=1}^{N} P_{i,m} \Omega_{i,m}^{l} - I_{th}^{l} \right) + \sum_{m=1}^{M} \beta_m \left(\sum_{i \in \mathrm{N}_m} P_{i,m} - \overline{P_m} \right) - \sum_{i=1}^{N} P_{i,m} \mu_i \,. \tag{5.61}$$

The Karush-Kuhn-Tucker (KKT) conditions can be written as follows

$$
\begin{aligned}
&\alpha^l \geq 0 \qquad \forall l \in \{1,2,\cdots,L\}; \qquad \beta_m \geq 0 \qquad \forall m \in \{1,2,\cdots,M\};\\
&\mu_i \geq 0 \qquad \forall i \in \{1,2,\cdots,N\}; \qquad P_{i,m}^* \geq 0;\\
&\alpha^l \left(\sum_{i=1}^{N} P_{i,m}^* \Omega_{i,m}^l - I_{th}^l \right) = 0\\
&\beta_m \left(\sum_{i \in \mathrm{N}_m} P_{i,m}^* - \overline{P_m} \right) = 0; \qquad \forall m \in \{1,2,\cdots,M\}\\
&\mu_i P_i^* = 0; \qquad \forall i \in \{1,2,\cdots,N\}\\
&\sum_{i=1}^{N} P_{i,m} \Omega_{i,m}^l - I_{th}^l \leq 0\\
&\sum_{i \in \mathrm{N}_m} P_{i,m} - \overline{P_m} \leq 0; \qquad \forall m \in \{1,2,\cdots,M\}\\
&\frac{\partial G}{\partial P_{i,m}^*} = \frac{-1}{\frac{\sigma_i^2}{\left|h_{i,m}\right|^2} + P_{i,m}^*} + \sum_{l=1}^{L} \alpha^l \Omega_{i,m}^l + \sum_{m=1}^{M} \beta_m - \mu_i = 0
\end{aligned}
\tag{5.62}
$$

Rearranging the last condition in (5.62) we get

$$
P_{i,m}^* = \frac{1}{\sum_{l=1}^{L} \alpha^l \Omega_{i,m}^l + \sum_{m=1}^{M} \beta_m - \mu_i} - \frac{\sigma_i^2}{\left|h_{i,m}\right|^2}. \tag{5.63}
$$

Since $P_{i,m}^* \geq 0$, we get

$$
\frac{\sigma_i^2}{\left|h_{i,m}\right|^2} \leq \frac{1}{\sum_{l=1}^{L} \alpha^l \Omega_{i,m}^l + \sum_{m=1}^{M} \beta_m - \mu_i}. \tag{5.64}
$$

If $\frac{\sigma_i^2}{\left|h_{i,m}\right|^2} < \frac{1}{\sum_{l=1}^{L} \alpha^l \Omega_{i,m}^l + \sum_{m=1}^{M} \beta_m}$, then $\mu_i = 0$ and hence

$$
P_{i,m}^* = \frac{1}{\sum_{l=1}^{L} \alpha^l \Omega_{i,m}^l + \sum_{m=1}^{M} \beta_m} - \frac{\sigma_i^2}{\left|h_{i,m}\right|^2}. \tag{5.65}
$$

Moreover, if $\frac{\sigma_i^2}{\left|h_{i,m}\right|^2} > \frac{1}{\sum_{l=1}^{L} \alpha^l \Omega_{i,m}^l + \sum_{m=1}^{M} \beta_m}$, from (5.63) we get

$$\frac{1}{\sum_{l=1}^{L}\alpha^{l}\Omega_{i,m}^{l}+\sum_{m=1}^{M}\beta_{m}-\mu_{i}}\geq\frac{\sigma_{i}^{2}}{\left|h_{i,m}\right|^{2}}>\frac{1}{\sum_{l=1}^{L}\alpha^{l}\Omega_{i,m}^{l}+\sum_{m=1}^{M}\beta_{m}} \tag{5.66}$$

and since $\mu_i P_{i,m}^{*}=0$ and $\mu_i \geq 0$, we get that $P_{i,m}^{*}=0$.

Therefore, the optimal solution can be written as follows

$$P_{i,m}^{*}=\left[\frac{1}{\sum_{l=1}^{L}\alpha^{l}\Omega_{i,m}^{l}+\sum_{m=1}^{M}\beta_{m}}-\frac{\sigma_{i}^{2}}{\left|h_{i,m}\right|^{2}}\right]^{+} \tag{5.67}$$

where $\left[x\right]^{+}=\max\left(0,x\right)$. If only one SU is assumed with interference constraint I_{th}^{l*}, (5.67) is reduced to

$$P_{i,m}^{*}=\left[\frac{1}{\alpha^{l*}\Omega_{i,m}^{l*}+\sum_{m=1}^{M}\beta_{m}}-\frac{\sigma_{i}^{2}}{\left|h_{i,m}\right|^{2}}\right]^{+}. \tag{5.68}$$

6 The "Good Neighbour" Strategy for Decentralized Dynamic Spectrum Allocation

The ultimate implication of the concept of cognitive radio is that a communication system, for example a base station and its users, which detect an unoccupied frequency band in the spectrum, should have the freedom to exploit it, without having to go through a lengthy clearance procedure and coordinate with other systems in the same geographical area. Hence, the denomination of opportunistic unsynchronized networks.

A first condition for such an environment to be realistic is the availability of an adequate physical layer. The FBMC technique can meet the objectives in terms of performance and flexibility. Then, a protocol must be developed to ensure global convergence and an overall transmission capacity close to the optimal possible value at a given place and a given time. To that purpose, the approach called "Good Neighbour" (GN) has been presented in deliverables [D8.1] [D8.2] and published in article [Kuz10].

The subsections are organized as follows. In section 6.1 the GN approach is briefly reviewed in the methodology level. Some corresponding technical details are provided in section 6.2. The issue of practical adaptation of spectrum allocation solutions is discussed in section 6.3. A summary is given in section 6.4.

6.1 Overview of the GN Approach

The approach consists of building the capacity requested by the users through a threshold regulated local search and with minimum changes in frequency band allocation to reduce interference non-stationarity to other systems. In fact, it can be viewed as some kind of rule-regulated cooperation between spectrum sharing subsystems without explicit data exchange between them and the emphasis is on decentralized dynamic spectrum allocation. A brief overview of the main characteristics is as follows.

A. Local search based on antenna array interference mitigation

In the context under consideration, the base stations dynamically allocate the spectral resources to their users, according to their requests. If the available capacity, in terms of number of sub-channels and bit rate per sub-channel, is sufficient to meet the needs of the users, the allocation procedure is simple. There is just the option to use more sub-channels than strictly needed and distribute the power, or maximize the bit rate and occupy the minimum number of sub-channels. The latter approach requires more power, but it facilitates the access for other systems. However, in some circumstances and at some time, the resources might be insufficient and several systems have to share the same frequency bands. Then, provided the base stations are equipped with multiple antennas, they can resort to beamforming to mitigate interference and maximize the Signal-to-Interference-plus-Noise Ratio (SINR) for each of their users. The SINR values obtained locally constitute the basis for spectrum allocation.

B. Threshold based spectrum allocation

The challenge for the opportunistic protocol is to distribute the total spectral capacity, taking into account the beamforming contribution to interference reduction, among the systems, in real time

and with minimum delay. A simple approach consists of defining a capacity threshold C_0, and preventing the extension of the present frequency band and the selection of a new band at the base station for a particular user, if its capacity C is already above the threshold C_0. The objective of the concept is to guarantee resource sharing and increase the probability of global convergence of the process. An issue is how to determine the threshold. If it is too low, convergence is fast but some users might be frustrated and the total spectrum capacity might end up below the maximum possible value. If it is too high, convergence may be long or hazardous. Under the hypothesis of non-cooperation, the threshold value must be determined locally by each base station. A technique exploiting the SINR measurements for all the available sub-channels has been described in [D8.1].

C. Minimum number of band extensions or new band allocations to achieve the given threshold

In a dense exploitation of the spectrum, any new band allocation in a system causes interference to other systems. Then, the objective of this concept is to speed up convergence by minimizing the non-stationarity caused by the changes in frequency allocations and the resulting interference modifications.

Clearly, space-time spectrum sensing is critical for the "Good Neighbour" (GN) dynamic spectrum allocation algorithm and it has to be implemented at each base station to estimate the weight vectors and SINR in all the available frequency bands. To do this, it is assumed that users transmit pilot symbols during sensing intervals and data signals during data intervals. In [D8.2], the GN algorithm has been modified to exploit estimated second order statistics. A space-time spectrum sensing protocol has been designed that allows such estimation. The impact on the performance of the finite amount of data has been investigated and the minimization of the required amount of the training data has been studied.

6.2 Further Details on GN and Spectrum Allocation

In this section, the major contributions of [D8.1] and [D8.2] on Decentralized Dynamic Spectrum Allocation (DDSA) with multiple antenna array and interference mitigation are briefly reviewed and some additional details are provided.

6.2.1 System Model

The cognitive radio system shown in Figure 6.1 is considered. It consists of N independent subsystems with respect to base stations BS_n, $n=1,\ldots,N$. Each Base Station (BS) offers service for M users or Subscriber Stations (SS), denoted as users SS_{nm} ,. $m=1,\ldots,M$. The available frequency bands are denoted by F with $F \geq M$. Let assume that each base station deploys K antenna elements to receive and detect signals. The narrowband receive signal model of the *n*-th subsystem can be presented as

$$\mathbf{x}_{nf}(t) = \sum_{l=1}^{N}\sum_{m=1}^{M} \delta_{fd_{lm}} \cdot q_{lm}\mathbf{h}_{d_{lm}mln}s_{lm}(t) + \mathbf{z}_{nf}(t), n=1,\ldots,N,\ f=1,\ldots,F, \qquad (6.1)$$

where $\mathbf{x}_{nf}(t)$ denotes the $K\times 1$ receive signal vector by BS_n in the *f*-th band at the time instant t, $\mathbf{h}_{fmln}$ denotes the $K\times 1$ propagation channel vector in the *f*-th band between BS_n and the *m*-th user

within the *l*-th subsystem, $s_{nm}(t)$ is the SS_{nm} transmitted signal with $\mathrm{E}\{|s_{nm}(t)|^2\}=1$ and q_{nm}^2 is its power with constraint $\sum_{m=1}^{M} q_{nm}^2 = Q$, $n=1,\ldots,N$, $\mathbf{z}_{nf}(t)$ is a $K\times 1$ Additive White Gaussian Noise (AWGN) vector with $\mathrm{E}\{\mathbf{z}_{nf}(t)\mathbf{z}_{nf}^{*}(t)\}=\sigma^2\mathbf{I}_K$, d_{nm} is the *nm*-th element of the $N\times M$ decision matrix **D** denoting the frequency band assigned to user SS_{nm}, $\mathrm{E}\{\cdot\}$ is the averaging operator, $(\cdot)^*$ is the conjugate transpose operation, $\mathbf{I}_K$ is the $K\times K$ unity matrix, and

$$\delta_{ij}=\begin{cases}1 & \text{if } i=j\\ 0 & \text{if } i\neq j\end{cases}. \tag{6.2}$$

BSs have full information and control of their own users. In particular, they can estimate propagation channels $\mathbf{h}_{fmln}$ in all the available bands and assign the individual bands and transmit powers to their own users.

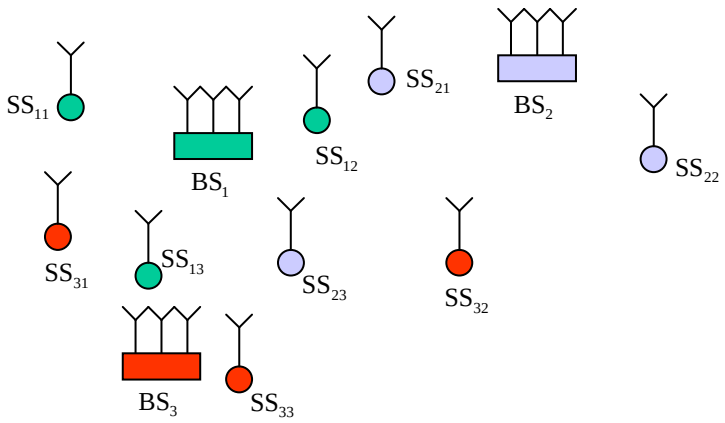

Figure 6.1: System model for horizontal CR scenario

6.2.2 Random Channel Allocation

To understand and obtain the analytical performance bound of DDSA strategy, the random channel allocation has to be considered, as shown in Figure 6.2. The system consists of N subsystems, M users per subsystem and F available frequency bands. Assume that the total MN users are uniformly distributed with F frequency bands, in order to utilize the spectral resource in a very balanced manner.

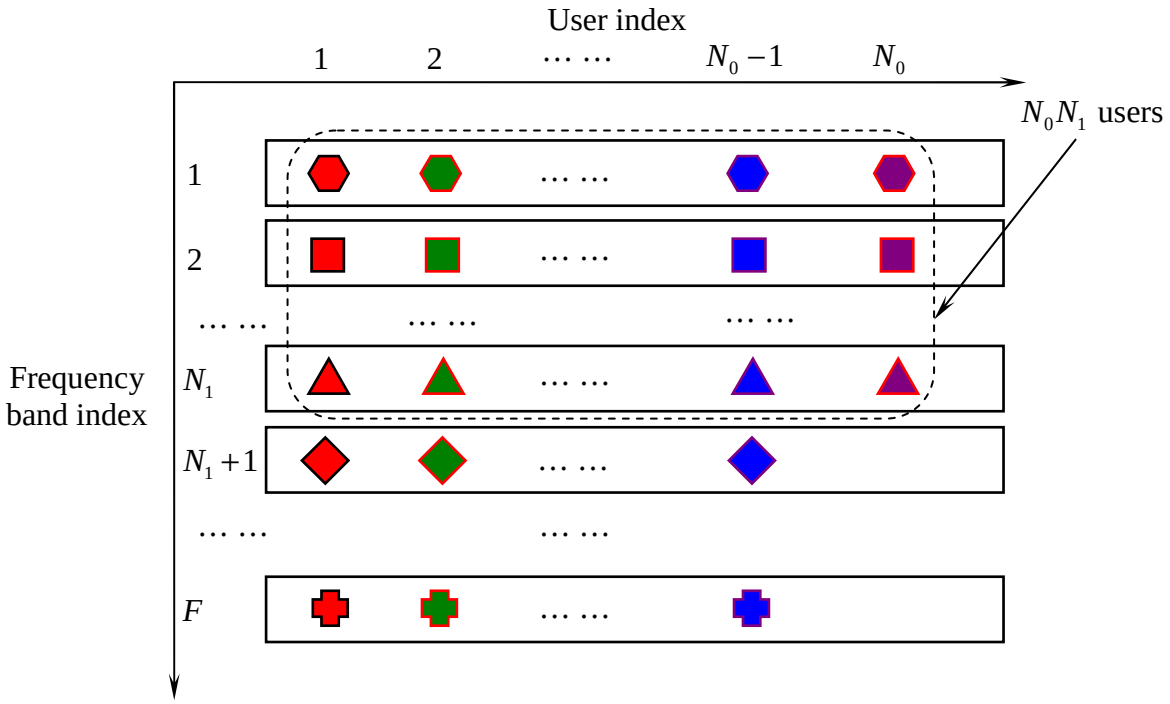

Figure 6.2: Illustration of random channel allocation

As shown in Figure 6.2, N_1 frequency bands include N_0 users per band, and the rest $F-N_1$ frequency bands include N_0-1 per band. The factors N_0 and N_1 can be straightforward given by

$$N_0 = \left\lceil \frac{MN}{F} \right\rceil \tag{6.3}$$

and

$$N_1 = MN - F(N_0 - 1), \tag{6.4}$$

respectively, where $\lceil \cdot \rceil$ denotes the ceiling function. Notice that the users in an arbitrary frequency are selected from different base stations, which is demonstratively shown in Figure 6.2, by distinguishing the symbols from their corresponding colors. The following prerequisite needs to be satisfied

$$N \geq N_0 . \tag{6.5}$$

Throughout the investigation, the inequality is assumed to hold

$$K \geq N_0 . \tag{6.6}$$

Thus, the diversity gain can be theoretically achieved in a multiple antenna system with K receive antennas and N_0 users within a frequency band. For a base station with $K < N_0$ receive antennas, the strong Co-Channel Interference (CCI) cannot be statistically avoided, which yields a relative low Signal-to-Interference-plus-Noise Ratio (SINR) for a user of interest. In the real practical

implementation, the network operator is required to estimate the system load and adaptively adjust the number of receive antennas K, to satisfy (6.6).

In [D8.1] the performance bound for the $N_0 N_1$ users within N_1 frequency bands is discussed. In this report, this issue about the spectrum allocation candidates is investigated again with respect to all MN users. Let the system with $M=2$, $N=6$ and $F=3$ be considered as an example. It yields $N_0=4$ and $N_1=3$ by considering (6.3) and (6.4). Obviously, this is a special case, due to $F=N_1=3$. The spectrum allocation procedure can be summarized as:

1. Select $N_0=4$ users from $N=6$ different base stations. The number of combination is $C_{N_0}^{N}=\left[\frac{N!}{(N-N_0)!N_0!}\right]_{N=6,\,N_0=4}=15$. This step is represented by the black arrows in Figure 6.3.
2. The unallocated users of the rest BS can be allocated in the rest frequency bands uniquely. This step is represented by the green arrows in Figure 6.3.
3. Channel Spectrum allocation for the rest $N_0=4$ users. The number of combination is $C_{2N_0-N}^{N_0}C_{N-N_0}^{N-N_0}=\left[\frac{N_0!}{(2N_0-N)!(N-N_0)!}\cdot\frac{(N-N_0)!}{0!(N-N_0)!}\right]_{N=6,\,N_0=4}=6$. This step is represented by the red arrows in Figure 6.3.
4. As the users in the same BS are independent, the factor M^N should be thus considered.

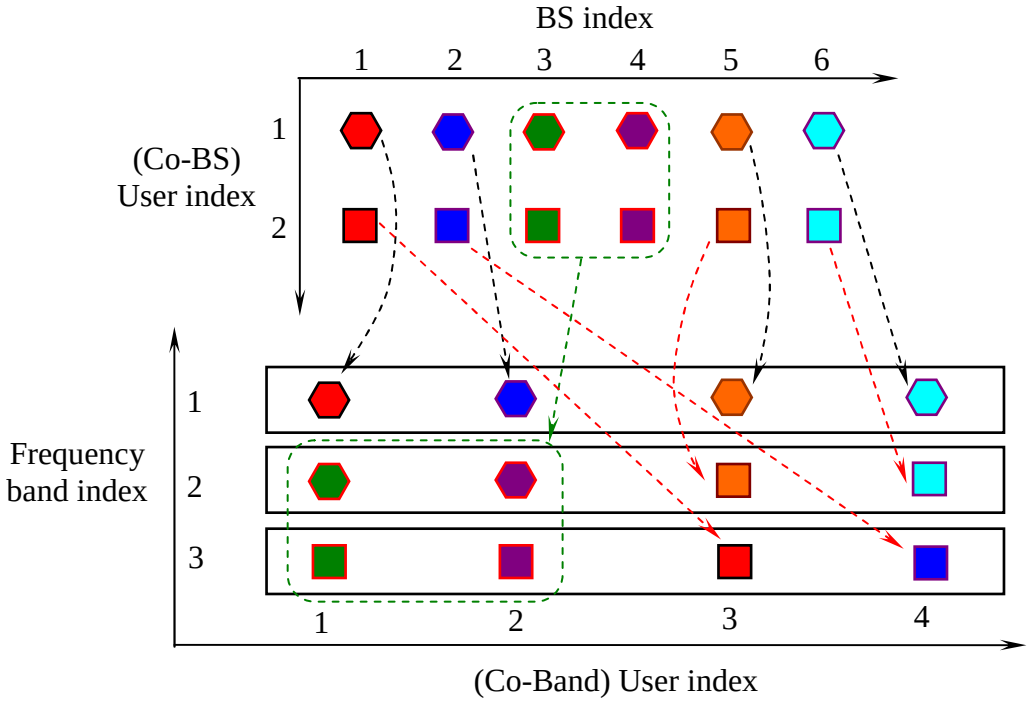

Figure 6.3: Illustration of channel spectrum allocation procedure for a system with $M=2$, $N=6$ and $F=3$

Hence, the number of all the channel resource allocation candidates can be given by

$$L=C_{N_0}^{N}(C_{N_0}^{2N_0-N}C_{N-N_0}^{N-N_0})M^N=5760.$$

In the general case, it holds $F > N_1$. Let the system with $M = 2$, $N = 5$ and $F = 3$ be considered as another example. It yields straightforward $N_0 = 4$ and $N_1 = 1$ by deploying (6.3) and (6.4). The channel allocation procedure can be similarly summarized as:

1. Selecting one frequency band from $F = 3$ bands and allocating $N_0 = 4$ users from $N = 5$ different base stations due to the asymmetric allocation, the number of combination is $C_1^F C_{N_0}^N = 15$. This step is represented by the black arrows in Figure 6.4.
2. The unallocated users of the rest BS can be allocated in the rest frequency bands uniquely. This step is represented by the green arrows in Figure 6.4.
3. Channel allocation for the rest $N_0 = 4$ users. The number of combination is $C_{2N_0-N-1}^{N_0} C_{N-N_0+1}^{N-N_0+1} = \left[\frac{N_0!}{(2N_0 - N - 1)!(N - N_0 + 1)!} \cdot \frac{(N - N_0 + 1)!}{0!(N - N_0 + 1)!} \right]_{N=5,\, N_0=4} = 6$. This step is represented by the red arrows in Figure 6.4.
4. Finally, the factor $M^N = 2^5 = 32$ should be also considered.

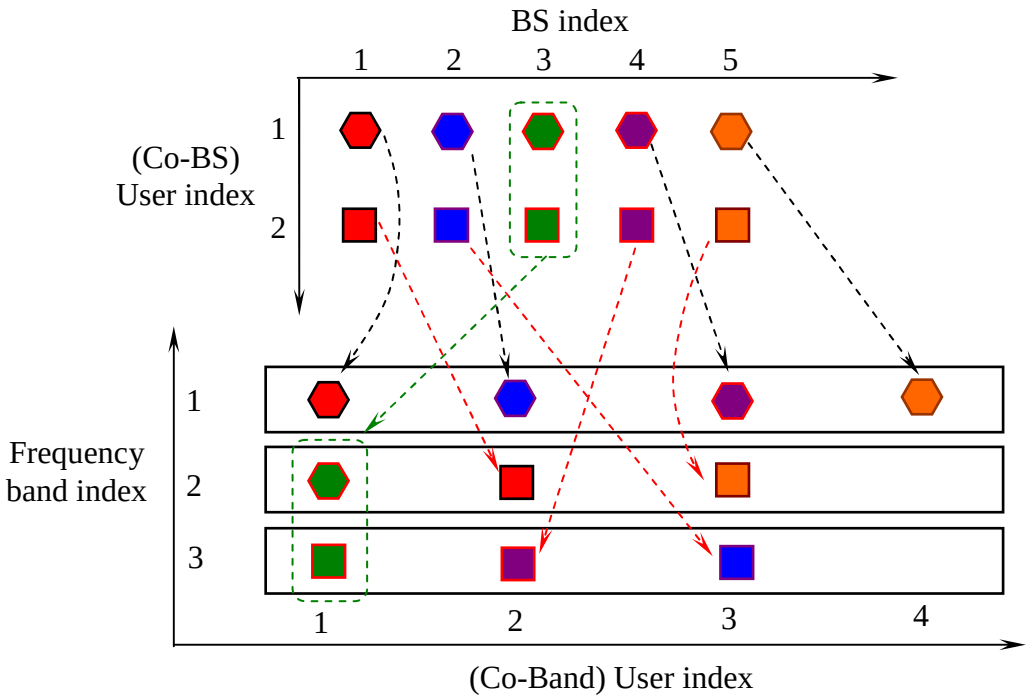

Figure 6.4: Illustration of channel allocation procedure for a system with $M = 2$, $N = 5$ and $F = 3$

Hence, the number of all the channel allocation candidates can be given by

$$L = (C_1^F C_{N_0}^N)(C_{2N_0-N-1}^{N_0} C_{N-N_0+1}^{N-N_0+1}) M^N = 2880.$$

Both examples above present the methodology to estimate and compute the number of the spectrum allocation candidates with respect to the scheme in Figure 6.2, instead of providing a closed mathematical expression, which can be different from case to case, and depends on e.g. whether $F > N_1$ or $F = N_1$. In Table 6.1, the number of the channel allocation candidates L is provided for

some systems with different dimensions. As the reference, by the exhaustive search, the number of the resource allocation candidate is presented by

$$L_{\text{ex}} = (A_M^F)^N = \left[\frac{F!}{(F-M)!} \right]^N . \tag{6.7}$$

Table 6.1: Number of channel allocation of given systems

N	F	M	N_0	N_1	$L_{\text{ex}} = (A_M^F)^N$	L
3	3	2	2	3	216	48
4	3	2	3	2	1296	576
5	3	2	4	1	7776	2880
6	3	2	4	3	46656	5760
7	3	2	5	2	279936	80640

6.2.3 System SINR Distribution

For the given statistically independent normal distributed variables $X_i \sim \mathcal{N}(0,1)$, $i = 1,\cdots,k$, the random variable $x = \sum_{i=1}^{k} X_i^{\,2}$ obeys chi-square distribution with k degrees of freedom, denoted as $x \sim \chi^2(k)$. The Probability Density Function (PDF) of chi-square distribution with k degrees of freedom is given by

$$f_X(x) = \begin{cases} \dfrac{1}{2^{k/2}\Gamma(k/2)} x^{k/2-1} e^{-x/2} & \text{for } x \geq 0 \\ 0 & \text{for } x < 0 \end{cases} ,$$

where $\Gamma(\cdot)$ denotes the Gamma function. Let the channel coefficient of an arbitrary user from the overall N_0 user be denoted as $[\mathbf{h}_i]_j$, with $i = 0,\cdots,N_0 - 1$ and $j = 1,\cdots,K$. The corresponding channel coefficients are assumed to have following distribution as

$$\text{Re}\{[\mathbf{h}_i]_j\} \sim \mathcal{N}(0,\frac{1}{2}) \text{ and } \text{Im}\{[\mathbf{h}_i]_j\} \sim \mathcal{N}(0,\frac{1}{2}).$$

Obviously, it is necessary to focus on the probability density function of random variable $y = g(x) = \frac{1}{2}x = \sum_{i=1}^{k} X_i^{\,2}$. With respect to the dependency property of probability density function, it holds

$$f_Y(y) = \left| \frac{1}{d\left[g^{-1}(y)\right]/dy} \right| \cdot f_X\left[g^{-1}(y)\right] = \left| \frac{1}{d(2y)/dy} \right| \cdot f_X(2y)$$

$$= \begin{cases} 2 \cdot \frac{1}{2^{k/2}\Gamma(k/2)} (2y)^{k/2-1} e^{-2y/2} = \frac{1}{\Gamma(k/2)} y^{k/2-1} e^{-y} & \text{for } y \geq 0 \\ 0 & \text{for } y < 0 \end{cases}.$$

Throughout the investigation, the modified chi-square distribution $f_Y(y)$ is thus considered. In the cognitive radio network, an arbitrary subsystem establishes an $N_0 \times K$ multiuser Multiple Input Multiple Output (MIMO) system, where K denotes the number of receive antennas at the base station, and $N_0 - 1$ stands for the number of users, who produce CCI. It is well known, that the diversity order of the $N_0 \times K$ MIMO system is $K - N_0 + 1$ at high SINR. According to the previous study on the relationship between diversity and chi-square distribution, the $N_0 \times K$ MIMO system has $2(K - N_0 + 1)$ degrees of freedom, and thus the SINR distribution can be obtained straightforward as

$$w(y) = f_Y(y) = \frac{1}{\Gamma(k/2)} y^{k/2-1} e^{-y} = \frac{1}{\Gamma(K - N_0 + 1)} y^{K-N_0} e^{-y}. \quad (6.8)$$

As the diversity order corresponds especially to the high SINR, the function $w(y)$ is the asymptote with respect to high SINR. In Figure 6.5, this effect can be observed, by comparing the 2×4 to the 2×12 MIMO system. Because the 2×12 MIMO system yields higher SINR, the measured PDF function perfectly matches the theoretical PDF function.

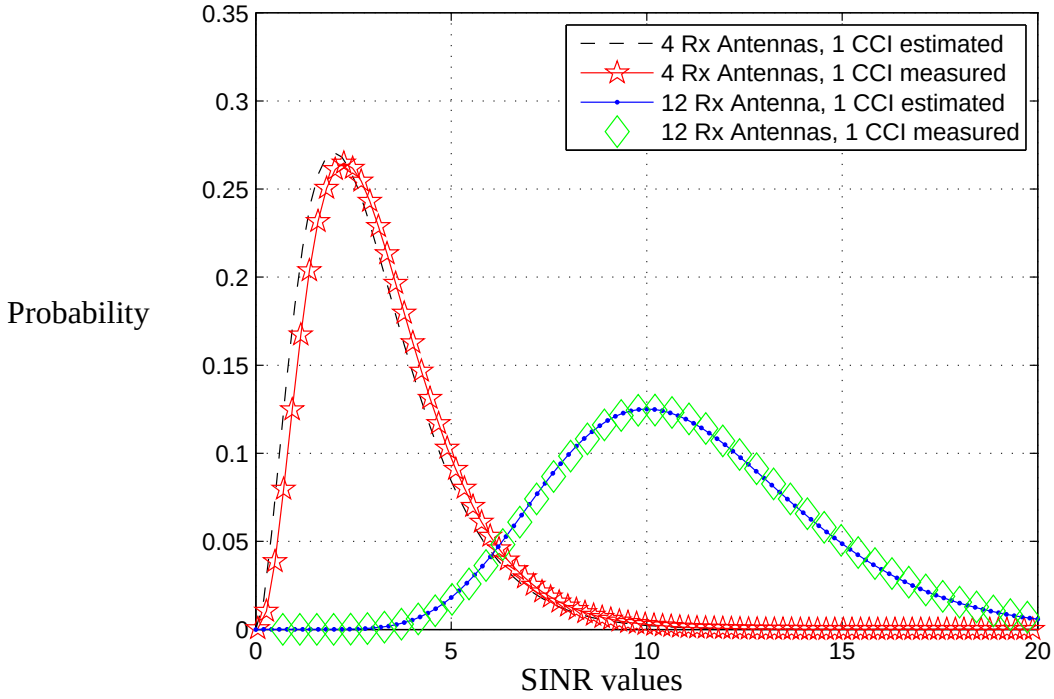

Figure 6.5: Comparison between measured and theorethical PDF curves

For a given PDF function $w(y)$, the term $P_1\left(\frac{\alpha}{\mu_s}, N_0\right) = \int_{\frac{\alpha}{\mu_s}}^{+\infty} w(y)dy$ stands for probability, that an arbitrary user's SINR is bigger than α, shown in Figure 6.6. The term $P_1\left(\frac{\alpha}{\mu_s}, N_0\right)^{N_0 N_1}$ stands for thus the probability, that the SINR of $N_0 N_1$ users are all bigger than α. Consequently, the probability $1 - P_1\left(\frac{\alpha}{\mu_s}, N_0\right)^{N_0 N_1}$ denotes that at least one user out of all $N_0 N_1$ users does exist, whose SINR is smaller than α. Hence, the term $\left[1 - P_1\left(\frac{\alpha}{\mu_s}, N_0\right)^{N_0 N_1}\right]^L$ indicates the probability, that in an arbitrary spectrum allocation option out of all L candidates, one user does exist, whose SINR is smaller than α. An equivalent expression can be given for a system with L spectrum allocation candidates, namely, the maximal value of minimum SINR out of $N_0 N_1$ users is always smaller than α. This expression is presented in the (8.16) of [D8.1] as

$$\Pr\left(\max_{L} \min_{N_0 N_1} \text{SINR} < \alpha\right) = \left[1 - P_1\left(\frac{\alpha}{\mu_s}, N_0\right)^{N_0 N_1}\right]^L .$$

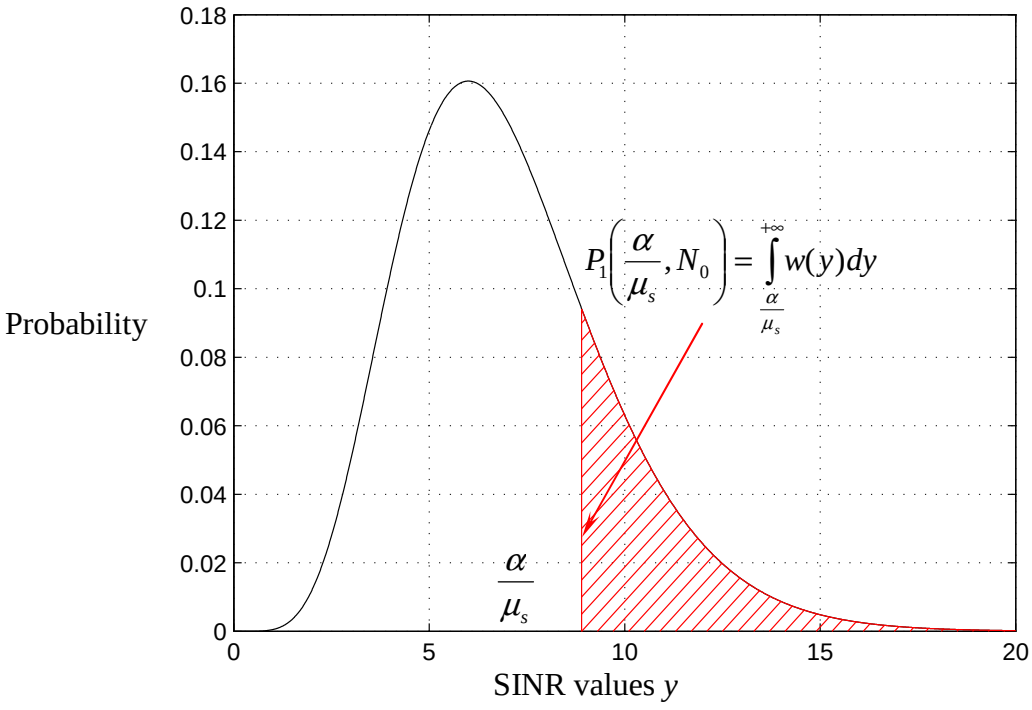

Figure 6.6: Illustration of the probability that an arbitrary user's SINR is bigger than α

By deploying the rule of integration by parts, the probability $P_1\left(\frac{\alpha}{\mu_s}, N_0\right)$ can be straightforward obtained by

$$P_1\left(\frac{\alpha}{\mu_s}, N_0\right) = \int_{\frac{\alpha}{\mu_s}}^{+\infty} w(y)dy = \frac{1}{\Gamma(K-N_0+1)} \int_{\frac{\alpha}{\mu_s}}^{+\infty} y^{K-N_0} e^{-y} dy = \frac{1}{(K-N_0)!} \int_{\frac{\alpha}{\mu_s}}^{+\infty} y^{K-N_0} e^{-y} dy$$

$$= \left[-\frac{y^{K-N_0} e^{-y}}{(K-N_0)!} - \frac{y^{K-N_0-1} e^{-y}}{(K-N_0-1)!} - \cdots - \frac{y e^{-y}}{1!} - \frac{y^0 e^{-y}}{0!} \right]_{\frac{\alpha}{\mu_s}}^{+\infty} = e^{-\frac{\alpha}{\mu_s}} \sum_{j=0}^{K-N_0} \frac{1}{j!} \left(\frac{\alpha}{\mu_s}\right)^j .$$

For the system resource allocation scheme in Figure 6.2, let all MN users be considered. The equation above can be straightforward extended as

$$\Pr\left(\max_{L} \min_{MN} \text{SINR} < \alpha \right) = \left[1 - P_1\left(\frac{\alpha}{\mu_s}, N_0\right)^{N_0 N_1} P_1\left(\frac{\alpha}{\mu_s}, N_0 - 1\right)^{MN - N_0 N_1} \right]^L . \qquad (6.9)$$

The term $P_1\left(\frac{\alpha}{\mu_s}, N_0 - 1\right)^{MN - N_0 N_1}$ indicates the probability, that the SINR of $MN - N_0 N_1$ users in the rest $F - N_1$ frequency bands are all bigger than α. Note that the user number in each band of the rest $F - N_1$ frequency bands is $N_0 - 1$. Hence, the number of CCIs with respect to an arbitrary user is $N_0 - 2$, which is lower than that of previous N_1 frequency bands and thus yields higher diversity order.

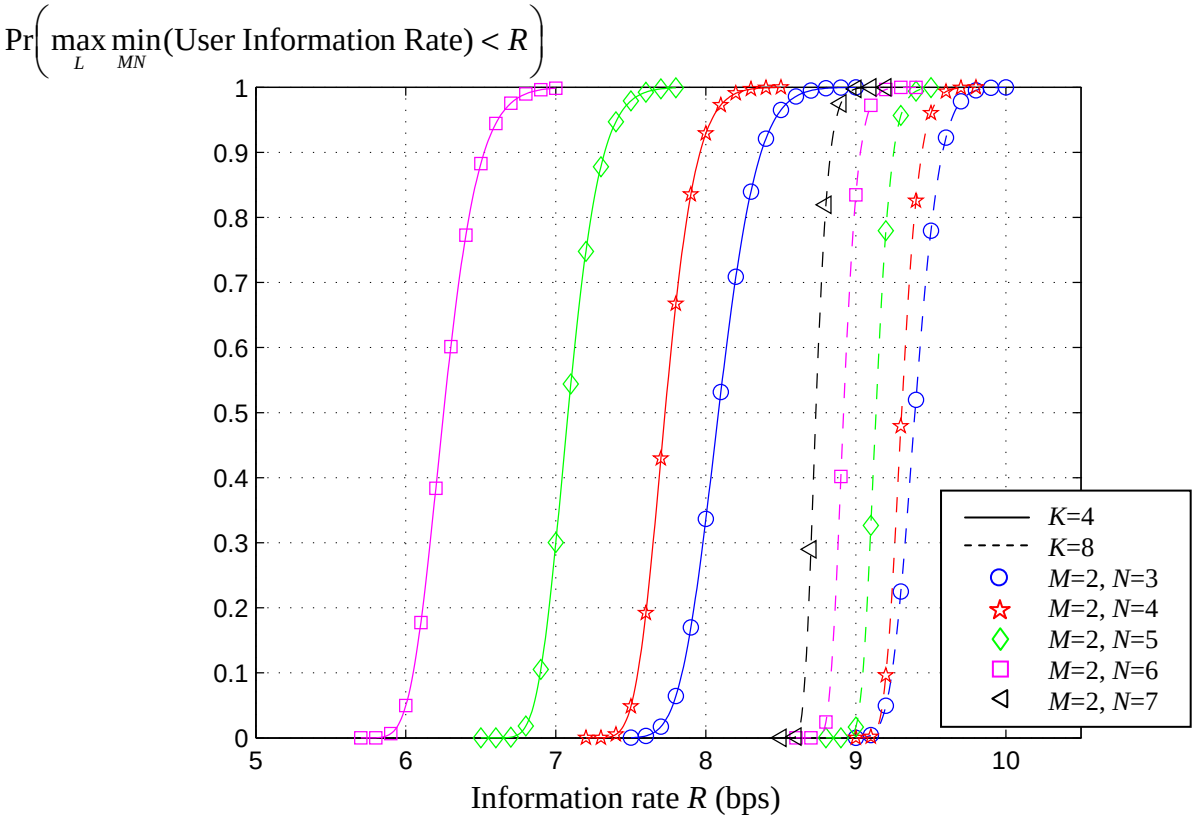

Figure 6.7: CDF curves of information rate of the CR systems in Table 6.1 (F=3)

In Figure 6.7 the theoretical Cumulative Distribution Function (CDF) curves for the user information rate of the cognitive radio systems in Table 6.1 are presented with respect to (6.9). Apparently, the system performance can be influenced by multiple variants, e.g. by limiting the number of the users, or increasing the number or receive antenna elements at BS. Let the straightforward solutions be focused on, by introducing additional available frequency bands. As the SINR bound for the CCI free cognitive radio system, equation (6.9) can be represented by

$$\Pr\left(\max_{L}\min_{MN}\mathrm{SINR}<\alpha\right)=\left[1-P_1\left(\frac{\alpha}{\mu_s},1\right)^{MN}\right]^{L} \tag{6.10}$$

$$\approx \Pr\left(\min_{N}\max_{A_M^F}\min_{M}\mathrm{SINR}<\alpha\right)=1-\left\{1-\left[1-P_1\left(\frac{\alpha}{\mu_s},1\right)^{M}\right]^{A_M^F}\right\}^{N},$$

where $F=MN$ and $L=A_F^F$ hold, and the approximation is presented in [D8.1] equation (8.19). In Figure 6.8, the CDF curves are presented for a cognitive radio system with $M=2$ and $N=3$. Obviously, the minimal user information rate in the system can be improved by either deploying additional frequency bands or increasing the number of receive antenna elements. With increasing number of antenna elements, the performance bound without CCI can be extremely approached. On the other hand, the trade-off should be considered between the cost of additional frequency bands and additional antenna elements. Figure 6.8 shows the potential of interference mitigation with multiple antenna arrays for cognitive radio system.

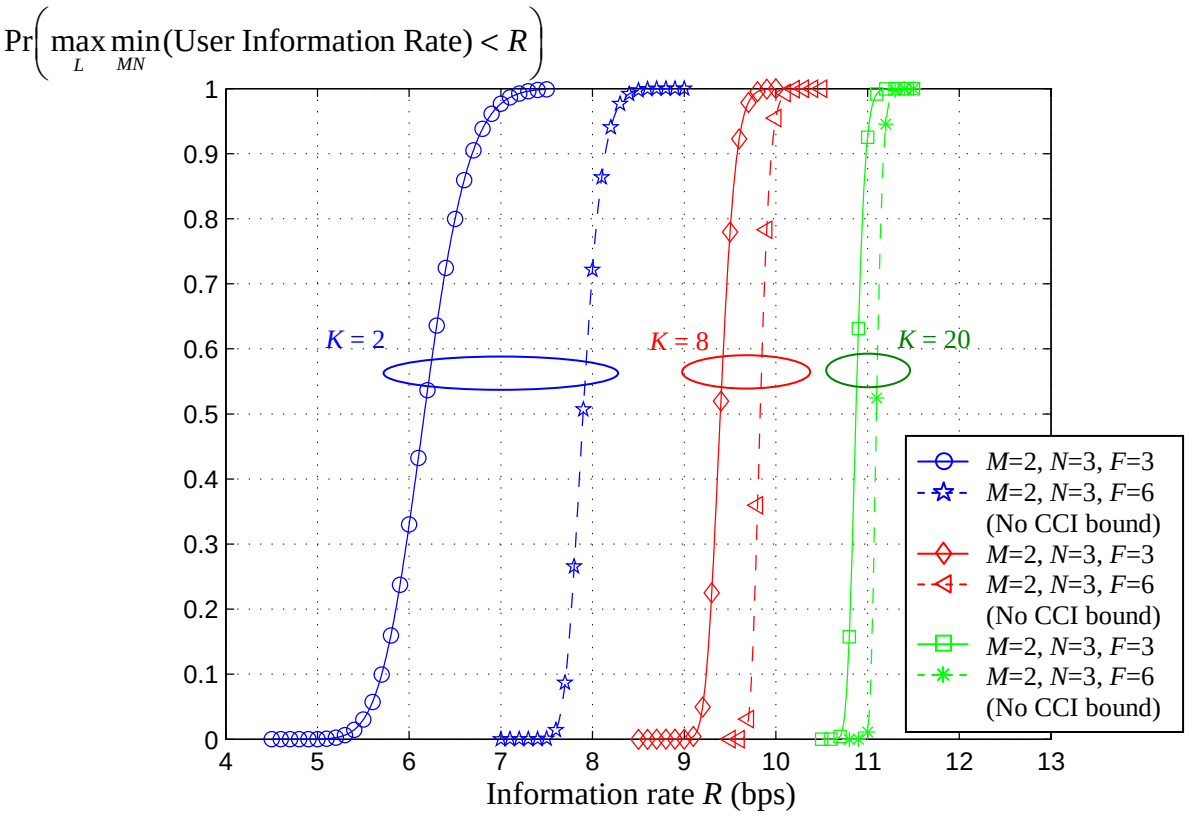

Figure 6.8: CDF curves of information rate of the CR system with M=2, N=3

6.2.4 "Good Neighbour" Approach and Evaluation

Let's now review the basic Good Neighbour (GN) Interference Mitigation (IM) based DDSA algorithm developed in [D8.1] and [D8.2].

GN IM-based DDSA algorithm

- Sensing interval

  1. Calculate antenna weights: $\mathbf{w}_{nm} = \frac{\mathbf{R}^{-1}_{d^{(0)}_{nm}n}\mathbf{h}_{d^{(0)}_{nm}mnn}}{\mathbf{h}^{*}_{d^{(0)}_{nm}mnn}\mathbf{R}^{-1}_{d^{(0)}_{nm}n}\mathbf{h}_{d^{(0)}_{nm}mnn}}$

     Calculate the minimal SINR: $\gamma_{\mathrm{n}} = \log_2(1+\min_{m=1,\ldots,M}\mathbf{h}^{*}_{d^{(0)}_{nm}mnn}\mathbf{R}^{-1}_{d^{(0)}_{nm}n}\mathbf{h}_{d^{(0)}_{nm}mnn})$

     with $m=1,\ldots,M$, $d^{(0)}_{nm}$ denotes the allocated frequency band for *m*-th user in *n*-th BS, and $\mathbf{R}_{d^{(0)}_{nm}n}$ denotes the interference covariance matrix of this user (*m*-th user in *n*-th BS);

  2. If the minimal SINR γ_n is not smaller than a given threshold γ_0, then go to the "Data interval" stage without updating $\mathbf{d}_n$; otherwise, go to Step 3;
  3. Update the band allocation vector $\mathbf{d}_n$ by

     $$\mathbf{d}_n = \arg\min_{m=1,\ldots,M;\, f_m\in\Phi;\, f_m\neq f_q,\, q=1,\ldots,M,\, q\neq m}\sum_{\mathrm{m}=1}^{\mathrm{M}}|\,\mathrm{sign}(f_m - d^{(0)}_{\mathrm{nm}})\,|$$

     subject to

     $$\log_2(1+\mathbf{h}^{*}_{f_m mnn}\mathbf{R}^{-1}_{f_m n}\mathbf{h}_{f_m mnn}) \geq \gamma_0$$

     with the optimal weight vector $\mathbf{w}_{nm} = \frac{\mathbf{R}^{-1}_{d_{nm}n}\mathbf{h}_{d_{nm}mnn}}{\mathbf{h}^{*}_{d_{nm}mnn}\mathbf{R}^{-1}_{d_{nm}n}\mathbf{h}_{d_{nm}mnn}}$, $m=1,\ldots,M$;

- Data interval

  SS_{nm}, $m=1,\ldots,M$ transmit data in bands assigned in $\mathbf{d}_n$;

  BS_n receives data with the optimal weight vectors $\mathbf{w}_{nm}$, $m=1,\ldots,M$ for interference suppression.

The general system assumptions are summarized as follows.

1. BSs allocate different bands for all users in their subsystems, i.e., all rows in matrix **D** contain different elements
2. Rayleigh propagation channels are stationary independent random Gaussian vectors $\mathbf{h}_{fmln} \propto CN(0,\sigma_h^2\mathbf{I}_K)$, where $\sigma_h^2 = 1$ is assumed to emphasize interference limited scenario, or σ_h^2 is a random variable according to the pathloss and shadowing models for particular system geometry.
3. For simplification, constant power for all users in the system is assumed, i.e., locally selectable frequency bands are the only adjustable parameters. Furthermore, exhaustive minimum switch (MinSwitch) local search in Step 3 of above algorithm is assumed to be feasible.

4. All subsystems know their own second order statistics, i.e., BS_n knows $\mathbf{R}_{fn}$ and $\mathbf{h}_{fmnn}$ for $n = 1, \ldots, N$, $m = 1, \ldots, M$, $f = 1, \ldots, F$, and has no information on $\mathbf{R}_{fl}$ and $\mathbf{h}_{fmln}$ for $l \neq n$. Assume that users transmit the pilot symbols during the sensing intervals and data signals during the data intervals, and the sensing intervals for different subsystems do not overlap. A low probability of overlapping of the sensing intervals can be achieved, for example, by means of random duration of the data intervals as illustrated in Figure 8.2 in [D8.1].

In [D8.1] and [D8.2] Markov chain model is exploited to analyse and evaluate the convergence of the GN IM-based DDSA algorithm above. As being a pure analytical study, the number of spectrum allocation candidates is assumed to be $L_{\text{ex}} = (A_M^F)^N$ in an exhaustive manner. The parameter L_{ex} for some cognitive systems is summarized in Table 6.1. Hence, the Markov chain model can be represented by an $L_{\text{ex}} \times L_{\text{ex}}$ transition probability matrix $\mathbf{P}$. The row index of matrix $\mathbf{P}$ denotes the current spectrum allocation schema, or the input allocation candidate for the GN IM-based DDSA algorithm to optimize or evaluate. The column index of matrix $\mathbf{P}$ denotes consequently the output spectrum allocation schema. If the solution is still not satisfactory, the iterations are required by deploying the GN IM-based DDSA algorithm again. Apparently, the convergence is found, if output of the GN IM-based DDSA algorithm is exactly its input. Namely, an arbitrary convergence point locates on the diagonal of the matrix the $\mathbf{P}$, whose row index is equal to its column index. In Figure 6.9 this procedure is illustrated. Assume that the *i*-th channel realization is invariable within the temporal duration $t_0 \le t \le t_0 + T$, which corresponds to a constant transition probability matrix $\mathbf{P}_i$. Figure 6.9 demonstratively presents the iterations by deploying the GN IM-based DDSA algorithm, and finally approaching the convergence spectrum allocation schema after $N_{\text{iter}} - 1$ iterations, where T_s denotes the sensing interval.

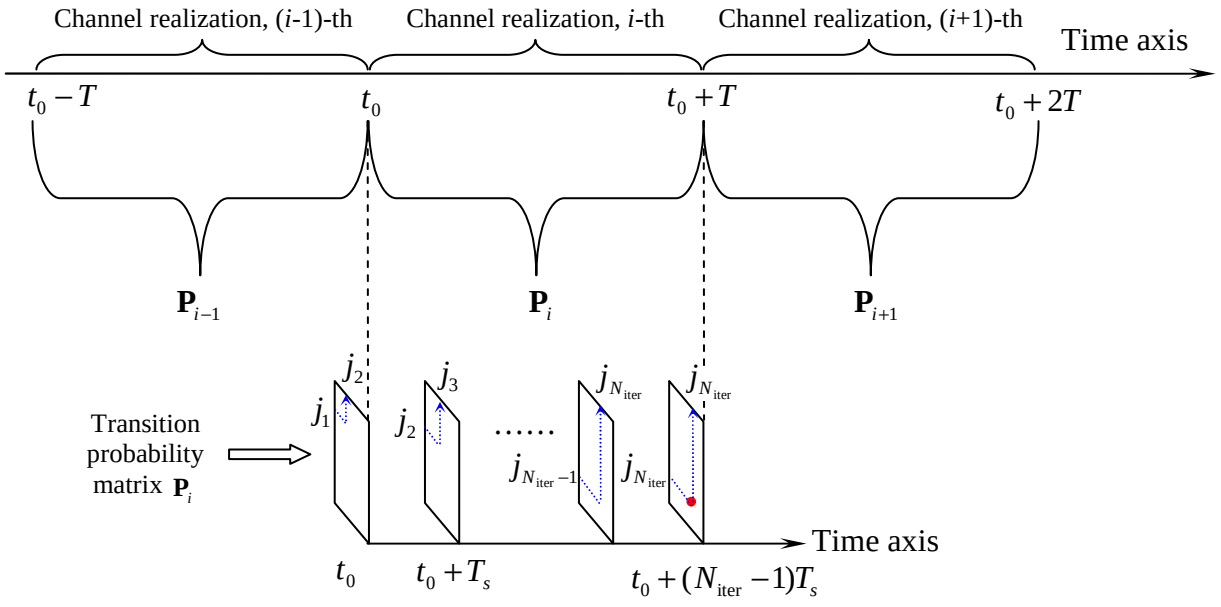

Figure 6.9: Illustration for the sensing the subsystems to iteratively find the convergence (red point), with respect to $L_{\text{ex}} \times L_{\text{ex}}$ transition probability matrix $\mathbf{P}$

6.3 Adaptation of DDSA Solution in Practise

The Markov chain model is a prominent analytical tool to evaluate the GN IM-based DDSA algorithm. In [D8.1] and [D8.2], considerable simulation results can be referred to. In this section, let's come back to focus on the algorithm application in practise, and think about the variant and modification of the algorithm to adapt to the reality. Three aspects need to be considered.

- Antenna configuration – due to the limitation of dimension of the multiple antenna arrays in the reality, Uniform Linear Array (ULA) or circular array will be deployed. The correlation of the channel coefficients between the antenna elements increases.
- Number of iteration – in the reality, the duration of an arbitrary channel realization is quite limited. The system convergence cannot be guaranteed within such a short term. Sub-optimal spectrum allocation solution is thus important with few or even no iterations.
- BS channel allocation – highly correlated channels can even allow the BS allocates its own users to the same frequency band, which can thus introduce additional degree of freedom as the control mechanism in the decentralized system.

The aspects above motivate the study on coherent DDSA solutions in this section. Throughout the investigation, the half-wavelength ULA is taken into account. The coherent DDSA schemes introduce additional degrees of freedom to coordinate the beam patterns and to suppress the interference. Additionally, the concept of virtual antennas can be deployed in uplink to improve the interference suppression. As shown in Figure 6.10, if the signal source is far away enough, the equal phase planes of electric and magnetic waves are vertical to the propagation direction. The phase difference between Antenna 1 and Antenna 2 corresponds to the path in the red mark. The phase difference can be quantized by

$$\Delta\phi_{12} = \frac{2\pi}{\lambda} d \sin\theta,\ -90° < \theta < 90°, \tag{6.11}$$

where λ stands for the wavelength of the carrier frequency, and θ denotes Direction of Arrival (DoA). In the illustration in Figure 6.10, Antenna 2 has the advanced phase. In the general case, this depends on θ, namely Antenna 2 has the advanced phase for $0 < \theta < 90°$, and Antenna 2 has lagged phase for $-90° < \theta < 0°$. The conclusion can be extended for antenna array with multiple elements.

Figure 6.11 illustrates the phase difference between an arbitrary receive antenna and the reference antenna (Antenna 1). A so-called array steering vector $\mathbf{s}$ can be introduced as

$$\mathbf{s}(\theta) = \left[1 \quad e^{j\frac{2\pi}{\lambda} d \sin\theta} \quad e^{j\frac{2\pi}{\lambda} 2d \sin\theta} \quad e^{j\frac{2\pi}{\lambda} 3d \sin\theta} \right]^T. \tag{6.12}$$

Especially, if half-wavelength array is deployed, namely $d = \frac{\lambda}{2}$, it yields

$$\mathbf{s}(\theta) = \left[1 \quad e^{j\pi \sin\theta} \quad e^{j2\pi \sin\theta} \quad e^{j3\pi \sin\theta} \right]^T. \tag{6.13}$$

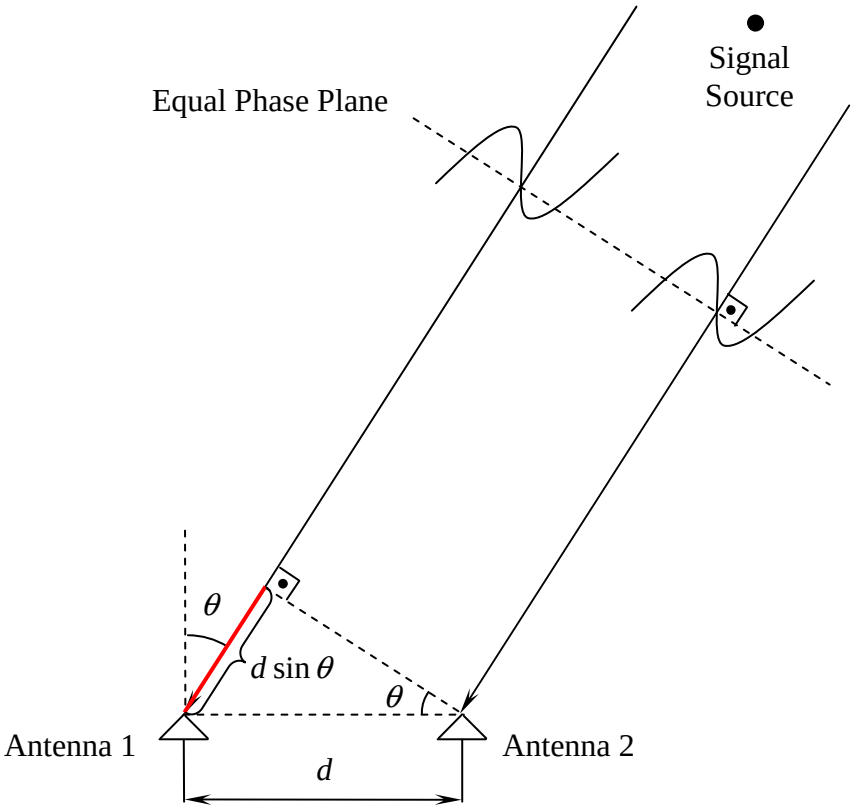

Figure 6.10: Calculation of the phase difference

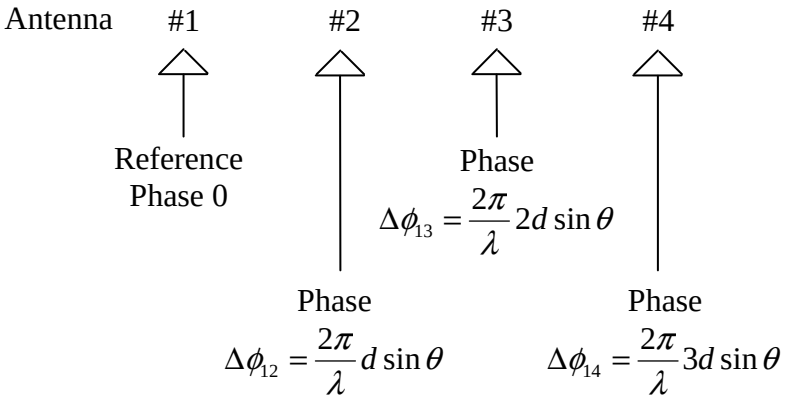

Figure 6.11: Phase difference between an arbitrary receive antenna and the reference antenna

Notice that the channel estimation can be done with respect to pilot or so-called sounding signaling. Let the pilot based channel estimates be denoted by $\mathbf{h}_0$. The DoA θ can be straightforward estimated by evaluating the eigenvector of matrix $\mathbf{h}_0\mathbf{h}_0^H$. A rotated channel vector can be computed by

$$\mathbf{h} = \mathrm{diag}\left[\mathbf{s}^H(\theta)\right] \cdot \mathbf{h}_0 . \tag{6.14}$$

Due to the high correlation, the elements of channel vector can be averaged, it yields

$$h_0 = \frac{1}{K}\sum_{k=1}^{K}\mathbf{h}[k]. \tag{6.15}$$

With the DoA θ and mean channel response h_0, K_v virtual antenna elements [Doh02] [Hon10] can be introduced to improve the uplink performance. Figure 6.12 illustrates the procedure to generate the channel response for the virtual antenna elements. It holds

$$\mathbf{h}_{0,\mathrm{va}} = \left[\mathbf{h}_0^{\ T} \quad h_0 e^{jK\pi\sin\theta} \quad \cdots \quad h_0 e^{j(K+K_v-1)\pi\sin\theta}\right]^T. \tag{6.16}$$

In Figure 6.13 illustrates a $Q\times K$ MIMO system. The BS of interest has K receive antennas. Each user has a single transmit antenna. The user of interest delivers the signal s_0. And the rest $Q-1$ users are the interferers. The MIMO system equation is given by

$$\mathbf{y} = \mathbf{H}\mathbf{s} + \mathbf{n} = \left[\mathbf{h}_0 \quad \mathbf{h}_1 \quad \cdots \quad \mathbf{h}_{Q-1}\right]\cdot\begin{bmatrix} s_0 \\ s_1 \\ \vdots \\ s_{Q-1}\end{bmatrix} + \mathbf{n} \tag{6.17}$$

$$= \begin{bmatrix} h_{1,0} \\ h_{2,0} \\ \vdots \\ h_{K,0}\end{bmatrix}\cdot s_0 + \begin{bmatrix} h_{1,1} \\ h_{2,1} \\ \vdots \\ h_{K,1}\end{bmatrix}\cdot s_1 + \cdots + \begin{bmatrix} h_{1,Q-1} \\ h_{2,Q-1} \\ \vdots \\ h_{K,Q-1}\end{bmatrix}\cdot s_{Q-1} + \begin{bmatrix} n_1 \\ n_2 \\ \vdots \\ n_K\end{bmatrix}.$$

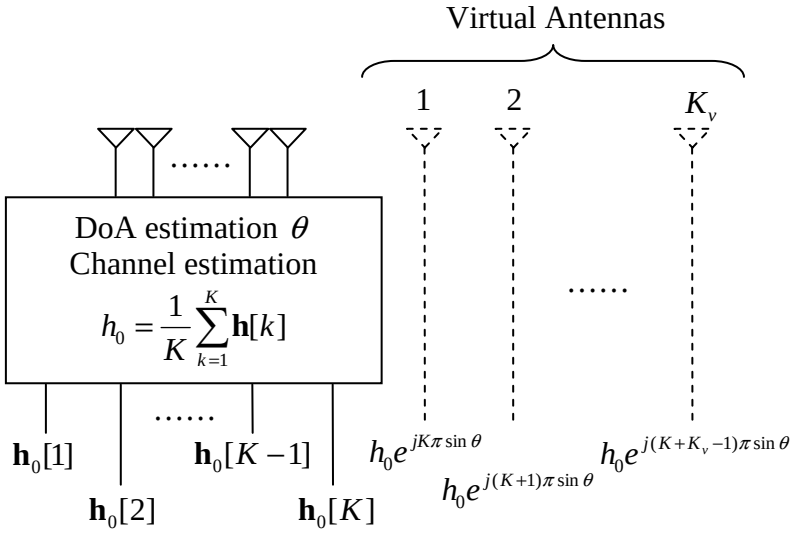

Figure 6.12: Procedure to generate the channel response for the virtual antenna elements

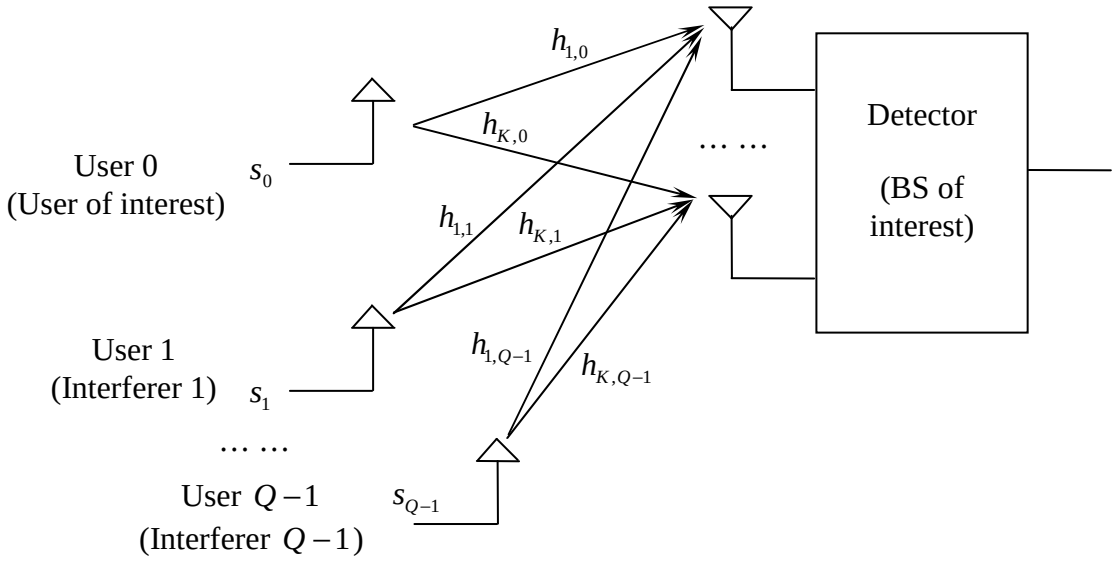

Figure 6.13: Uplink MIMO system with K receive elements for Q users

The classical Wiener-Hopf solution allows estimating the useful signal by minimizing the square root of error with respect to the pilot signalling. It holds

$$\mathbf{w}_{\mathrm{WH}} = \mathbf{R}_{\mathbf{yy}}{}^{-1}\mathbf{h}_0 = E[\mathbf{y}\mathbf{y}^H]^{-1}\mathbf{h}_0 . \tag{6.18}$$

Being denoted as Minimum Mean Square Error (MMSE) algorithm, equation (6.18) can be approximated as

$$\begin{aligned}\mathbf{w}_{\mathrm{WH}} \approx \mathbf{w} &= (\sum_{i=0}^{Q-1} E_{s_i}\mathbf{h}_i\mathbf{h}_i{}^H + \sigma^2\mathbf{I})^{-1}\mathbf{h}_0 \\ &= (E_{s_0}\mathbf{h}_0\mathbf{h}_0{}^H + \sum_{i=1}^{Q-1} E_{s_i}\mathbf{h}_i\mathbf{h}_i{}^H + \sigma^2\mathbf{I})^{-1}\mathbf{h}_0 \\ &= (\mathbf{h}_0\mathbf{h}_0{}^H + \sum_{i=1}^{Q-1}\mathbf{h}_i\mathbf{h}_i{}^H + \sigma^2\mathbf{I})^{-1}\mathbf{h}_0 ,\end{aligned} \tag{6.19}$$

where σ^2 denotes the variance of AWGN, the unity transmit power is assumed, namely $E_{s_i} \equiv 1$.

Throughout the investigation, the cognitive radio system in Figure 6.14 is studied. There are $N = 5$ BSs, each of which has $M = 2$ users. There are $F = 3$ available frequency bands. The coverage of each BS is also shown in Figure 6.14. Throughout the investigation, the users only drop in the hot spot in the middle.

Being the lower and upper bound, the random resource allocation and max-min resource allocation corresponds to the decentralized and centralized cognitive scheme, respectively. The max-min resource allocation can be represented by the criterion in (6.20)

$$\max_{\mathbf{D}} \min \frac{\mathbf{w}^H \mathbf{h}_i \mathbf{h}_i{}^H \mathbf{w}}{\sum_{j=1, j\neq i}^{Q-1} \mathbf{w}^H \mathbf{h}_j \mathbf{h}_j{}^H \mathbf{w} + \mathbf{w}^H \mathbf{n}\mathbf{n}^H \mathbf{w}}, \text{ for } i = 0, 1, \cdots, Q-1. \tag{6.20}$$

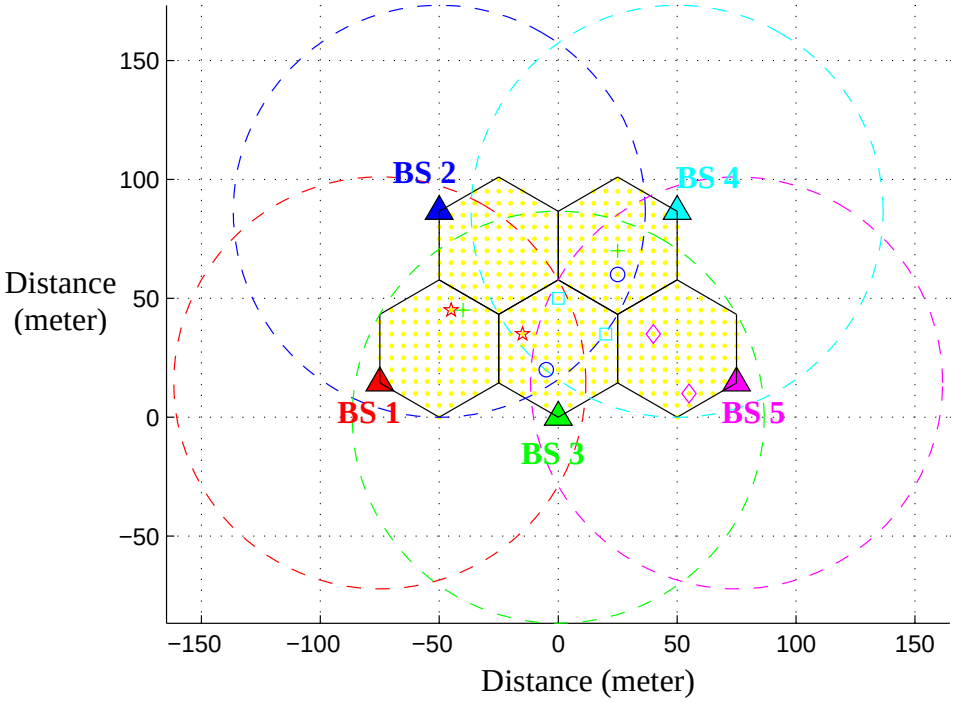

Figure 6.14: Investigated cognitive radio system layout

A central unit is required to compare and find out the optimal solution. The $N \times M$ frequency band allocation matrix **D** indicates the m-th user of the n-th BS to occupy one of the F available frequency band. For the example in Figure 6.14 above, the frequency allocation matrix **D** can be obtained as

$$\mathbf{D} = \begin{array}{c} \\ \#1 \\ \#2 \\ \#3 \\ \#4 \\ \#5 \\ \text{BS index} \end{array} \overset{\begin{array}{cc}\#1 & \#2\end{array} \rightarrow \text{User index}}{\begin{bmatrix} 1 & 2 \\ 2 & 1 \\ 2 & 1 \\ 2 & 3 \\ 1 & 3 \end{bmatrix}}, \tag{6.21}$$

by considering random allocation. In Figure 6.15, the beam patterns of the BSs in $F = 3$ frequency bands are presented with respect to equation (6.19). The users with negative low SINR values are marked.

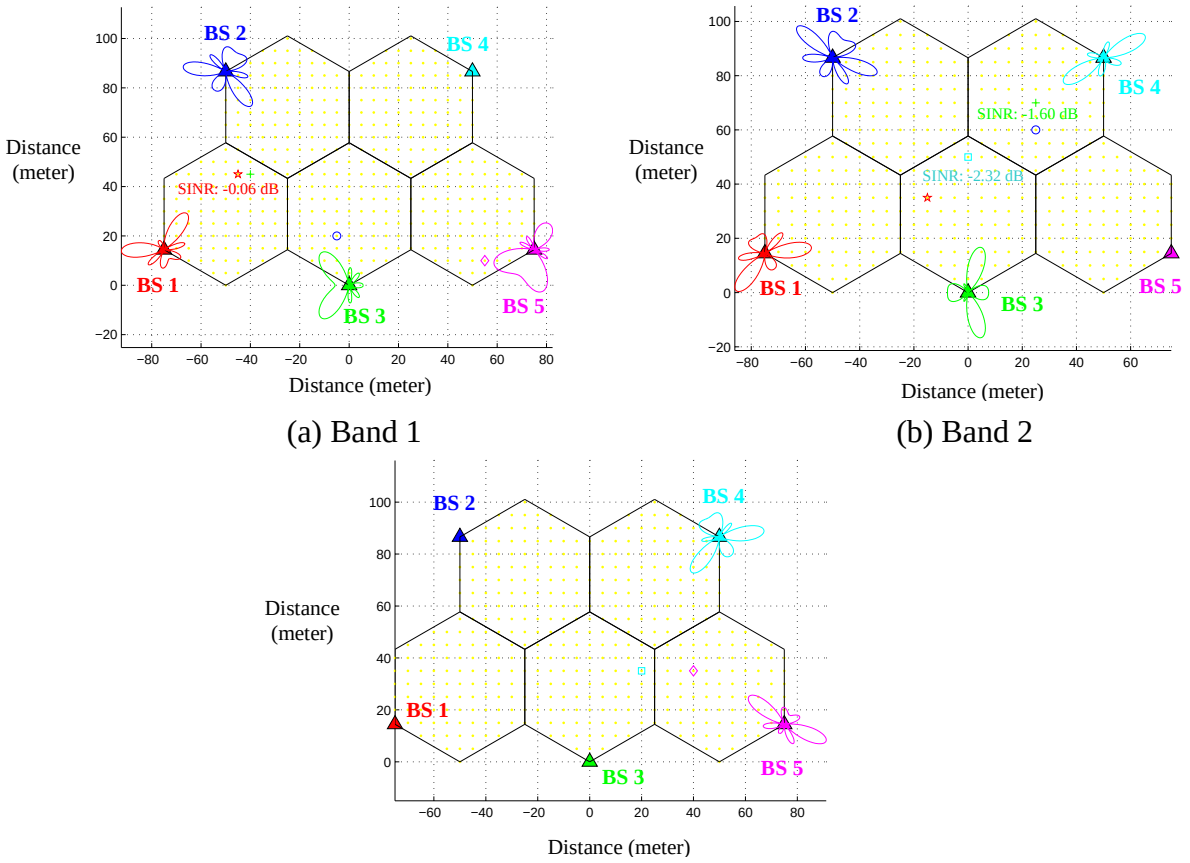

Figure 6.15: Beam patterns of the BSs with random allocation ($F = 3$, $K = 4$)

Being a decentralized system, the low SINR value can be only detected by the own BS. According to the conventional solution, the user needs to switch to another frequency band. Let's denote it as a transition from state $\mathbf{D}_i$ to state $\mathbf{D}_{i+1}$ within the i-th sensing interval. Nevertheless, it can lead to the unexpected solutions. For instance, a couple of users with low SINR occasionally and simultaneously shift to another frequency band together due to being decentralized. The situation will not be improved either, or other users with low SINR appear in the new state $\mathbf{D}_{i+1}$. Obviously, a number of iterations are required to approach a solution for the complete cognitive network. If the convergence hasn't be approached before the channel realization changes, the resource allocation has to be started over again.

Hence, the first algorithm is proposed under this context, to avoid shifting to another frequency band, if the SINR is not adequate. The virtual antenna arrays are introduced to improve the SINR. The flow diagram is provided in Figure 6.16.

- Algorithm 1: virtual antenna solution

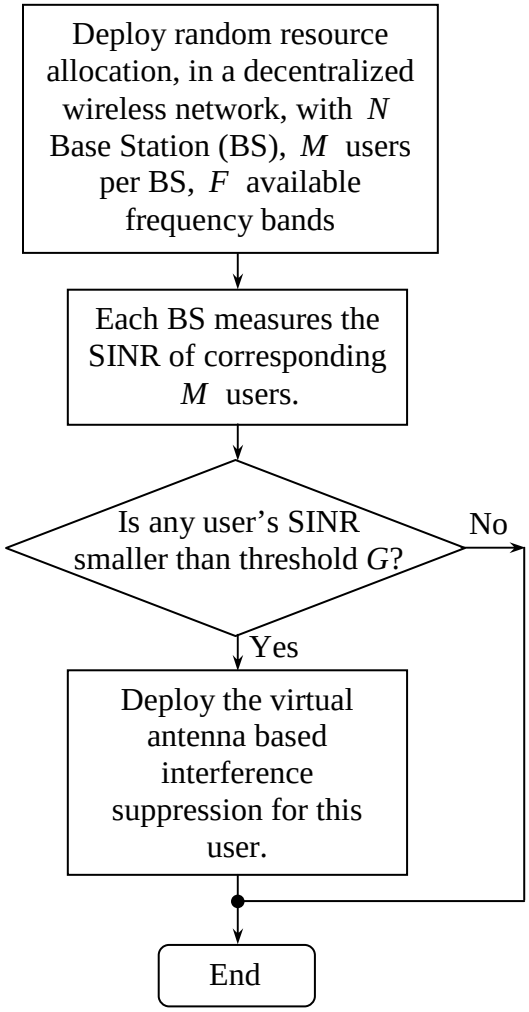

Figure 6.16: Algorithm 1: virtual antenna solution

Let the example in Figure 6.14 and Figure 6.15 be considered again. The SINR threshold is defined as $G = 0\,\text{dB}$. The number of virtual antenna is $K_v = 4$. In Figure 6.17, the beam patterns are presented. Notice that the user of BS 1 in band 1 has now an improved SINR value, by introducing virtual antennas. The beam pattern is thus narrower, and can suppress the interference from the user of BS 3. In band 2, the similar effect can be observed. The SINR value of the user of BS 3 is now above the SINR threshold $G = 0\,\text{dB}$. Nevertheless, the SINR of the user of BS 4 does not satisfy the SINR threshold. Further resource allocation strategy will be discussed after presenting some numeric results.

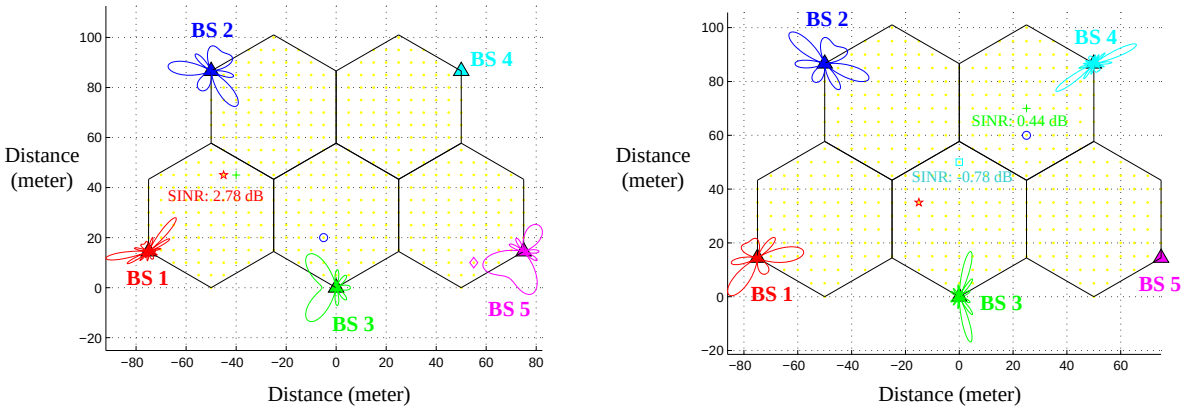

(a) Band 1 (b) Band 2

Figure 6.17: Updated beam patterns of the BSs in Band 1 and Band 2 with $K_v = 4$ virtual antennas

In Figure 6.18, the CDF curves of minimal SINR of the determined allocation state $\mathbf{D}_i$, denoted as $\mathrm{SINR}_{\min}^{(i)}$, are shown with respect to different resource allocation schemes. The result reveals that the virtual antenna solution can flexibly bring in the improvement by defining a SINR threshold G.

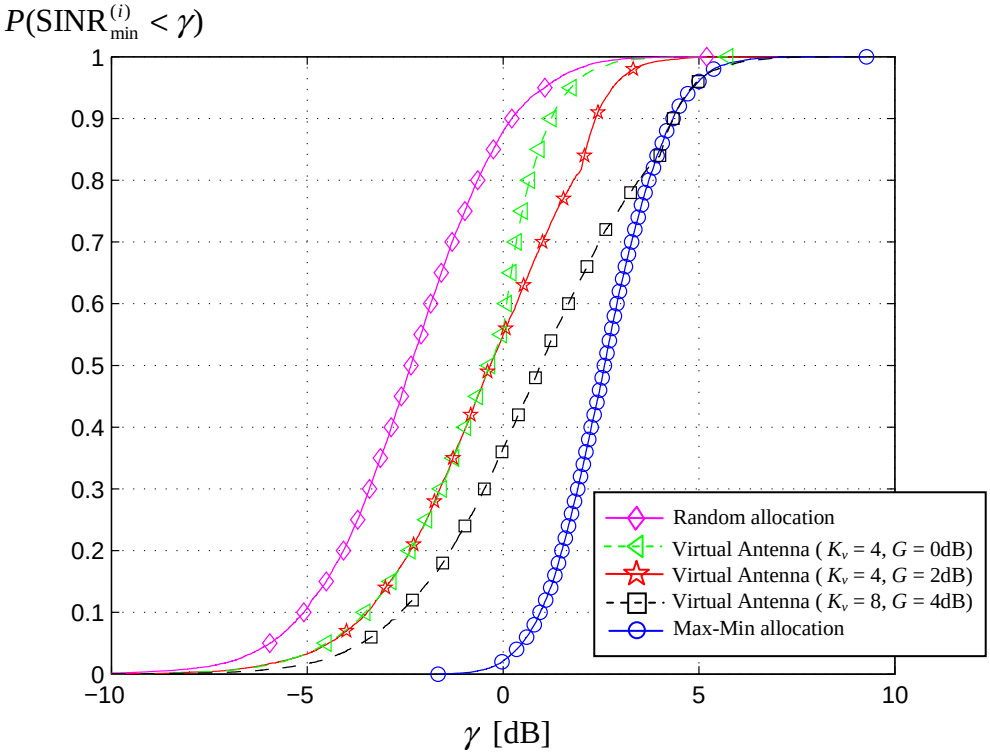

Figure 6.18: Performance of algorithm 1, CDF curves of minimal SINR with respect to K_v virtual antenna and SINR threshold G (F = 3, K = 4, N = 5)

Notice that it can happen that the minimal SINR cannot satisfy the given SINR threshold G, even virtual antennas are deployed. In Figure 6.17 (b), the SINR of the user of BS 4 cannot be improved due to the distribution of interferers. For this scenario, another solution should be considered. The corresponding flow diagram is provided in Figure 6.19.

- Algorithm 2: virtual antenna and band switch solution

After deploying the virtual antenna solution for a certain user, the updated SINR will be again compared to the SINR threshold G. If it is still not satisfactory, the user will switch to use another frequency band. Thus, the spectrum allocation state $\mathbf{D}_i$ of the cognitive system transits to state $\mathbf{D}_{i+1}$. This is so-called an iteration. The number of iterations N_{iter} is defined. It has to be emphasized that the channel realization within all the iterations should be constant. Otherwise, the spectrum allocation state $\mathbf{D}_i$ will be irrelevant, and cannot be regarded as the start of a new iteration. In order to strictly satisfy this assumption, the number of iterations for the following investigation is $N_{\text{iter}} = 1$.

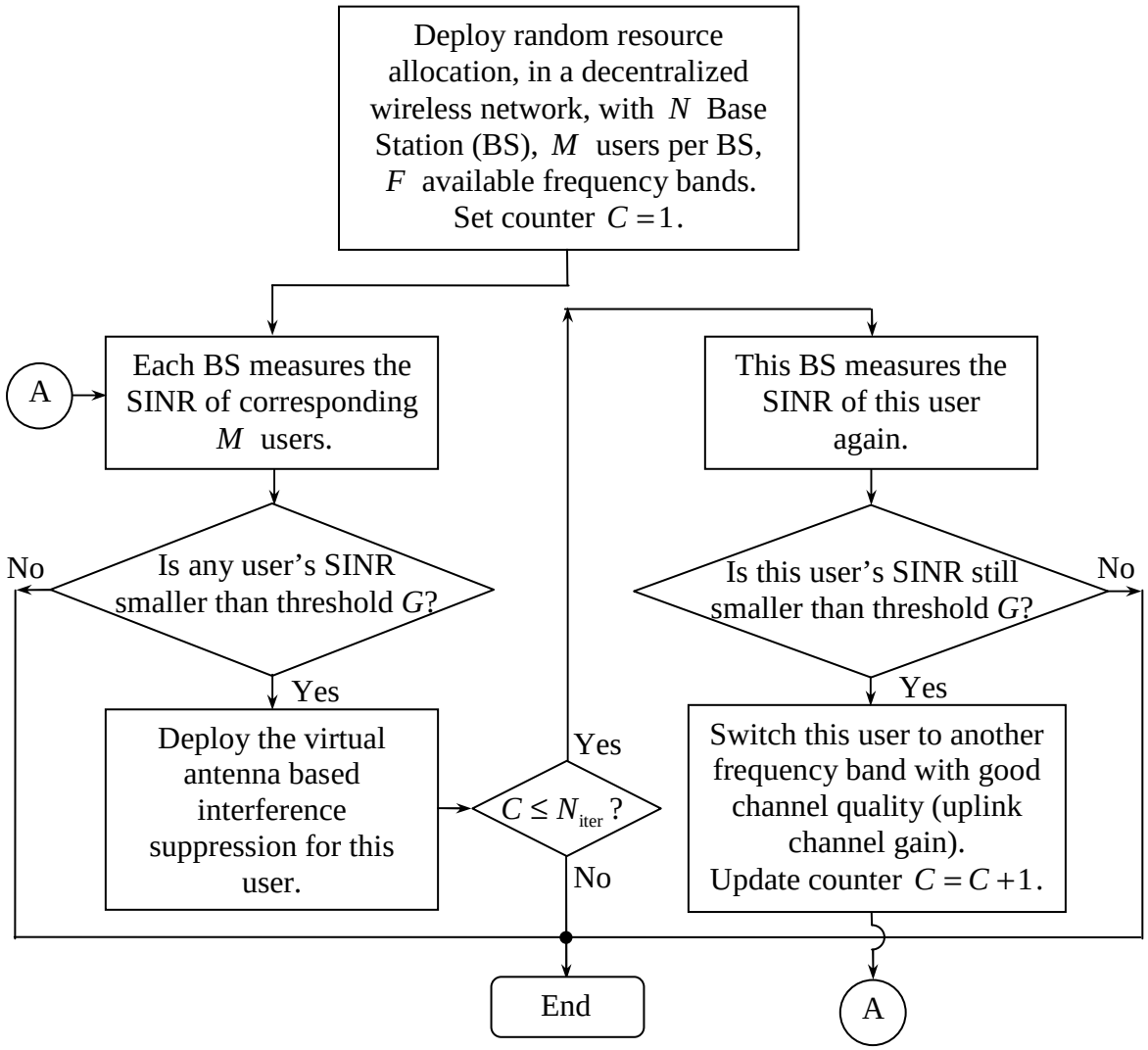

Figure 6.19: Algorithm 2: virtual antenna and band switch solution

In Figure 6.20 and Figure 6.21, the performance of algorithm 2 is presented for target SINR threshold $G = 0$ dB and $G = 4$ dB, respectively. By comparing the performance of algorithm 1 to algorithm 2 at the target SINR threshold with $K_v = 4$, the improvement can be apparently observed.

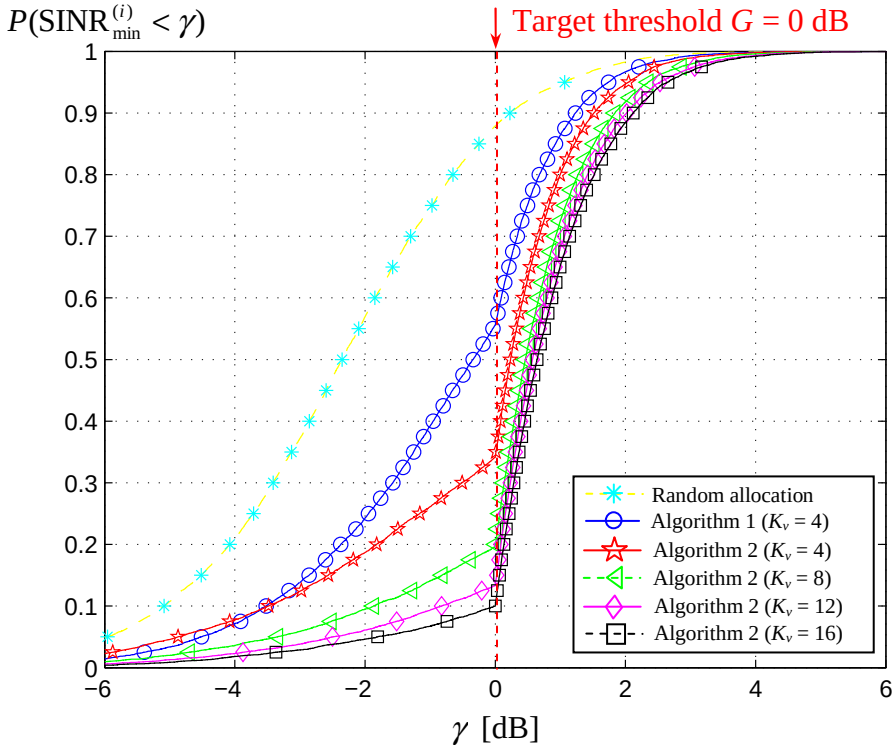

Figure 6.20: Performance of algorithm 2, CDF curves of minimal SINR with respect to K_v virtual antenna and SINR threshold G = 0dB (F = 3, K = 4, N = 5)

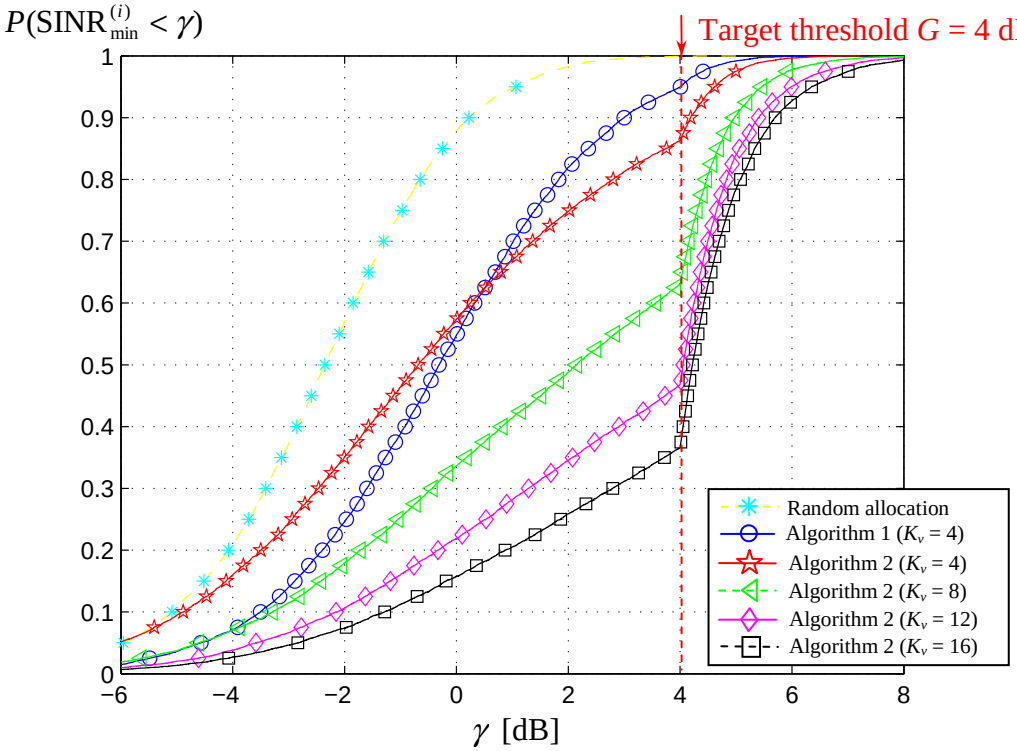

Figure 6.21: Performance of algorithm 2, CDF curves of minimal SINR with respect to K_v virtual antenna and SINR threshold G = 4dB (F = 3, K = 4, N = 5)

As discussed in [D8.1] and [D8.2], it is assumed that the optimum allocation will be found, if any BS will allocate its own users in different frequency bands. Nevertheless, in the coherent DDSA solution, this should be re-evaluated. Let the following sets be defined

$$\mathscr{A} = \{ \text{ All possible spectrum allocation candidates } \} \tag{6.22a}$$

$$\mathscr{A}_1 = \{ \text{ Spectrum allocation schemes } | \text{ Co-BS users are not Co-Band } \} \tag{6.22b}$$

$$\mathscr{A}_2 = \{ \text{ Spectrum allocation schemes } | \text{ At least one band accommodates Co-BS users } \}. \tag{6.22c}$$

Obviously the number of elements in set $\mathscr{A}$, $\mathscr{A}_1$ and $\mathscr{A}_2$ are L_{ex}, L and $L_{\text{ex}} - L$, respectively. It holds

$$\mathscr{A} = \mathscr{A}_1 \bigcup \mathscr{A}_2. \tag{6.23}$$

In Figure 6.22, the CDF curves of $\text{SINR}_{\text{min}}^{(i)}$ are presented for three search space. Notice that in the global optimum solution, there is almost at least one band accommodating Co-BS users.

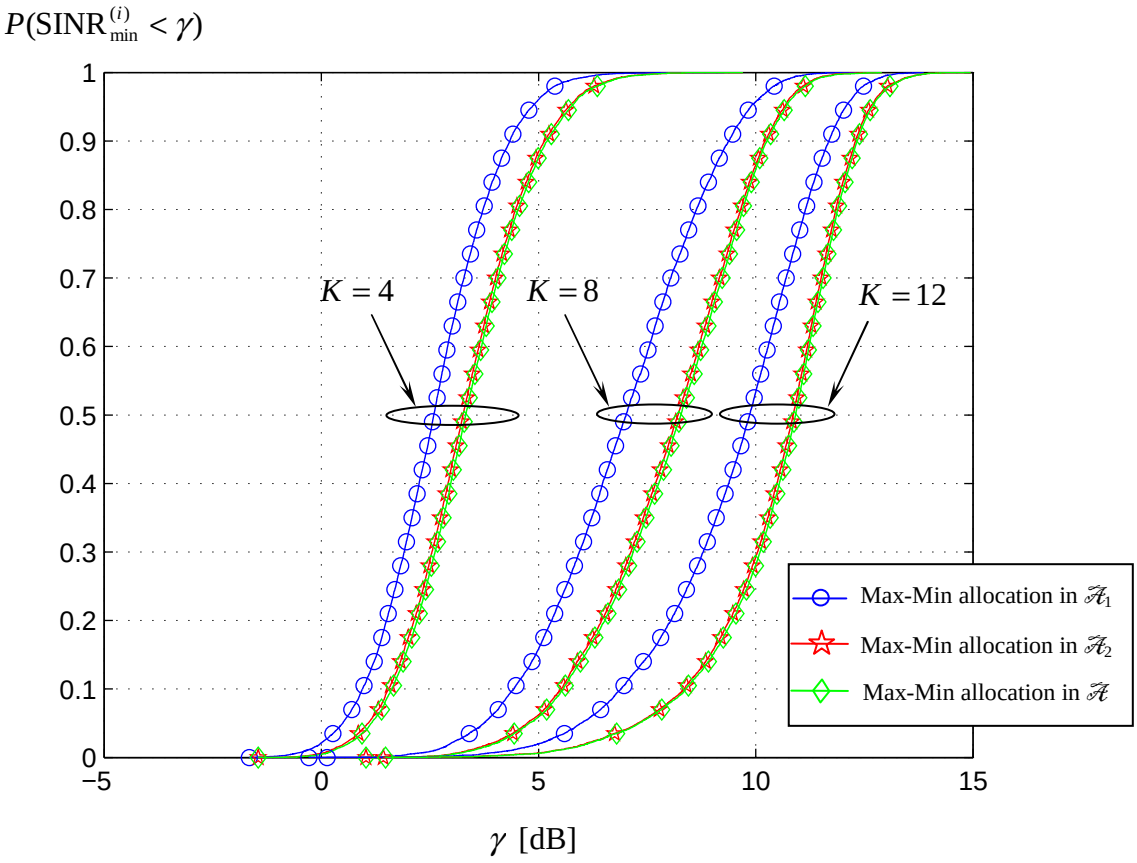

Figure 6.22: Performance of Max-Min allocation, curves of minimal SINR with respect to search space (F = 3; K = 4, 8 or 12; N = 5)

By allowing the Co-BS users in the same frequency band, a BS in the decentralized system has an additional degree of freedom to combat the interference. This is the motivation of the algorithm 3, whose flow diagram is presented in Figure 6.23.

- Algorithm 3: modified virtual antenna and band switch solution

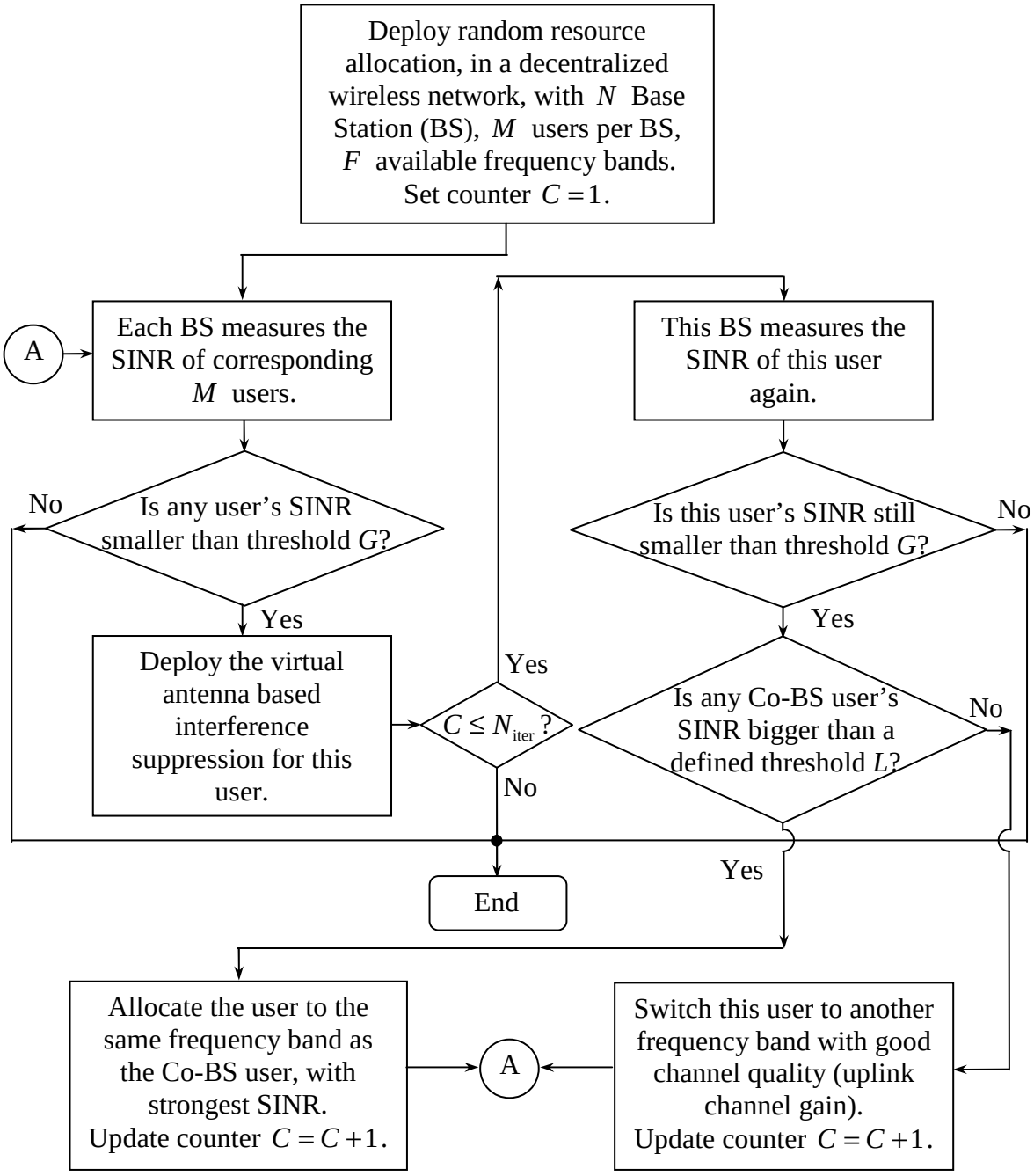

Figure 6.23: Algorithm 3: modified virtual antenna and band switch solution

After deploying the virtual antenna solution for a certain user as in algorithm 1, if the SINR of this user is still inadequate, instead of the immediate frequency band switch, the BS will check, whether another Co-BS user with extreme good SINR does exist by introducing another threshold L, e.g. $L=10\,\mathrm{dB}$. If this happens, it indicates that this band is not overloaded or the user distribution is fine. Hence, it allows the BS to reuse this frequency band and allocate the target user to this channel. Although both Co-BS users are thus in the same frequency band, they can still be spatially separated, by deploying virtual antenna, if necessary. Hence, further performance improvement can be expected. The numeric simulation results in Figure 6.24 and Figure 6.25 support this conclusion.

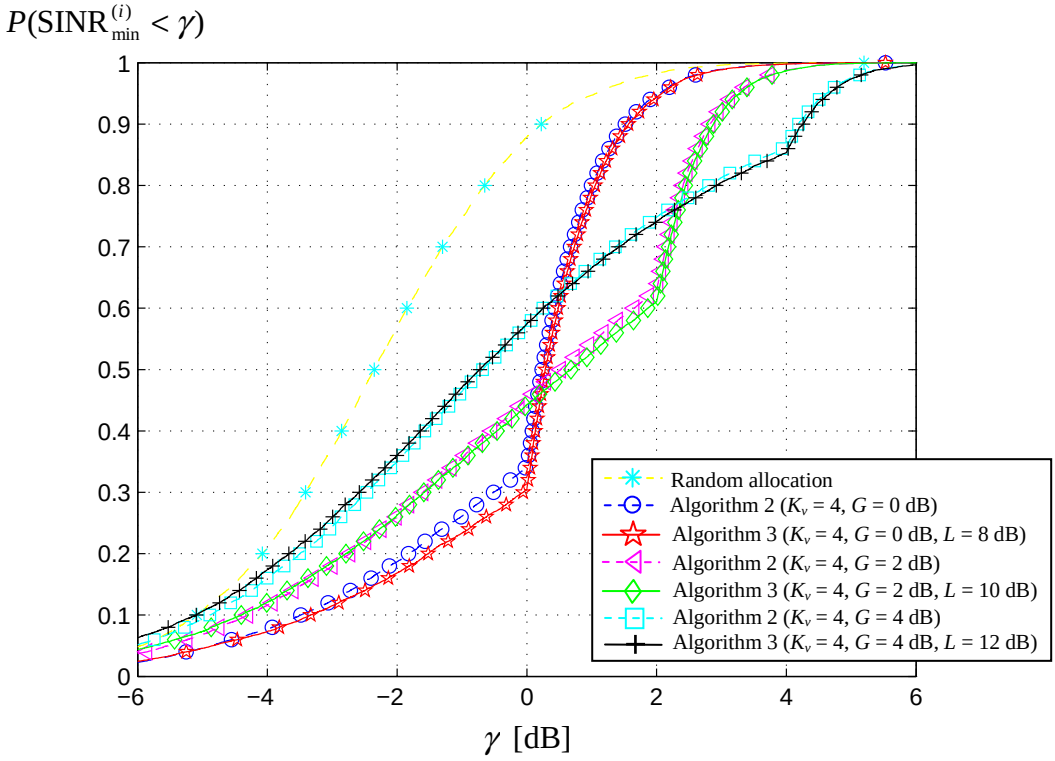

Figure 6.24: Performance comparison between algorithm 2 and algorithm 3, CDF curves of minimal SINR with respect to K_v = 4 virtual antenna and SINR threshold G and L (F = 3, K = 4, N = 5)

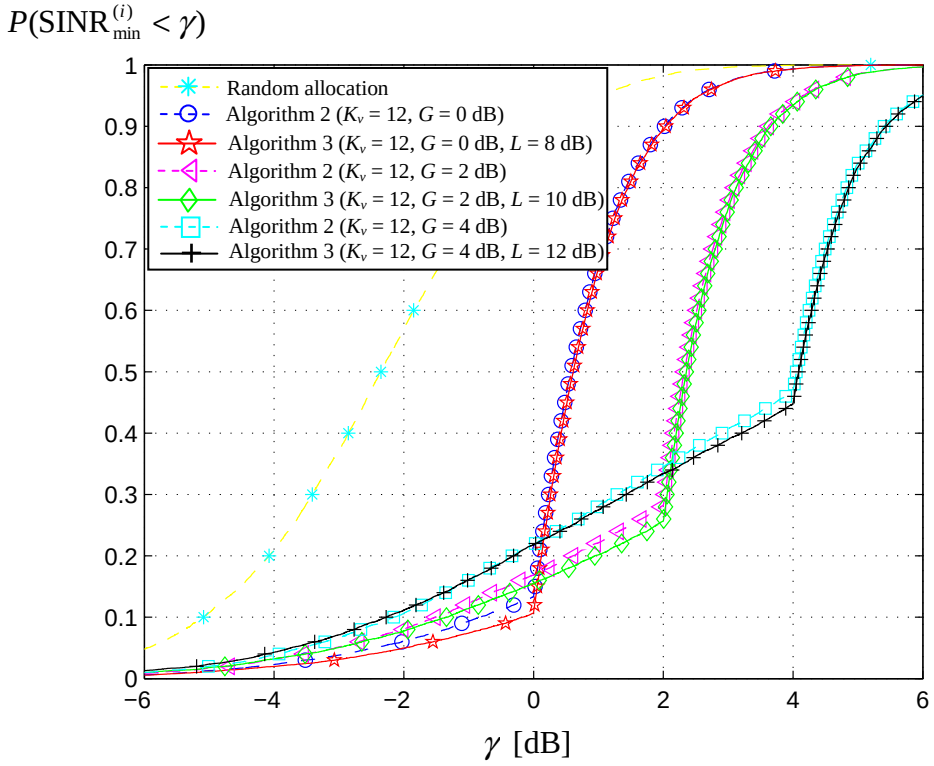

Figure 6.25: Performance comparison between algorithm 2 and algorithm 3, CDF curves of minimal SINR with respect to K_v = 12 virtual antenna and SINR threshold G and L (F = 3, K = 4, N = 5)

6.4 Summary

In this section, the "Good Neighbour" (GN) Interference Mitigation (IM) base Decentralized Dynamic Spectrum Allocation (DDSA) approach is generally reviewed, which is intensively investigated in [D8.1] [D8.2] and provides a promising solution for the issue on coexistence in the opportunistic unsynchronized cognitive radio networks. Additionally, a prominent analytical tool, Markov chain model, is exploited to evaluate the GN IM-based DDSA algorithm. The Markov chain model provides a brand new view point to illustrate the convergence of the GN IM-based DDSA algorithm. The corresponding investigation shows that GN IM-based DDSA algorithm holds excellent convergence characteristics and thus significantly outperforms the classical DDSA solution, such as "Selfish" IM-based DDSA algorithm. Abundant simulations from diverse view points support this conclusion.

Secondly, the adaptation of DDSA algorithm to the practise is focused on. Due to the invariance of the wireless radio channel, large number of iterations cannot be expected, which try to approach the optimal spectrum allocation scheme in a decentralized manner, and must be executed within a constant channel realization. Investigation shows that the performance gap between the DDSA algorithm and the optimum solution can be reduced, by appropriately introducing additional antenna elements, as presented in Figure 6.8 for the case $K = 8$. In the modern communication system, this is applicable and can be supported by intelligent physical antenna selection or deploying virtual antennas. Throughout this section, three corresponding DDSA mechanisms are proposed to improve the system performance with possibly limited iterations.

7 Opportunistic Unsynchronized CR Networks

The introduction of opportunistic networks in some particular frequency bands, such as the digital dividend, will be motivated by their economic impact and the perspective of enhanced spectrum utilization. A number of favourable situations can be envisaged for applications.

A. High speed local complement to cellular systems

Due to their universality, their rules of deployment and their rigid protocols, cellular systems are unable to support economically the high capacities which might be requested at particular times and particular places by some customers. Opportunistic networks, capitalizing on their capability to adaptively share the spectrum, may have the possibility to build up the frequency bandwidth needed by the high bit rates involved.

B. Broadband networks in rural areas

Opportunistic networks can help improve the coverage of rural areas and, through dynamic spectrum sharing, offer economical broadband local access to their users. In such a context, they might cooperate with cellular systems or with fixed networks to organize and optimize the global traffic.

C. Easy and cheap access in sparsely populated areas

With their light infrastructure and their versatility, they can adjust the capacity to the user instantaneous needs and follow the evolution in time and space.

D. Temporary high capacity networks for emergency and moving events

At some place and some time, the requested capacity may be so high that the networks are congested. It is the case in emergency situations or for large scale moving events, such as the cycling race “tour de France”. Then, opportunistic networks can make the best usage of the instantaneous available spectrum and divert a part of the traffic load.

E. Peer-to-peer communication

This classical way of communication between users, either people or machines, can be further developed by opportunistic broadband access, in terms of capacity, coverage and mobility.

8 Conclusion and Perspectives

In the field of cognitive radio, the most important contribution of the project concerns the opportunistic unsynchronized networks, which are able to access the spectrum on their own decision and without synchronizing and cooperating with other networks sharing the same frequency bands. With the FBMC physical layer, reliable spectrum sensing and monitoring can be achieved, as well as efficient data transmission and a guaranteed protection of the other systems. A tool box is now available for design and implementation.

The access protocol is a critical component of opportunistic networks, because of the numerous constraints and objectives, particularly the fair access which must be ensured to all the systems operating in the same area and the high level of global spectral efficiency. In that respect, the “Good Neighbour” strategy which has been proposed has a number of desirable features and its theoretical convergence has been proven. The next step is the reduction to practice, which will require simplification of the algorithms and some optimization, particularly regarding the adaptivity of the threshold involved in the spectrum allocation and the real time pilot based space-time spectrum sensing. Real world deployment and field trials will be necessary to validate the concepts.

The opportunistic unsynchronized network is a novel communication paradigm and its successful introduction amid existing networks and its proliferation depend on a number of conditions.

A first condition is the availability of spectral bands dedicated to cognitive radio. It is not realistic to imagine that networks which are based essentially on spectrum sensing can be deployed in the complete RF band, from 400 MHz to 6 GHz. Such systems need coordination and they have to rely on centralized data bases and employ specific schemes, such as the pilot control channel or the cognitive control channel. However, in a limited band, e.g. 100 MHz or 200 MHz, reliable spectrum sensing and monitoring can be achieved, particularly with the FBMC physical layer described above, and opportunistic unsynchronized networks can realize their potential in terms of flexibility and spectral efficiency.

A second condition is the existence of standards and regulatory policies. A key issue is coexistence of systems and acceptance by all the players in the field, i.e. administrations, operators and industries. Relevant parameters will have to be identified and specifications will have to be agreed. Among the key parameters are interference levels and signal detection thresholds. In any case, performance is critical. Regarding regulatory policies, the most important aspect is the spectrum allocation. It can be bands reserved for opportunistic networks or authorized access to already occupied bands under well defined rules and procedures. In this respect, the availability of spectrum space in the UHF band, after the shift from analogue to digital television, is a unique opportunity.

A third condition is related to business. An appropriate business model is essential for the start and the sustained growth of opportunistic networks. In fact, the approach will be successful if it is accepted by the administrations and current operators, if it satisfies needs of customers better than existing systems and if it is cost efficient. Referring to the history of WiFi, the availability of reserved appropriate frequency bands seems essential to launch the process of building the opportunistic business model. In the end, the operational and commercial success will be materialized by the presence of the opportunistic functionalities in PCs and communication sets.

In this respect, it is worth pointing out that the results of the PHYDYAS project will be transferred to the new COST action IC0905, “Techno-Economic regulatory framework for radio spectrum access for cognitive radio/software defined radio (TERRA)”:

> *The main objective of this Action is to develop a comprehensive techno-economic regulatory framework for radio spectrum access rules for CR/SDR based wireless applications, catering for envisaged CR/SDR deployment scenarios and shown to benefit most optimally the development of the wireless industries and consumer interests at large. Furthermore, the Action will provide assistance to European administrations in formulating a European position on radio spectrum access rules for CR/SDR applications.*

References

[Aky06] I. Akyildiz, L. Won-Yeol, M. Vuran, and S. Mohanty, "NeXt generation/dynamic spectrum access/cognitive radio wireless networks: A survey," Computer Networks, vol. 50, no. 13, pp. 2127 – 2159, 2006.

[Bal07] L. G. Baltar, D. S. Waldhauser, and J. Nossek, "Out-of-band radiation in multicarrier systems: a comparison," in *Proc. MC-SS Workshop*. Springer, May 2007, pp. 107–116.

[Ban07] G. Bansal, M. J. Hossain, and V. K. Bhargava, "Adaptive power loading for OFDM-Based cognitive radio systems," in *IEEE international conference on communication (ICC)*, 2007, pp. 5137–5142.

[Ban08] G. Bansal, M. J. Hossain, and V. K. Bhargava, "Optimal and suboptimal power allocation schemes for OFDM-based cognitive radio systems," *IEEE Transactions on Wireless Communications*, vol. 7, no. 11, pp. 4710–4718, Nov. 2008.

[Bel01] M. G. Bellanger, "Specification and design of a prototype filter for filter bank based multicarrier transmission," in *Proc. IEEE Int. Conf. Acoustics, Speech, and Signal Processing*, Salt Lake City, USA, May 2001, pp. 2417-2420.

[Boy04] S. Boyd and L. Vandenberghe, "Convex optimization," Cambridge, U.K.: Cambridge Univ. Press, 2004.

[Cha08] S. Chaudhari, V. Koivunen, and H. V. Poor, "Autocorrelation-based decentralized sequential detection of OFDM signals in cognitive radio," *IEEE Trans. Signal Processing*, vol. 57, pp. 2690-2700, Jul. 2008.

[D2.1] INFSO-ICT-211887 Project PHYDYAS, Deliverable 2.1, "Data-aided synchronization and initialization (single antenna)," Jul. 2008.

[D2.2] INFSO-ICT-211887 Project PHYDYAS, Deliverable 2.2, "Synchronization and initialization with single antenna. Blind Techniques," Jan. 2009.

[D3.1] INFSO-ICT-211887 Project PHYDYAS, Deliverable 3.1, "Equalization and demodulation in the receiver (single antenna)," Jul. 2008.

[D3.2] INFSO-ICT-211887 Project PHYDYAS, Deliverable 3.2, "Optimization of transmitter and receiver," Jul. 2009.

[D4.1] INFSO-ICT-211887 Project PHYDYAS, Deliverable 4.1, "MIMO channel matrix estimation and tracking," Jan. 2009.

[D4.2] INFSO-ICT-211887 Project PHYDYAS, Deliverable 4.2, "MIMO techniques and beamforming," Jan. 2010.

[D5.1] INFSO-ICT-211887 Project PHYDYAS, Deliverable 5.1, "Prototype filter and structure optimization," Jan. 2009.

[D6.1] INFSO-ICT-211887 Project PHYDYAS, Deliverable 6.1, "Duplexing and multiple access techniques, software description," Jan. 2009.

[D6.2] INFSO-ICT-211887 Project PHYDYAS, Deliverable 6.2, "Duplexing and multiple access techniques, software description," Jan. 2010.

[D8.1] INFSO-ICT-211887 Project PHYDYAS, Deliverable 8.1, "Application of the FBMC physical layer in a cognitive radio scenario," Jul. 2009.

[D8.2] INFSO-ICT-211887 Project PHYDYAS, Deliverable 8.2, "Space-time spectrum sensing, algorithms and software description," Feb. 2010.

[D9.3] INFSO-ICT-211887 Project PHYDYAS, Deliverable 9.3, "WiMAX simulation results – Lab setup and measurements," Jan. 2010.

[Doh02] M. Dohler, J. Dominguez and H. Aghvami, "Link capacity analysis for virtual antenna arrays," in *Proc. of IEEE Vehicular Technology Conference (VTC'02 Fall)*, Vancouver, Canada, vol. 1, pp. 440–443, Sep. 2002.

[Far08] B. Farhang-Boroujeny and R. Kempter, "Multicarrier communication techniques for spectrum sensing and communication in cognitive radios," *IEEE Commun. Mag. (Special Issue on Cognitive Radios for Dynamic Spectrum Access)*, vol. 48, no. 4, Apr. 2008.

[Fet09] G. Fettweis, M. Krondorf, S. Bittner, "GFDM - Generalized Frequency Division Multiplexing," in *Proc. VTC 2009 Spring*, Barcelona, Spain, Apr. 2009.

[Fou96] R. Fouler, C. Carlsson, "Fuzzy multiple criteria decision making: Recent developments," *Fuzzy Sets and Systems*, vol. 78, pp. 139-153, 1996.

[Fuj10] The Fujitsu 2G/3G/LTE Transceiver MB86L10A, data sheet, see http://www.fujitsu.com/downloads/MICRO/fma/pdf/RFTrans_MB86L10A.pdf

[Gao08] L. Gao and S. Cui, "Efficient subcarrier, power, and rate allocation with fairness consideration for OFDMA uplink," *IEEE Transactions on Wireless Communications*, vol. 7, no. 5, pp. 1507–1511, May 2008.

[Has09] Z. Hasan, G. Bansal, E. Hossain, and V. Bhargava, "Energy-efficient power allocation in OFDM-based cognitive radio systems: A risk-return model," IEEE Transactions on Wireless Communications, vol. 8, no. 12, pp. 6078 –6088, Dec. 2009.

[Hon10] X. Hong, C. Wang, M. Uysal, X. Ge and S. Ouyang, "Capacity of Hybrid Cognitive Radio Networks with Distributed VAAs," accepted by *IEEE Transactions on Vehicular Technology*, 2010.

[Hua05] J. Huang, R. A. Berry and M. L. Honig, “Spectrum sharing with distributed interference compensation,” in *Proc. 1st IEEE International Symposium on New Frontiers in Dynamic Spectrum Access Networks 2005 (DySPAN ’05)*, pp. 88–93, Nov. 2005.

[Iha09] T. Ihalainen, A. Viholainen, T. Hidalgo Stitz, M. Renfors and M. Bellanger, ”Filter bank based multi-mode multiple access scheme for wireless uplink”, in *Proc. EUSIPCO’09*, Glasgow, Scotland, Aug. 2009.

[ITU-R-A19] ITU-R, Annex 19 to document 5A/513, “Cognitive radio systems in the land mobile service,” Working document towards a preliminary draft new report, 31 May 2010.

[ITU-R-5A] ITU-R contribution- 5A/360-E, “Cognitive radio systems in the land mobile service – technical characteristics and functionalities of cognitive radio systems,” May 2009.

[Jan03] J. Jang and K. Lee, “Transmit power adaptation for multiuser OFDM systems,” *IEEE Journal on Selected Areas in Communications*, vol. 21, no. 2, pp. 171–178, Feb. 2003.

[Kan09] X. Kang, Y.-C. Liang, A. Nallanathan, H. Garg, and R. Zhang, “Optimal power allocation for fading channels in cognitive radio networks: Ergodic capacity and outage capacity,” *IEEE Transactions on Wireless Communications*, vol. 8, no. 2, pp. 940–950, Feb. 2009.

[Kim05] K. Kim, Y. Han, and S.-L. Kim, “Joint subcarrier and power allocation in uplink OFDMA systems,” *IEEE Communications Letters*, vol. 9, no. 6, pp. 526–528, Jun. 2005.

[Kim09] M. Kim, J. Naganawa, and J. Takada, “Multichannel Spectrum Sensing using Polyphase DFT Filter Bank for Opportunistic Cognitive Radios,” *The Institute of Electronics, Information and Communication Engineers (IEICE)*, vol. 109, pp. 121-127, May 2009.

[Kiv03] D. Kivanc, G. Li, and H. Liu, “Computationally efficient bandwidth allocation and power control for OFDMA,” *IEEE Transactions on Wireless Communications*, vol. 2, no. 6, pp. 1150–1158, 2003.

[Kuz10] A. Kuzminskiy and Y. Abramovich, “Decentralized dynamic spectrum allocation based on adaptive antenna array interference mitigation diversity,” *IEEE Transactions on Signal Processing*, vol. 58, no. 4, pp.2246-2260, Apr. 2010.

[Lek97] A. Leke and J. Cioffi, “A maximum rate loading algorithm for discrete multitone modulation systems,” in *IEEE Global Telecommunications Conference (GLOBECOM’97)*, vol. 3, pp. 1514–1518, 1997.

[Mar98] K. W. Martin, "Small Side-lobe Filter Design for Multitone Data Communication," IEEE Trans., CAS-II, Vol.45, pp. 1155-1161, Aug. 1998.

[Mer08] A. Merentitis, E. Patouni, N. Alonistioti, M. Doubrava, "To Reconfigure or Not to Reconfigure: Cognitive Mechanisms for Mobile Devices Decision Making," in *Proc. 68th IEEE Vehicular Technology Conference (VTC)*, Calgary, Canada, Sept. 2008.

[Mer09] A. Merentitis, A. Kaloxylos, M. Stamatelatos, N. Alonistioti, "Optimal Periodic Radio Sensing and Low Energy Reasoning for Cognitive Devices," in *Proc. of the Mediterranean Electrotechnical Conference (MELECON)*, 25 – 28 April 2010, Valetta, Malta.

[Mer10] A. Merentitis, D. Triantafyllopolou, "Transmission Power Regulation in Cooperative Cognitive Radio Systems Under Uncertainties," accepted for publication in *Proc. of the International Symposium on Wireless Pervasive Computing, (ISWPC)*, 5-7 May 2010, Modena, Italy.

[Mit99] J. Mitola, "Cognitive radio for flexible mobile multimedia communications," in *IEEE International workshop on Mobile multimedia communications, MoMuC'99*, pp. 3–10, Nov. 1999.

[Mun02] G. Munz, S. Pfletschinger, and J. Speidel, "An efficient waterfilling algorithm for multiple access OFDM," in *IEEE Global Telecommunications Conference (GLOBECOM'02)*, vol. 1, pp. 681– 685, Nov. 2002.

[Mus09] L. Musavian and S. Aissa, "Capacity and power allocation for spectrum-sharing communications in fading channels," *IEEE Transactions on Wireless Communications*, vol. 8, no. 1, pp. 148–156, Jan. 2009.

[Pap08] N. Papandreou and T. Antonakopoulos, "Bit and power allocation in constrained multicarrier systems: The single-user case," *EURASIP Journal on Advances in Signal Processing*, vol. 2008, Article ID 643081, 4 pages, 2008, doi:10.1155/2008/43081.

[Per09] A. I. Perez, M. A. Lagunas, M. A. Rojas, "Correlation Matching Approach for Spectrum Sensing," *IEEE Transactions on Signal Processing*, vol. 57, no. 12, pp. 4823-4836, Dec. 2009.

[PHY] "PHYDYAS-Physical layer for dynamic spectrum access and cognitive radio," Project website: www.ict-phydyas.org.

[Pro02] J. G. Proakis and M. Salehi, "Communication Systems Engineering," 2nd edition Upper Saddle River, NJ: Prentice-Hall, 2002.

[Qin07] T. Qin and C. Leung, "Fair adaptive resource allocation for multiuser OFDM cognitive radio systems," in *Second International Conference on Communications and Networking in China (CHINACOM'07)*, Aug. 2007.

[Raw08] O. A. Rawashdeh, "Towards Decentralized Management of Graceful Degradation in Distributed Embedded Systems," *IEEE Dependable Systems and Networks Conference (DSN)*, June 2008.

[Rah09] U. Rahim, T. Hidalgo Stitz and M. Renfors, "Analysis of clipping-based PAPR reduction in multicarrier systems", in *Proc. IEEE VTC'09*, Barcelona, Spain, Apr. 2009.

[Rin10] V. Ringset, H. Rustad, F. Schaich, J. Vandermot, M. Najar," Performance of a FilterBank MultiCarrier (FBMC) Physical Layer in the WiMAX Context," in *Proc. Future Network & Mobile Summit* (FNMS'2010, Florence, Italy), Jun. 2010.

[Roj08] Miguel A. Rojas, Miguel A. Lagunas, Ana I. Pérez-Neira, Petre Stoica, "Spectrum Labeling for Cognitive Radio Systems: Cadidate Spectral Estimation," in *Proc. 1st IARP in Cognitive Radio and Networks (CiP)*, Santoniri, Greece, Jun. 2008.

[Roj09] Miguel A. Rojas, Ana I. Pérez-Neira, Miguel A. Lagunas, "DVB-T Candidate Power Detector for Cognitive Radio," in *Proc of 17th European Signal Processing Conference (EUSIPCO'2009)*, Glasgow, Scotland, Aug. 2008.

[Saa08] H. Saarnisaari, "URANUS: Flexible Parameterized Baseband Transceiver Architecture Based on Filter Banks," in *Proc. ISCCSP 2008*, Malta, Apr. 2008.

[Sal10] G. Salami, O. Durowoju, A. Attar, O. Holland, R. Tafazolli and H. Aghvami, "A Comparison Between the Centralized and Distributed Approaches for Spectrum Management," accepted by *IEEE Communications Surveys & Tutorials*, 2010.

[Sha10] M. Shaat and F. Bader, "Computationally efficient power allocation algorithm in multicarrier-based cognitive radio networks: OFDM and FBMC systems," *EURASIP Journal on Advances in Signal Processing*, vol. 2010, Article ID 528378, 13 pages, 2010.

[She03] Z. Shen, J. Andrews, and B. Evans, "Optimal power allocation in multiuser OFDM systems," in *IEEE Global Telecommunications Conference (GLOBECOM'03)*, vol. 1, 2003.

[She09] F. Sheikh, S. Masud, and B. Bing, "Harmonic power detection in wideband cognitive radios," *Signal Processing, IET*, vol. 3, pp. 40-50, Jan. 2009.

[Skr06] A. Skrzypczak, P. Siohan, and J. Javaudin, "Power spectral density and cubic metric for the OFDM/OQAM modulation," in *IEEE ISSPIT*, Vancouver-Canada, Aug. 2006.

[Stu09] G. Stuber, S. Almalfouh, and D. Sale, "Interference analysis of TV-band whitespace," *Proceedings of the IEEE*, vol. 97, no. 4, pp. 741–754, Apr. 2009.

[Taj10] A. Tajer and X. Wang, "Multiuser Diversity Gain in Cognitive Networks," accepted by *IEEE/ACM Transactions on Networking*, 2010.

[Tos09] A. Toskala, H. Holma (Eds.), "LTE for UMTS - OFDMA and SC-FDMA Based Radio Access," Wiley 2009.

[Wan07] P. Wang, M. Zhao, L. Xiao, S. Zhou, and J. Wang, "Power allocation in OFDM-Based cognitive radio systems," in *IEEE Global Telecommunications Conference (GLOBECOM)*, pp. 4061–4065, 2007.

[Val06] M. Valkama, A. Shahed Hagh Ghadam, L. Anttila, M. Renfors, "Advanced digital signal processing techniques for compensation of nonlinear distortion in wideband multicarrier radio receivers," *IEEE Trans. Microwave Theory and Techniques*, vol. 54, pp. 2356-2366, Jun. 2006.

[Wal08] D. S. Waldhauser, L. G. Baltar, J. A. Nossek, "Filter Bank Based Multicarier systems," Techniken, Algorithmen und Konzepte für zukünftige COFDM Systeme (TakeOFDM).

[Wan09] W. Wang, W. Wang, Q. Lu, and T. Peng, "An uplink resource allocation scheme for OFDMA-based cognitive radio networks," *International Journal of Communication Systems*, vol. 22, no. 5, pp. 603–623, 2009.

[Wei03] W. Wei and M. J. Wang, "Fuzzy-MOGA-based Traffic Signal Control at Intersection," in *Proc. International Conference on Machine Learning and Cybernetics*, Nov. 2003.

[Wei04] T. Weiss and J. Hillenbrand, "Mutual interference in OFDM-based spectrum pooling systems," in *Vehicular Technology Conference (VTC)*, vol. 4, May 2004.

[Wei03b] T. Weiss, J. Hillenbrand, A. Krohn, F. K. Jondral, "Efficient signaling of spectral resources in spectrum pooling systems," in Proc. 10th Symp. Communications and Vehicular Technology, Eindhoven, Netherlands, Nov. 2003.

[Won99] C. Wong, R. Cheng, K. Lataief, and R. Murch, "Multiuser OFDM with adaptive subcarrier, bit, and power allocation," *IEEE Journal on Selected Areas in Communications*, vol. 17, no. 10, pp. 1747–1758, 1999.

[Yu04] W. Yu, W. Rhee, S. Boyd, and J. Cioffi, "Iterative water-filling for Gaussian vector multiple-access channels," *IEEE Transactions on Information Theory*, vol. 50, no. 1, pp. 145 – 152, Jan. 2004.

[Yuc09] T. Yucek and H. Arslan, "A survey of spectrum sensing algorithms for cognitive radio applications," *IEEE Communications Surveys Tutorials*, vol. 11, no. 1, pp. 116–130, First quarter 2009.

[Zen10] Y. Zeng, Y.-C. Liang, A. T. Hoang, and R. Zhang, "A review on spectrum sensing for cognitive radio: Challenges and solutions," *EURASIP Journal on Advances in Signal Processing*, vol. 2010, Article ID 381465, 15 pages, 2010.

[Zha08-1] R. Zhang and Y.-C. Liang, "Exploiting multi-antennas for opportunistic spectrum sharing in cognitive radio networks," *IEEE Journal of Selected Topics in Signal Processing*, vol. 2, no. 1, pp. 88–102, Feb. 2008.

[Zha08-2] Y. Zhang, "Resource allocation for OFDM-Based cognitive radio systems," *Ph.D. dissertation, Univ. of British Columbia, Vancouver*, Dec. 2008.

[Zha08-3] R. Zhang, "Optimal power control over fading cognitive radio channel by exploiting primary user CSI," in *IEEE Global Telecommunications Conference (IEEE GLOBECOM'08)*, Dec. 2008.

[Zha09-1] R. Zhang, "On peak versus average interference power constraints for protecting primary users in cognitive radio networks," *IEEE Transactions on Wireless Communications*, vol. 8, no. 4, pp. 2112–2120, Apr. 2009.

[Zha09-2] R. Zhang, S. Cui, and Y.-C. Liang, "On Ergodic sum capacity of fading cognitive multiple-access and broadcast channels," *IEEE Transactions on Information Theory*, vol. 55, no. 11, pp. 5161–5178, Nov. 2009.

[Zha09-3] H. Zhang, D. L. Ruyet, and M. Terre, "On spectral efficiency analysis between OFDM/OQAM and OFDM based CR networks," in *Vehicular Technology Conference, VTC*, Barcelona-Spain, 2009.

[Zha09-4] Y. Zhang and C. Leung, "Resource allocation in an OFDM-based cognitive radio system," *IEEE Transactions on Communications*, vol. 57, no. 7, pp. 1928 –1931, Jul. 2009.

[Zha10-1] H. Zhang, D. L. Ruyet, D. Roviras, Y. Medjahdi, and H. Sun, "Spectral efficiency comparison of OFDM/FBMC for uplink cognitive radio networks," *EURASIP Journal on Advances in Signal Processing*, vol. 2010, Article ID 621808, 14 pages, 2010.

[Zha10-2] C. Zhao and K. Kwak, "Power/Bit loading in OFDM-Based cognitive networks with comprehensive interference considerations: The single-SU case," *IEEE Transactions on Vehicular Technology*, vol. 59, no. 4, pp. 1910 –1922, May 2010.

[Zha10-3] H. Zhang, D. L. Ruyet, M. Terre, "Spectral efficiency comparison between OFDM/OQAM- and OFDM-based CR networks," Wiley's Wireless Communications and Mobile Computing, DOI in press.